

10. SITE 830¹

Shipboard Scientific Party²

HOLE 830A

Date occupied: 6 November 1990
Date departed: 6 November 1990
Time on hole: 19 hr, 30 min
Position: 15°57.00'S, 166°46.79'E
Bottom felt (rig floor; m; drill-pipe measurement): 1029.5
Distance between rig floor and sea level (m): 11.1
Water depth (drill-pipe measurement from sea level, m): 1018.4
Total depth (rig floor; m): 1126.4
Penetration (m): 96.9
Number of cores (including cores with no recovery): 11
Total length of cored section (m): 96.9
Total core recovered (m): 53.77
Core recovery (%): 55.5
Oldest sediment cored:
Depth below seafloor (m): 96.9
Nature: volcanic silt and sand
Age: Pleistocene
Measured velocity (km/s): 1.706

HOLE 830B

Date occupied: 6 November 1990
Date departed: 9 November 1990
Time on hole: 2 days, 23 hr
Position: 15°57.00'S, 166°46.8'E
Bottom felt (rig floor; m; drill-pipe measurement): 1029.5
Distance between rig floor and sea level (m): 11.1
Water depth (drill-pipe measurement from sea level, m): 1018.4
Total depth (rig floor; m): 1311.2
Penetration (m): 281.7
Number of cores (including cores with no recovery): 24
Total length of cored section (m): 233.20
Total core recovered (m): 48.77
Core recovery (%): 20.9
Oldest sediment cored:
Depth below seafloor (m): 281.7
Nature: volcanic breccia and sandstone
Age: unknown
Measured velocity (km/s): 2.281
Comments: Washed down to 48.5 m

HOLE 830C

Date occupied: 9 November 1990
Date departed: 12 November 1990
Time on hole: 3 days, 4 hr
Position: 15°57.00'S, 166°46.7'E
Bottom felt (rig floor; m; drill-pipe measurement): 1020.0
Distance between rig floor and sea level (m): 11.1
Water depth (drill-pipe measurement from sea level, m): 1008.9
Total depth (rig floor; m): 1370.6
Penetration (m): 350.6
Number of cores (including cores with no recovery): 12
Total length of cored section (m): 115.6
Total core recovered (m): 19.4
Core recovery (%): 16.8
Oldest sediment cored:
Depth below seafloor (m): 350.6
Nature: volcanic breccia
Age: unknown
Measured velocity (km/s): 4.44
Comments: Washed down to 235 m.

Principal results: Site 830 is located on the forearc slope in the collision zone between the Bougainville Guyot and the central New Hebrides Island Arc, about 6.5 km east of the plate boundary and about 30 km from the southern coast of Espiritu Santo Island. Based on a short pre-site geophysical survey run by the *JOIDES Resolution*, we selected a site close to the original proposed site DEZ-4, on a small flat area protruding out from a 10° south-dipping slope. At this location the Bougainville Guyot is impinging upon the arc slope, causing considerable uplift and shortening as indicated by a shallow bulge of accreted rocks (750 meters below seafloor, or mbsf) and well-developed, arcward-dipping thrust faults east of the impact zone. The site was chosen to penetrate a thrust slice in the forearc where thin surficial sedimentary rocks appear to overlie east-dipping strongly reflective horizons. We interpret these horizons to be either arc basement rock, old accretionary rocks, a piece of guyot broken off during subduction, or part of the guyot's debris apron. Our intent at this site was to determine if guyot fragments are being accreted to the forearc and to study the mechanical properties of the deformed forearc rocks, as well as to analyze interstitial fluids geochemically in order to contrast them with major results of Sites 827 and 829, which were drilled in the North d'Entrecasteaux Ridge–New Hebrides Island Arc collision zone.

Hole 830A was drilled with APC and XCB down to 96.9 mbsf with 55.5% core recovery rate. Hole 830B penetrated to 281.7 mbsf and was cored between 48.5 and 281.7 mbsf with a 20.9% core recovery rate and Hole 830C penetrated to 350.6 mbsf and was cored between 235 and 350.6 mbsf with a core recovery rate of 16.8%.

Two major lithostratigraphic units were described: Unit I (0–174.9 mbsf) consists of very dark gray volcanic silt and siltstone with various amounts of sand and clay, and is divided into three subunits. Subunit IA (0–21.0 mbsf, Hole 830A) is a 21-m-thick, fine-grained, nearly structureless un lithified silt. Subunit IB (21.0–

¹ Collot, J.-Y., Greene, H. G., Stokking, L. B., et al., 1992. *Proc. ODP, Init. Repts.*, 134: College Station, TX (Ocean Drilling Program).

² Shipboard Scientific Party is as given in the list of participants preceding the contents.

47.0 mbsf, Hole 830A) is a 26.0-m-thick sequence characterized by clayey sandy silt with numerous normally graded interbeds of black sand. Subunit IC (47.0–174.9 mbsf, Holes 830A and 830B) is a 127.9-m-thick sequence that contains interbedded sandy silts and silty sands. The upper part of Unit I shows some horizontal bedding planes whereas the bedding dip increases downhole from 5° to more than 40°. Few high-angle normal faults with throws of a few millimeters to a few centimeters are also observed in Unit I. Lithostratigraphic Unit I appears to lie unconformably upon lithostratigraphic Unit II. Unit II (174.9–350.6 mbsf) is a colorful sequence of altered, very poorly sorted, very coarse volcanoclastic, partially lithified sandstone with a matrix of sandy silt and has a 9.5-m-thick sequence containing pieces of basalt, sed-lithic breccia, and volcanic sandstone without surviving matrix distinctly marking the top of the unit. The sand grains throughout the unit are composed of black, well-lithified volcanic siltstone. Intervals of silty sandstone in varying shades of grayish green, reddish black clayey silts, white zeolite veins, gray clay laminae, and black volcanic sand lenses compose sections of Unit II. These sections alternate with layers of dark gray volcanoclastic sandstone. Rocks of Unit II are deformed and considered as cataclases. They show increasing occurrences of scaly fabric downhole.

Clasts and isolated pebbles of igneous rocks were encountered only in Unit II. Based on their mineralogy and structure, they can be divided into volcanic breccia with crystals of clinopyroxene and plagioclase and with rock fragments of altered basalts, and andesite with a generally altered ground mass including vesicles filled with chlorite, calcite, and some zeolites.

Foraminiferal and nannofossil analysis indicate that lithostratigraphic Unit I is not older than Pleistocene. All samples from lithostratigraphic Unit II were barren.

Initial interpretations of the cores suggest that lithostratigraphic Unit I consists of turbidites that were deposited along an unstable slope. Lithostratigraphic Unit II represents a highly altered epiclastic sequence whose components were probably derived from the nearby islands.

Paleomagnetic studies indicate that the upper 48 m of lithostratigraphic Unit I are in the upper part of the Brunhes Chron and have high ($1-10 \times 10^{-2}$ SI) magnetic susceptibility. Magnetization overprint due to drilling and the mixed magnetic orientation of the volcanic breccia preclude any determination of the magnetostratigraphy in the deep part of the holes.

Analyses of the fluid geochemistry from whole-round samples indicate that chloride concentration strongly increases with depth to about 11% higher than seawater. Alteration of ash and the coarse volcanic siltstone and breccia is clearly seen in extreme calcium, magnesium, potassium, and sodium concentrations. In the most altered pore-fluid sample, which was collected near the total depth of the hole, calcium increases to 229.2 mM. There is no magnesium or potassium and only 172 mM of sodium. Similar, although not as extreme, abnormal variations in concentrations occur between 50 and 100 mbsf in the overlying Pleistocene sediments. These variations could reflect local diagenetic alteration of ash layers or lateral flow of deep fluids along a slightly sandier layer. Similar deviations in the gradients of alkalinity, silica, phosphate, and ammonia support the hypothesis of lateral flow of deep fluids.

Physical properties of the cores recovered at Site 830 were also measured. Porosity and water content have very high values of 72% and 85% at the mudline, but decrease extremely rapidly in the first 50 mbsf to less than 40% porosity and 25% water content. Bulk density shows a corresponding increase in the first 50 mbsf from the 1.6 to 2.24 Mg/m³. Shear strength also increases rapidly within the first 50 mbsf from 5 to 135 kPa. Sonic velocity shows a normal gradient down to 175 mbsf, and then increases sharply. The rapid decrease in porosity and water content provides evidence that dewatering may be occurring as a result of tectonic compression.

Hole 830C was logged only to 260 mbsf because of deteriorating conditions in the bottom part of the hole. The formation microscanner was not used in this hole because of irregular hole conditions, including areas of oversized diameter. Consequently only the Schlumberger quad combo and the geochemical combination were deployed. Excellent results were obtained and con-

firm the major boundary between lithostratigraphic Units I and II near 160 mbsf. Geochemical logs indicate a change in chemical composition of rocks at 185 mbsf and the seismic log suggests a boundary just below 200 mbsf.

BACKGROUND AND OBJECTIVES

Site 830 is the fourth of a series of sites (Sites 827–831) located within the collision zone between the d'Entrecasteaux Zone (DEZ) and the central New Hebrides Island Arc. The site is located high on the upper forearc slope 30 km due south of the southern tip of Espiritu Santo Island, about 7 km east of the collision zone, and approximately 15 km from Site 831 (Fig. 1). The slope to the south of the site is the northern wall of a semicircular bathymetric reentrant that is interpreted as a morphological scar from a previously subducted seamount (Collet and Fisher, 1989). Sites within the collision zone were selected to determine the influence that ridge composition and structure exert on a forearc and to determine the style of accretion and the type of arc structures produced during the collision.

The South d'Entrecasteaux Chain (SDC) is the southern ridge of the DEZ, a two-ridge system that also includes the North d'Entrecasteaux Ridge (NDR). This submarine mountain chain extends in an arcuate fashion over 600 km from the northern New Caledonia Ridge to the New Hebrides Trench. The eastern terminus of the SDC is represented by the Bougainville Guyot, which appears to be subducting beneath the central New Hebrides Island Arc or accreting to the forearc slope (Fisher et al., 1986). To the west, another guyot, Sabine Bank, which rests on the outer rise, is about to follow Bougainville Guyot down the subduction zone. Bougainville Guyot is an eastward-tilted seamount that clogs the New Hebrides Trench. Collision of the Bougainville Guyot with the arc has deformed the upper forearc slope immediately east of where the guyot impinges upon the outer arc slope. Seabeam bathymetric data show that the impingement of the guyot formed an anticlinal dome (Fig. 1), oriented generally north-south, whose summit is elevated nearly 1 km above the eastern summit platform surface of the guyot (Daniel et al., 1986). Compressional forces associated with the collision of

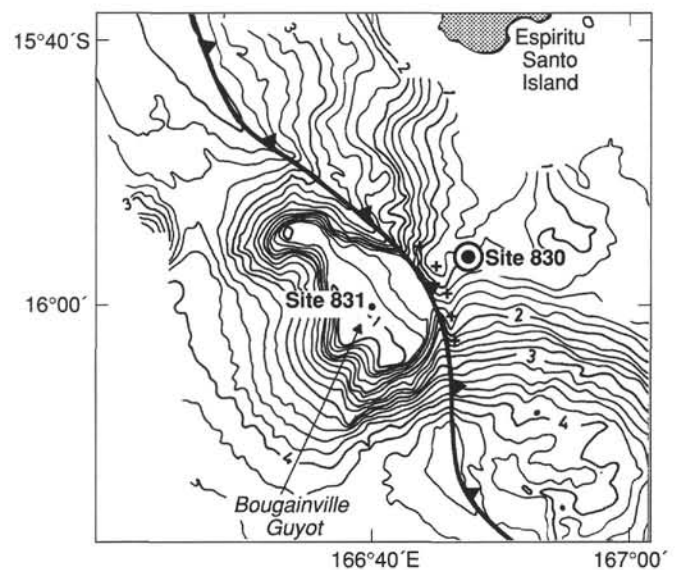


Figure 1. Bathymetric map showing location of Site 830. Bathymetry is in kilometers. Heavy line indicates trace of subduction zone, teeth are on upper plate. Crosses indicate the anticlinal dome (modified after Daniel et al., 1986).

the guyot deformed and foreshortened the sedimentary and volcanic rocks of the forearc. This deformation is reflected by arcward-dipping beds and shallow eastward-dipping imbricate thrust faults (Fisher et al., 1986). Observations made during recent dives along the exposed eastern edge of the Bougainville Guyot, using the French deep-diving submersible *Nautille*, revealed steeply to gently arcward-dipping sedimentary and volcanic rocks (Collot et al., 1989). Seafloor samples collected with *Nautille* near the base of the arc slope, near the collision zone of the guyot, consist of upper Eocene to lower Miocene highly fractured and deformed reefal limestone, calcarenite, and mudstone. Overlying the area where the samples were collected are less-deformed Pliocene to Pleistocene volcanic and calcareous siltstone and sandstone that were observed to dip 30° toward the arc (Collot et al., unpubl. data).³

The exposed part of Bougainville Guyot appears intact and unbroken in spite of its trip down the subduction zone. A few step faults appear to offset the guyot's carbonate cap, but otherwise, little deformation is observed. The eastern part of the guyot may be step-faulted down to the east and may be buried beneath the anticlinal dome immediately east of the collision zone. If so, broken-up pieces of the guyot may lie at shallow depths (400–1000 m) beneath the seafloor east of the collision zone.

A short single-channel seismic reflection survey was made in the area of proposed site DEZ-4 (see Fig. 2, "Seismic Stratigraphy" section, this chapter). This survey defined a series of eastward-dipping, low-angle imbricate thrust sheets just east of the collision zone (see Fig. 3, "Seismic Stratigraphy" section, this chapter). Site 830 was located near the westward toe of the most westerly thrust sheet and along the southeastern flank of the anticlinal dome (Fig. 1). Here the sole of the thrust lies about 1.5 seconds (s) (seismic two-way traveltime) deep and older island-arc rocks or broken pieces of the guyot may lie about 1.7–1.8 s deep.

Three hypotheses are proposed for the origin of arc slope rocks in the collision zone of the SDC with the New Hebrides Island Arc. The arc-slope rocks may be (1) composed of remnants of an accretionary wedge that predates the collision and is deformed and uplifted by the collision, (2) formed of deformed and tilted New Hebrides Island Arc basement rocks, or (3) comprised of guyot cap rock and detrital apron that has been accreted to the forearc. Based on these hypotheses the scientific objectives for drilling at Site 830 are as follows:

1. To penetrate imbricated arc rocks so as to determine whether these rocks are part of an uplifted old accretionary wedge, recently accreted guyot rocks, or island-arc basement.
2. To study stress orientation in relation to compressive forces associated with the guyot collision.
3. To determine the amount and timing of Neogene uplift of the forearc.
4. To determine the role of pore fluids in collisional subduction or obduction processes.

Results obtained from drilling at Site 830 will be compared and contrasted with those obtained near the NDR and on the Bougainville Guyot to determine why arc structures induced by collision of the two ridges (NDR and SDC) differ from each

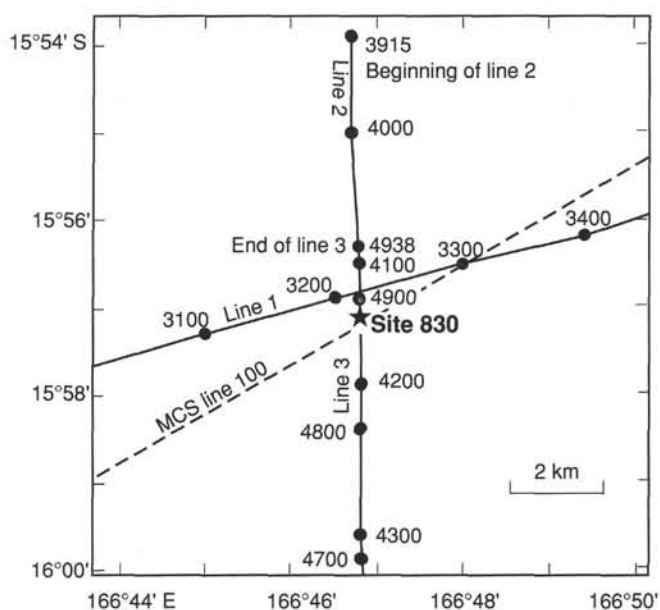


Figure 2. Trackline map showing the locations of Site 830, single-channel seismic lines 1, 2, and 3, as well as multichannel seismic line 100 (USGS, L5-84-SP).

other. The rate of uplift of the accretionary wedge will be determined and compared to the rate at which onshore areas emerge during the late Quaternary (Taylor et al., 1987).

SEISMIC STRATIGRAPHY

Multichannel Seismic Data

Crossing multichannel seismic lines collected over Site 830 show shallow, east-dipping reflections that outline arc structures caused by the collision of the Bougainville Guyot. For example, line 100 (Figs. 2 and 4) indicates that one set of east-dipping reflections occur at 1.5 s below shotpoint (SP) 550; they lie within a large antiform that developed along the east side of the Bougainville Guyot as a direct product of the eastward encroachment of the guyot into forearc rocks. Another of the east-dipping reflections, one of the main targets for drilling at Site 830, lies at 1.5 s below the site; yet another is at 2.0 s below SP 440. The spatial relationships among these reflections suggest imbricated thrust faults: either the reflections are from one stratigraphic horizon wholly within arc rocks that was disrupted by thrust faulting, or the reflections are from blocks of guyot rocks that were accreted to the arc during the ongoing collision. The antiform below SP 550 (Fig. 4) lies just east of the plate boundary and is another manifestation of collision-zone structure.

The east-dipping reflections are segmented by thrust faults that strike north and dip east, but southward from the drill site this strike is less well constrained by seismic data. The strike may differ to the south because the stress caused by collision is asymmetric—the guyot encounters arc rocks on its north and east sides but the south side of the guyot is a free surface, owing to a large reentrant in the lower arc slope (see Fig. 1, "Background and Objectives" section, this chapter). Seismic data show that rocks forming the wall of the reentrant are well bedded and appear to be part of the thick debris apron that forms the lower guyot flank. Before drilling began at Site 830, the east-dipping reflections were thought to be accreted parts of this apron, and since the drill failed to penetrate the rocks

³ Collot, J.-Y., Lallemand, S., Pelletier, B., Eissen, J.-P., Glaçon, G., Fisher, M. A., Greene, H. G., Boulin, J., Daniel, J., and Monzier, M. Geology of the d'Entrecasteaux–New Hebrides island arc collision: results from a deep-sea submersible survey (submitted to *Tectonophysics*).

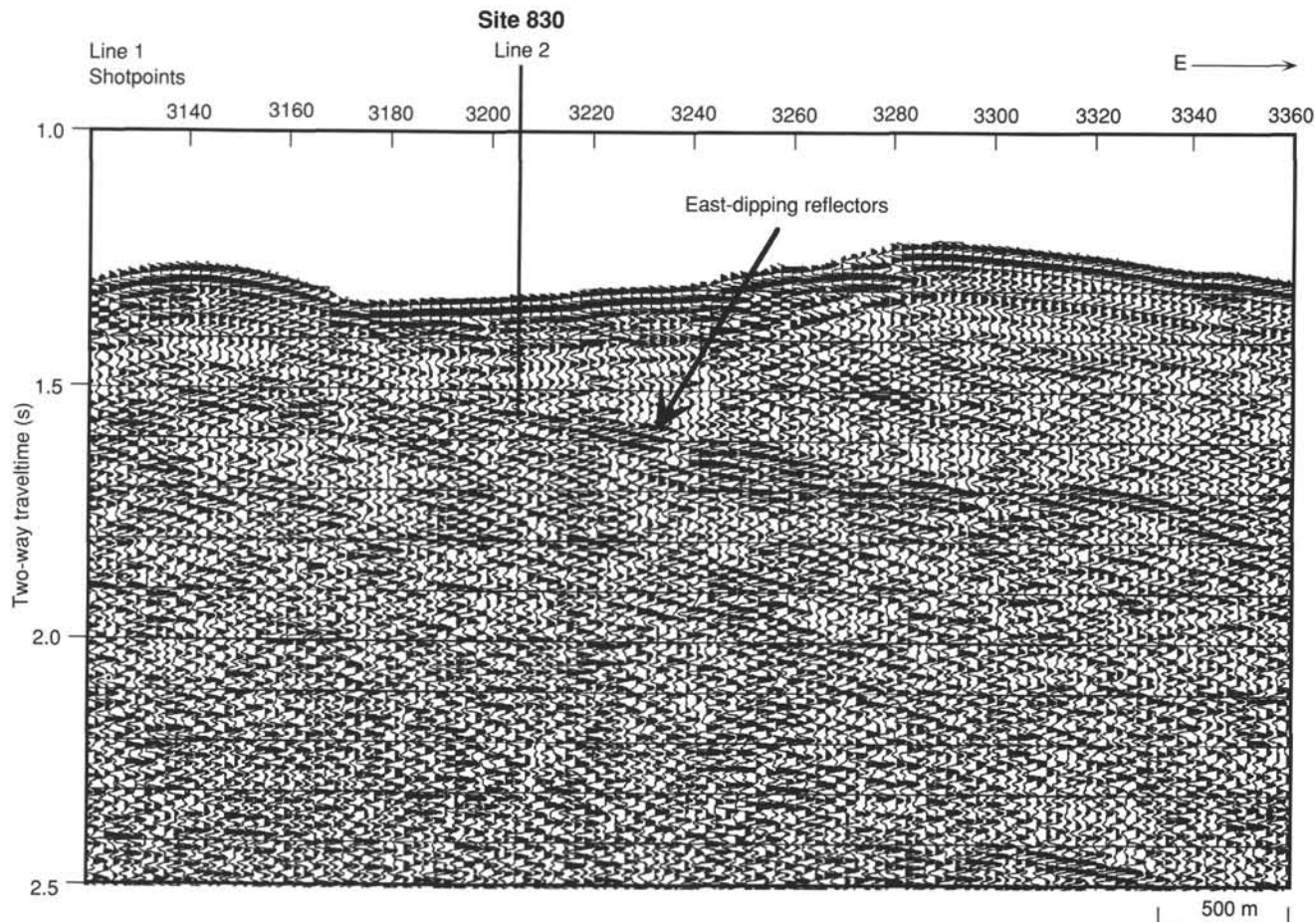


Figure 3. Part of single-channel seismic line 1 that crosses just north of Site 830.

that cause these reflections, the affinity of the rocks remains uncertain.

Single-Channel Seismic Data

Single-channel seismic reflection data were collected over Site 830, using two 80-in.³ water guns for the source and a streamer that has a 100-m-long active section. Aboard-ship processing included predictive deconvolution, bandpass filtering, and automatic gain control. Velocity data used to convert depth in the hole to traveltime come primarily from the sonic log and partly from physical properties measurements, which were used where well logs are not available, from the very shallowest part of the hole.

Site 830 lies just south of the intersection of seismic lines 1 and 2 (Figs. 2, 3, and 5). Unfortunately, strong noise of undetermined cause affected seismic section 2 just over the drill site, but line 1 is unaffected. Seismic section 1 shows that one of the east-dipping reflections lies at about 0.25 s below the seafloor (Fig. 3). The interface that causes this reflection lies at the top of a rock unit that returns parallel reflections for about 0.4 s. Rocks within the forearc area are not usually so reflective, thick and coherently bedded.

Lithostratigraphic Unit I is Pleistocene clayey volcanic siltstone and Unit II is an undated, very poorly sorted volcaniclastic sand with a chloritic matrix; both of these units overlie the east-dipping reflectors that were the target of this hole (Fig. 6). Drilling at Hole 830C, which had the deepest penetration (350.5 mbsf) at this drill site, apparently just penetrated the top of these reflectors but had to stop because of unstable hole conditions before a sample of the reflectors

could be recovered. That drilling stopped short of the reflectors is indicated by the poor bedding of Unit II, which would not generate the parallel reflections evident from just below the total depth of the hole. Furthermore, no major change in rock type or structure is described from material recovered at the bottom of the hole.

OPERATIONS

Transit from Site 829 to proposed site DEZ-4 was made in 14 hr. Preliminary surveys were conducted at proposed sites DEZ-5 and DEZ-4 and a beacon was dropped at proposed site DEZ-5. At 0230 Universal Time Coordinated (UTC) on 6 November, a second beacon was launched on DEZ-4 to begin Site 830.

Hole 830A

The first advanced piston coring system (APC) core was taken from the seafloor at 1018.4 meters below sea level (mbsl). Core orientation began with Core 134-830A-2H, but coring strokes were incomplete from Core 134-830A-3H onward. After Core 134-830A-6H, at 48.5 mbsf, we switched to the extended core barrel (XCB) system and penetrated to 96.9 mbsf, although recovery averaged only 55.5% (Table 1). The final of a series of three water sampler temperature probe (WSTP) temperature measurements was then taken and the pipe was tripped so that rotary core barrel (RCB) coring could begin.

Hole 830B

The vessel was offset 10 m northwest of Hole 830A in a water depth 1018.4 mbsl. Hole 830B was drilled without

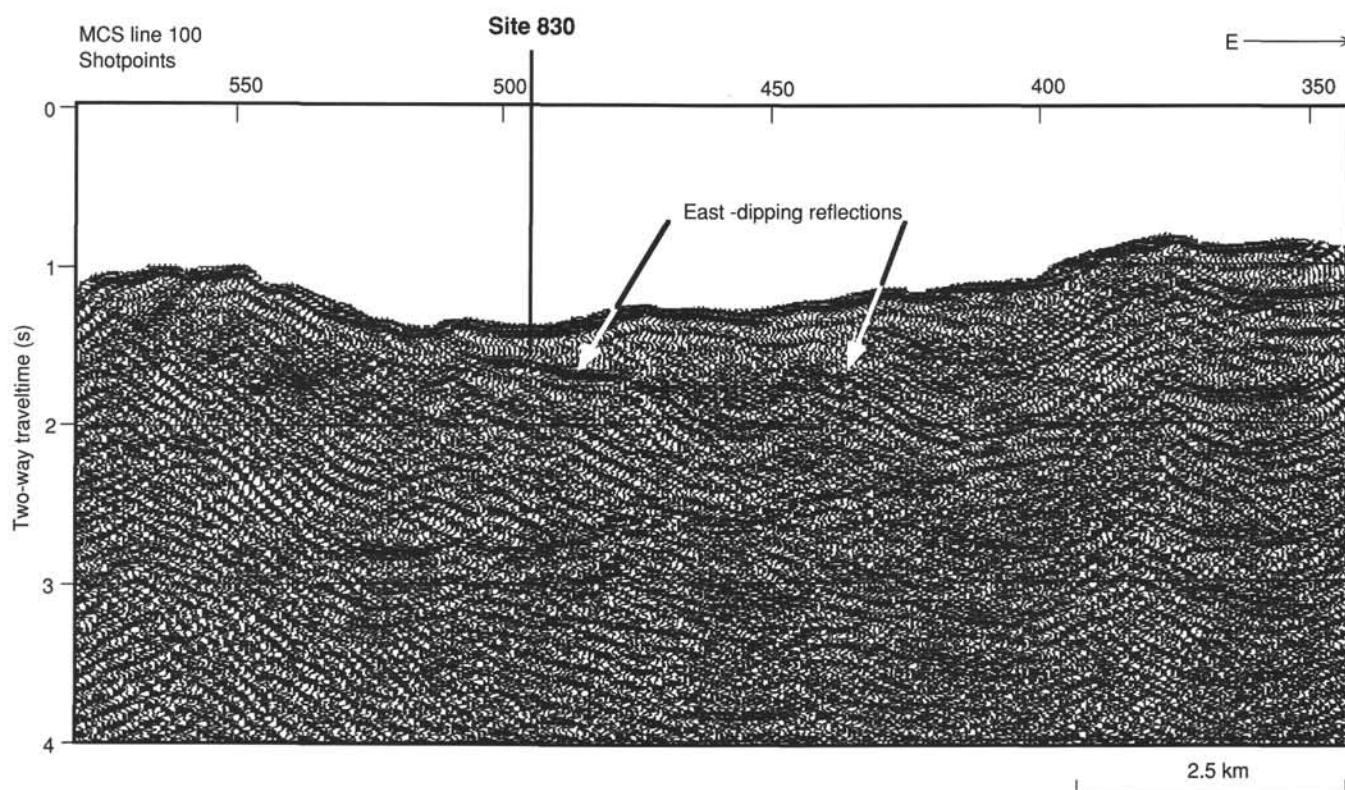


Figure 4. Part of multichannel seismic line 100 (USGS, L5-84-SP) that crosses the arc near Site 830.

coring to 48.5 mbsf, where RCB coring began. At 175 mbsf, an interval of sheared volcanic rocks and sediments containing sand- and gravel-sized particles was encountered that was quite difficult to drill, although the material within the poorly recovered cores was relatively soft.

Hole conditions were excellent to about 260 mbsf, where the drill string packed off and stuck without warning after a core barrel retrieval and reconnection. The drill string was worked free and pulled to about 38 m above the base of the hole. When the bottom-hole assembly was returned to the bottom of the hole, coring continued. The core liner contained drill cuttings that were quite fine, suggesting that the pipe had stuck because of an avalanche of cuttings from the seafloor. When circulation was stopped to recover subsequent cores, however, packing problems recurred. Back flow from the drill pipe occurred when the connection was broken to retrieve Core 134-830B-24R and to drop the next core barrel. After the pipe connection, the drill string became plugged and circulation could not be re-established. The drill string was stuck vertically, but could be rotated, and was eventually freed and recovered. Hole 830B was cored from 48.5 to 281.7 mbsf, for a recovery rate of 20.9% (Table 1).

Hole 830C

The ship was offset 143 m to the west in a water depth of 1008.9 mbsl, where the sedimentary layer previously drilled appeared to be thinner in seismic reflection profiles. The hole was drilled without coring to 244.4 mbsf, after which continuous RCB coring began. Despite increased RPM and circulation rate, penetration rate and core recovery both were low. Packing-off problems began upon retrieval of the first core and indicated poor annular cleaning even after mud flushing. Hole-cleaning problems increased with depth in the volcanic breccia and sandstone (see "Lithostratigraphy" section, this

chapter). At 330 mbsf, the drill string became plugged while a core was being retrieved. The drill string also became stuck because of annular packing. The bit was "worked" 30 m up the hole and circulation was re-established through the throat of the bit. A short trip was made up to 180 mbsf, and 2 hr was required to clear three of the four bit nozzles so that coring could be resumed. The hole was cleaned to total depth, through 10 m of fill, and an additional core was cut. After more packing-off, plugging, and sticking of the drill string, it became apparent that the drilling targets were unattainable at Site 830. A final core was cut to 351 mbsf and the bit was raised 20 m above the base of the hole before retrieving the core. A "wiper trip" to 90 mbsf was made and the hole was cleaned in preparation for logging. Hole 830C was cored from 235.0 to 350.6 mbsf for a recovery rate of 16.8% (Table 1).

Two Schlumberger logging combinations were run beginning at a bridge at 272 mbsf. The first was the geophysical combination, consisting of the dual induction tool, the long-spaced sonic tool, the lithodensity tool, and the LDGO temperature tool. The second was the geochemical combination, including the natural gamma-ray spectrometry tool, the aluminum clay tool, the induced gamma-ray spectrometry tool, and the LDGO temperature tool. The caliper curve indicated that the diameter of most of the interval logged was greater than 19 in., the maximum reading possible. Because the hole diameter was so large, no other logs were attempted, and the drill string was recovered.

LITHOSTRATIGRAPHY

Sedimentary Units

Three holes drilled at Site 830 penetrated 351 m of epiclastic sediment and rock. Two lithostratigraphic units have been defined at Site 830 based on grain size, texture, sedimentary

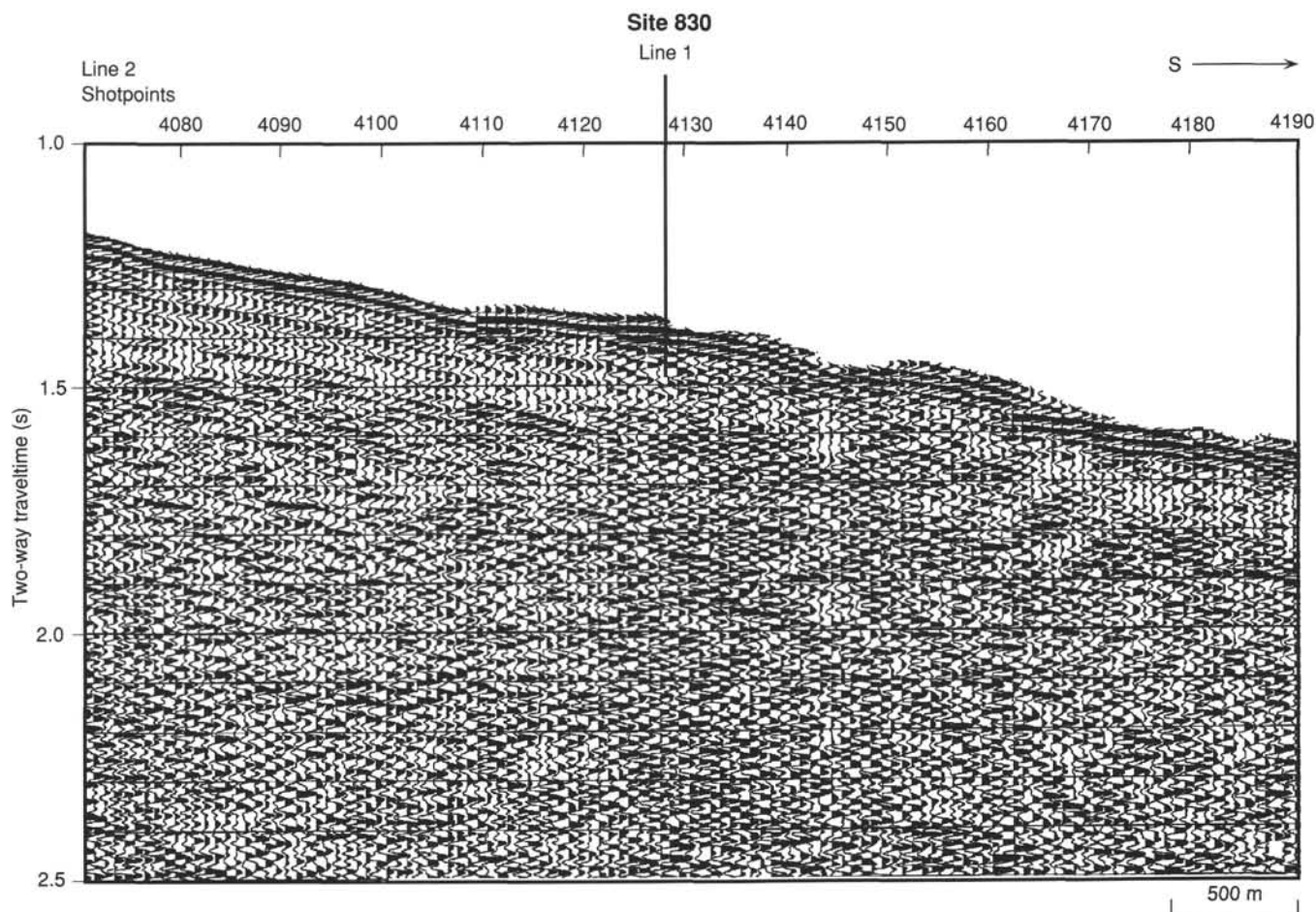


Figure 5. Part of single-channel seismic line 2 that crosses the arc near Site 830. Shipboard processing has not removed all traces of strong noise that affect this seismic section right over the site.

structures, and mineralogy (Fig. 7 and Table 2). Unit I occurs in Holes 830A and 830B; it is broken into three subunits. Unit II occurs in Holes 830B and 830C. Unit I contains Pleistocene fossils; Unit II is barren (see "Biostratigraphy" section, this chapter). The descriptions of the units are presented below hole by hole.

Hole 830A

Unit I

Depth: 0–96.9 mbsf
Interval: Sections 134-830A-1H-1, 0 cm, to 134-830A-11X-1, 34 cm
Thickness: 96.9 m
Age: Pleistocene

Unit I consists of very dark gray (5Y 3/1) volcanic silt and siltstone with varying amounts of sand and clay. Three subunits are defined based primarily on the presence and character of sandy interbeds: Subunit IA is fine-grained, nearly structureless, unlithified volcanic silt. Subunit IB is characterized by clayey sandy silt with numerous normally graded interbeds of black volcanic sand. Subunit IC contains interbedded sandy silts and silty sands in intervals ranging from less than 1 cm to over 50 cm.

Subunit IA

Depth: 0–21.0 mbsf
Interval: Sections 134-830A-1H-1, 0 cm, to 134-830A-3H-3, 150 cm
Thickness: 21 m
Age: Pleistocene

Subunit IA is primarily composed of dark greenish gray (10Y 4/1) volcanic silt with occasional pumice fragments. Ash layers 1 to 5 cm thick with bioturbated upper surfaces occur throughout the subunit. The interval from 0–10 mbsf has a carbonate content above 20% (Fig. 8), as well as intermittent shell fragments and thin layers rich in shell fragments. Below 10 mbsf (Section 134-830A-2H-3, 0 cm), the clay content increases to more than 25%, and normally graded, foraminiferal, sandy interbeds appear. The thickest of these graded beds occurs from 11.15 to 11.85 mbsf (Sections 134-830A-2H-3, 115 cm, to -2H-4, 35 cm); here a 40-cm-thick, dark greenish gray to black (10Y 5/1 to 2.5Y 2/0), sandy unit lies above an olive gray to greenish gray (5Y 5/2 to 10Y 5/1) clayey silt (Fig. 9). This 40-cm-thick sequence appears to represent an oxidized former sediment-water interface overlain by a turbidite. In the bottom 60 cm of the subunit, the frequency of the sandy layers increases, forming a gradational contact with Subunit IB, which is rich in graded beds.

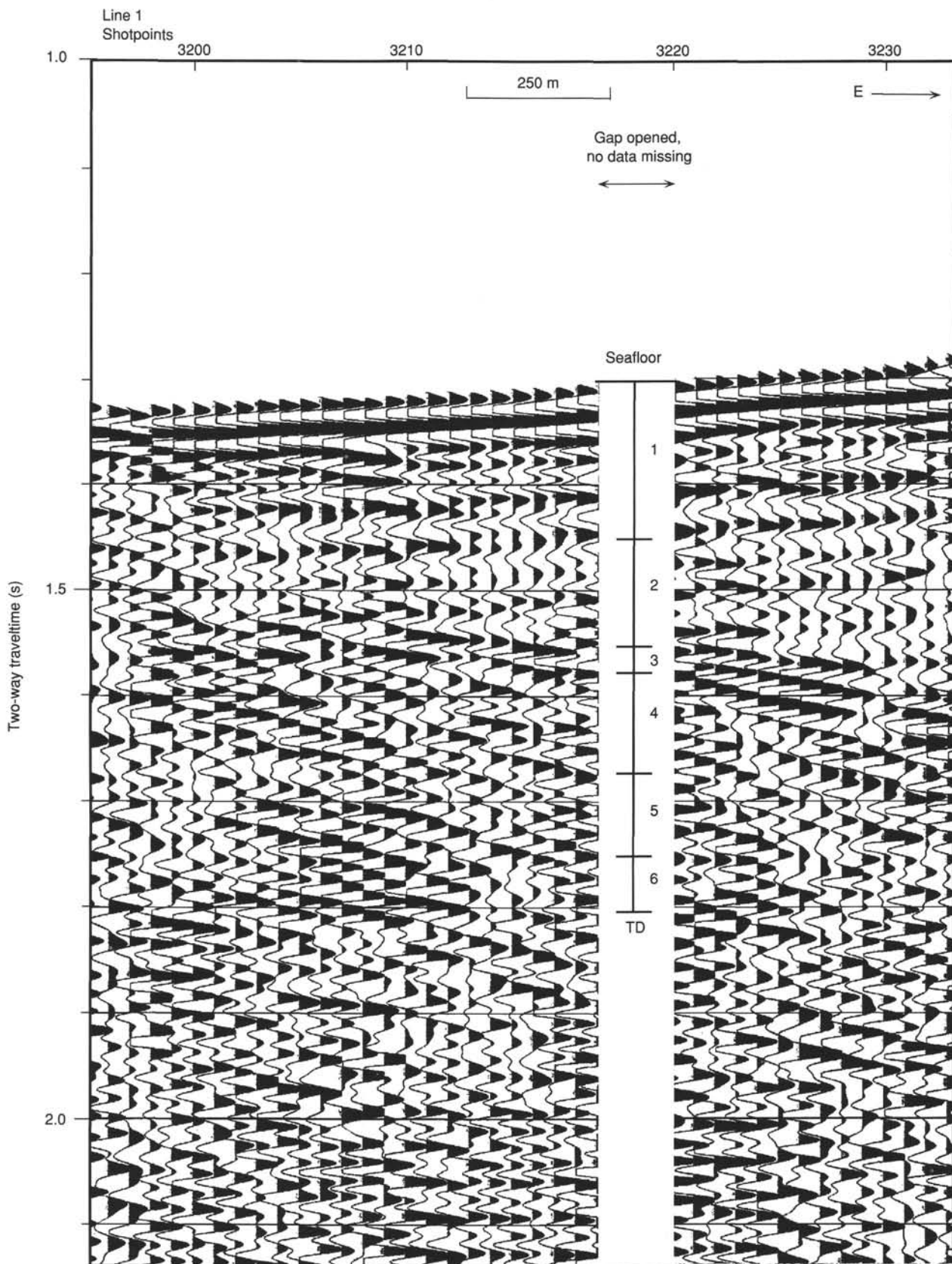


Figure 6. Detailed part of single-channel seismic line 1 that crosses just north of Site 830. Lithostratigraphic units are explained in the "Lithostratigraphy" section (this chapter). Vertically along the line in the gap at the center of the section are numbers that stand for the lithostratigraphic unit. TD = total depth of the hole.

Table 1. Coring summary, Holes 830A, 830B, and 830C.

Core	Date (1990)	Time (UTC)	Depth (mbsf)	Length cored (m)	Length recovered (m)	Recovery (%)	Age
134-830A-							
1H	6 November	0600	0.0–7.0	7.0	6.99	99.8	Pleistocene
2H	6 November	0645	7.0–16.5	9.5	10.09	106.2	Pleistocene
3H	6 November	0715	16.5–26.0	9.5	9.73	102.0	Pleistocene
4H	6 November	0750	26.0–30.4	4.4	4.44	101.0	Pleistocene
5H	6 November	0940	30.4–39.9	9.5	9.93	104.0	Pleistocene
6H	6 November	1030	39.9–48.5	8.6	8.62	100.0	Pleistocene
7X	6 November	1205	48.5–58.2	9.7	1.51	15.5	Pleistocene
8X	6 November	1310	58.2–67.9	9.7	0.43	4.4	
9X	6 November	1530	67.9–77.6	9.7	0.51	5.3	Pleistocene
10X	6 November	1645	77.6–87.3	9.7	1.18	12.1	?Pleistocene
11X	6 November	1800	87.3–96.9	9.6	0.34	3.5	
Coring totals				96.9	53.77	55.5	
134-830B-							
1R	7 November	0340	48.5–58.1	9.6	2.06	21.4	Pleistocene
2R	7 November	0430	58.1–67.7	9.6	2.84	29.6	Pleistocene
3R	7 November	0500	67.7–77.5	9.8	2.10	21.4	Pleistocene
4R	7 November	0540	77.5–87.4	9.9	2.10	21.2	Pleistocene
5R	7 November	0630	87.4–97.1	9.7	3.18	32.8	Pleistocene
6R	7 November	0710	97.1–106.8	9.7	2.21	22.8	Pleistocene
7R	7 November	0825	106.8–116.5	9.7	1.66	17.1	
8R	7 November	0905	116.5–126.2	9.7	2.07	21.3	Pleistocene
9R	7 November	1005	126.2–135.9	9.7	2.23	23.0	Pleistocene
10R	7 November	1115	135.9–145.6	9.7	2.69	27.7	Pleistocene
11R	7 November	1215	145.6–155.3	9.7	6.35	65.4	Pleistocene
12R	7 November	1320	155.3–165.2	9.9	3.10	31.3	Pleistocene
13R	7 November	1420	165.2–174.9	9.7	3.40	35.0	Pleistocene
14R	7 November	1540	174.9–184.6	9.7	0.82	8.5	?
15R	7 November	1845	184.6–194.2	9.6	1.60	16.6	?
16R	7 November	2045	194.2–203.8	9.6	0.00	0.0	
17R	7 November	2300	203.8–213.4	9.6	0.72	7.5	?
18R	8 November	0145	213.4–223.1	9.7	1.71	17.6	?
19R	8 November	0410	223.1–232.9	9.8	1.92	19.6	?
20R	8 November	0630	232.9–242.6	9.7	1.49	15.3	?
21R	8 November	0840	242.6–252.4	9.8	0.78	8.0	?
22R	8 November	1110	252.4–262.2	9.8	1.09	11.1	?
23R	8 November	1525	262.2–272.0	9.8	1.58	16.1	?
24R	8 November	1730	272.0–281.7	9.7	1.07	11.0	?
Coring totals				233.2	48.77	20.9	
134-830C-							
1R	10 November	0715	235.0–244.4	9.4	1.03	10.9	
2R	10 November	1000	244.4–254.1	9.7	1.65	17.0	
3R	10 November	1245	254.1–263.7	9.6	1.34	13.9	
4R	10 November	1500	263.7–273.3	9.6	2.85	29.7	
5R	10 November	1645	273.3–282.9	9.6	0.83	8.6	
6R	10 November	1900	282.9–292.6	9.7	1.65	17.0	
7R	10 November	0205	292.6–302.3	9.7	1.07	11.0	
8R	10 November	2300	302.3–311.9	9.6	2.37	24.7	
9R	11 November	0030	311.9–321.5	9.6	1.32	13.7	
10R	11 November	0315	321.5–331.2	9.7	2.29	23.6	
11R	11 November	1100	331.2–340.9	9.7	1.09	11.2	
12R	11 November	1400	340.9–350.6	9.7	1.91	19.7	
Coring totals				115.6	19.40	16.8	

Subunit IB

Depth: 21.0–47.0 mbsf
Interval: Sections 134-830A-3H-3, 150 cm, to 134-830A-6H-5, 110 cm
Thickness: 26.0 m
Age: Pleistocene

Subunit IB consists primarily of graded beds, 1–16 cm thick, with sharply defined bases of black (5Y 2.5/1) volcanic sand fining upward to very dark gray (5Y 3/1) clayey sandy volcanic silt (Fig. 10). A sharp increase in volcanogenic mineral content, notably plagioclase, clinopyroxene, and opaque minerals such as magnetite and hematite, and a slight decrease in carbonate mark the boundary of the unit (Fig. 8). Apparent dips of the beds range from subhorizontal to about

35°. The beds are offset and truncated in about five places in the sequence, but it is difficult to know whether the deformation results from drilling, microfaulting, or slumping. Silt intervals and the tops of sand layers in graded sequences appear bioturbated (Fig. 10).

The subunit is broken by intervals, 2.9–5.25 m thick, of soupy, black (5Y 2.5/1) volcanic sand (23–25.9, 34.3–39.5, and 41.75–47.0 mbsf; Sections 134-830A-3H-5, 45 cm, to -3H-7, 55 cm, Sections 134-830A-5H-3, 95 cm, to -5H-7, 57 cm, and Sections 134-830A-6H-2, 35 cm, to -6H-5, 110 cm). These, along with a 65-cm layer of sandy clayey silt at the top of Core 134-830A-5H (30.6–31.25 mbsf), are highly disturbed by drilling, so that any previously existing bedding has been obliterated.

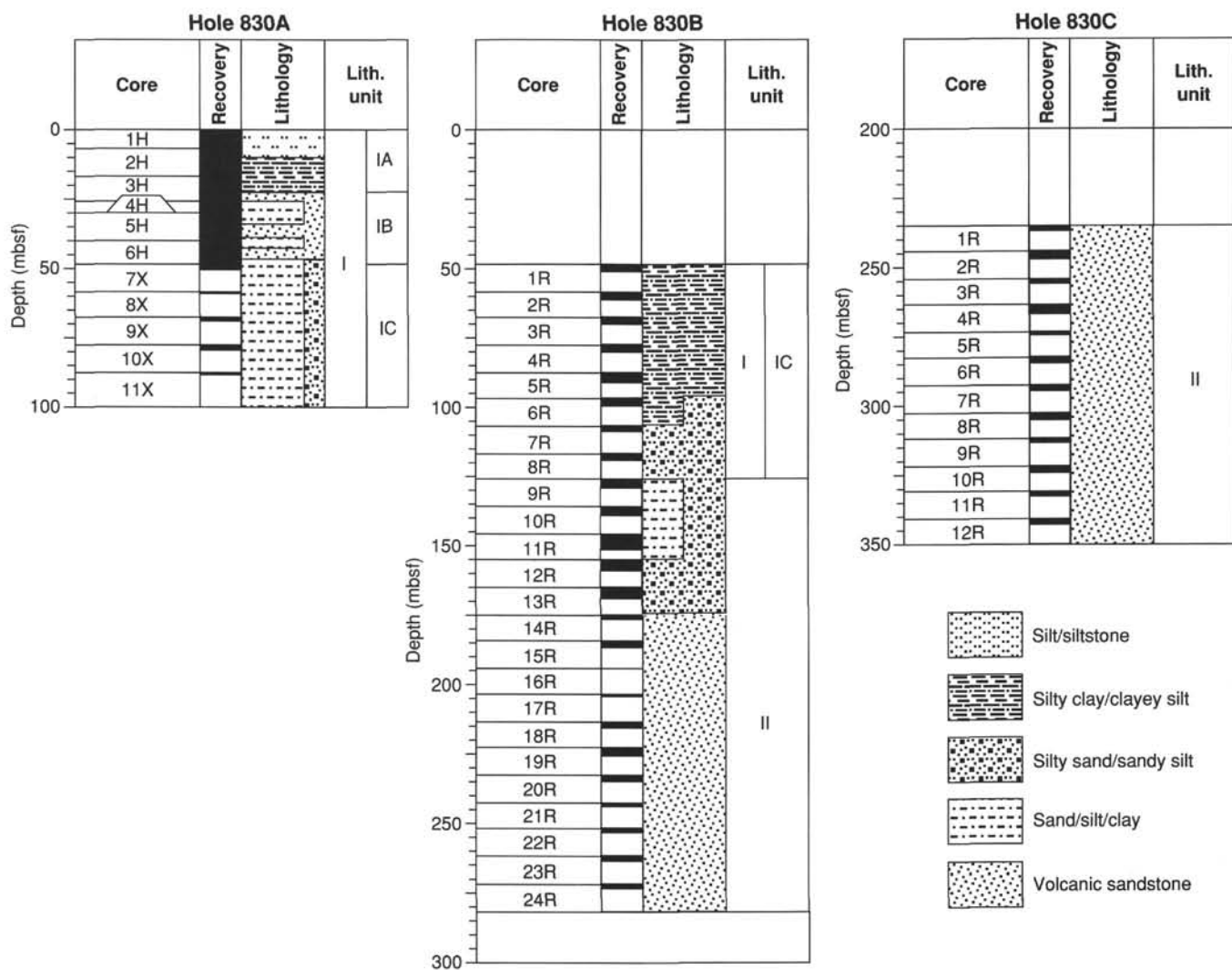


Figure 7. Lithostratigraphy of Site 830.

Table 2. Lithostratigraphic units, Site 830.

Interval	Unit	Subunit	Depth (mbsf)	Thickness (m)	Age
Sections 134-830A-1H-1, 0 cm, to 134-830A-11X-1, 34 cm	I		0–96.9	96.9	Pleistocene
Sections 134-830A-1H-1, 0 cm, to 134-830A-3H-3, 150 cm		IA	0–21.0	21.0	Pleistocene
Sections 134-830A-3H-4, 0 cm, to 134-830A-6H-5, 110 cm		IB	21.0–47.0	26.0	Pleistocene
Sections 134-830A-6H-5, 110 cm, to 134-830A-11X-1, 34 cm		IC	47.0–96.9	49.9	Pleistocene
Sections 134-830B-1R-1, 0 cm, to 134-830B-14R-1, 0 cm	I	IC	48.5–174.9	126.4	Pleistocene
Sections 134-830B-14R-1, 0 cm, to 134-830B-24R-CC, 15 cm	II		174.9–281.7	106.8	Unknown (barren)
Sections 134-830C-1R-1, 0 cm, to 134-830C-12R-CC, 14 cm	II		235.0–350.6	115.6	Unknown (barren)

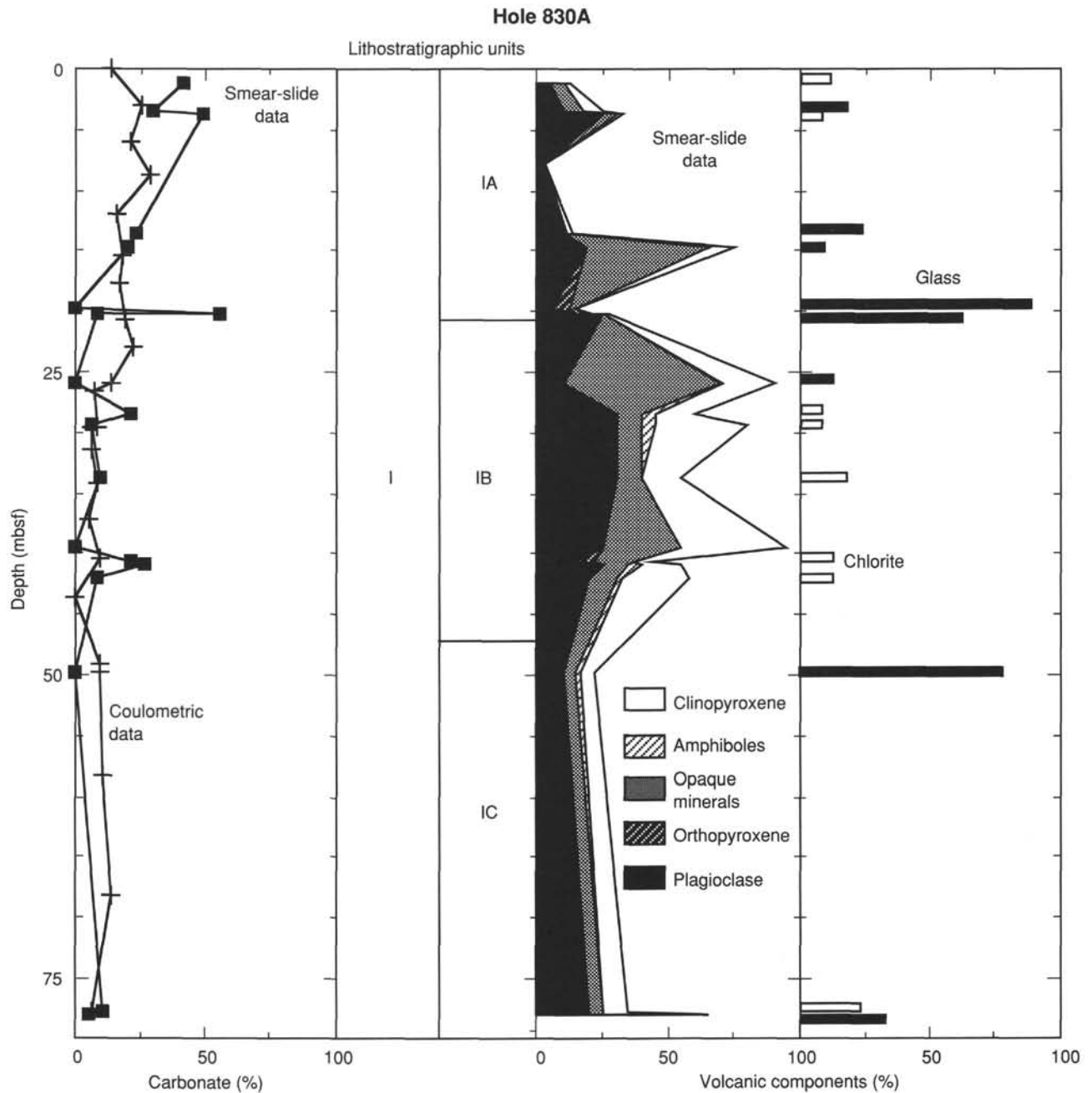


Figure 8. Variation in carbonate content and volcanic components with depth in Holes 830A and 830B. Carbonate content was determined both by coulometric and smear-slide analyses; volcanic component was determined by smear-slide analysis.

Subunit IC

Depth: 47.0–96.9 mbsf
 Interval: Sections 134-830A-6H-5, 110 cm, to 134-830A-11X-1, 34 cm
 Thickness: 49.9 m
 Age: Pleistocene

Subunit IC consists of very dark gray (5Y 3/1) beds of clayey sandy volcanic silt interbedded with layers of silty volcanic sand, 2 to 12 cm thick. No evidence of bioturbation is present. The beds have sharp bases and are approximately horizontal. These sequences appear to be normally graded, though the grading is often difficult to distinguish. They differ from the graded beds in Subunit IB in mineralogy,

color, and texture: the basal sands are much siltier and are gray in color, and the percentage of clinopyroxene and opaque mineral grains drops significantly from the overlying subunit (Fig. 8).

Hole 830B

Hole 830B was washed to a depth of 48.5 mbsf, then cored to 281.7 mbsf. The 233.2-m interval produced 48.77 m of recovered sediment, which was divided into two units. The upper unit consists of volcanic silts that correlate to Subunit IC in Hole 830A; the lower unit is a poorly sorted sandstone, classified as Unit II with similar rocks recovered in Hole 830C.

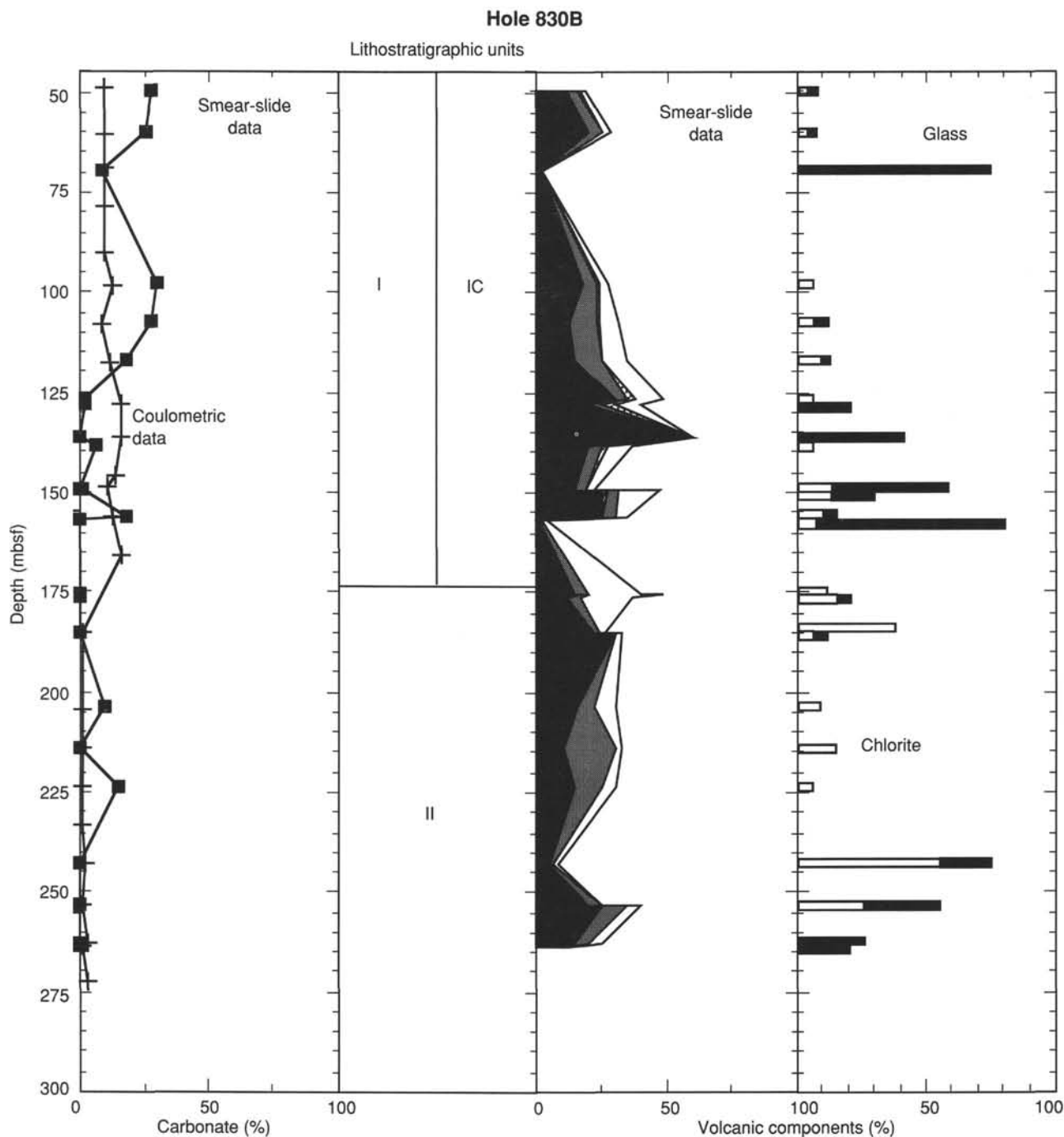


Figure 8 (continued).

Unit I**Subunit IC**

Depth: 48.5–174.9 mbsf
Interval: Sections 134-830B-1R-1, 0 cm, to 134-830B-14R-1, 0 cm
Thickness: 126.4 m
Age: Pleistocene

Subunit IC in Hole 830B consists of 126.4 m of very dark gray (5Y 3/1) clayey and sandy volcanic silts, becoming more lithified with depth so that it is classified as partially lithified

siltstone at approximately 97.1 mbsf (Core 134-830B-6R). The upper part of the subunit, approximately 48.5–99.0 mbsf (Cores 134-830B-1R through -6R), is characterized by thin (1–2 cm), laminated sandy layers and occasional lenses of gray (N5) clays and volcanic sand.

Below about 97.1 mbsf (the top of Section 134-830-6R-1), the sand content of the siltstone increases, and evidence of bioturbation (trace fossils and structureless beds) increases. Interbeds of silty sands and sandy silts with poorly defined normal grading begin in Core 134-830B-10R (about 136 mbsf) and continue to the bottom of the subunit.

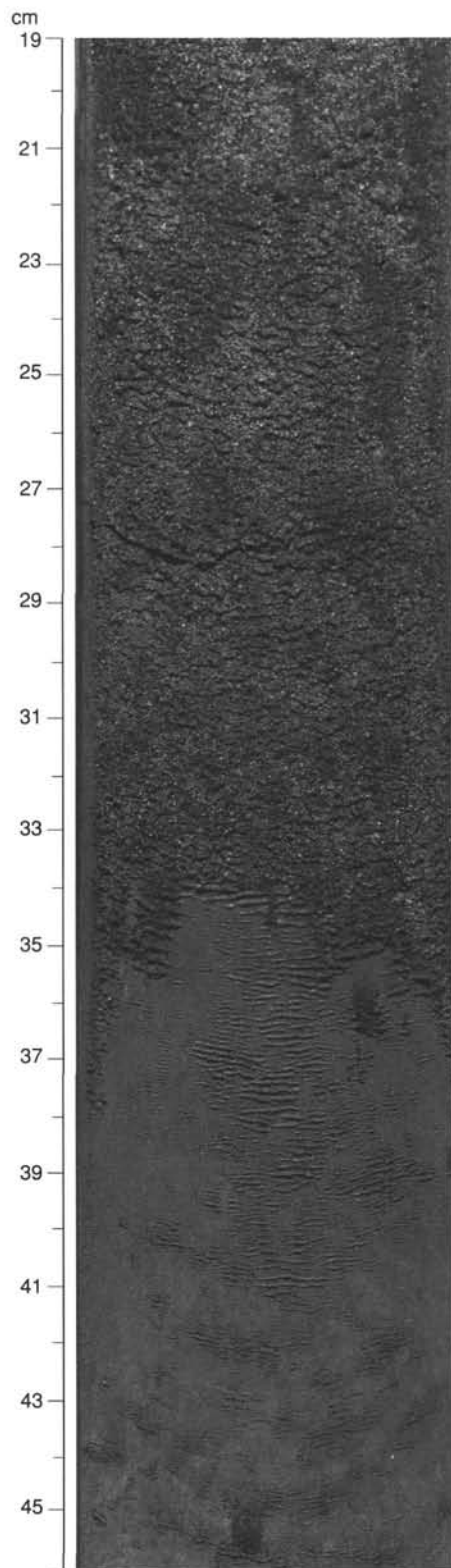


Figure 9. Photograph of interval 134-830A-2H-4, 19–46 cm, showing sharp contact between silty sand overlying clayey silt that grades in color from olive gray to greenish gray. The sequence is interpreted as an oxidized former sediment-water interface overlain by a turbidite deposit.

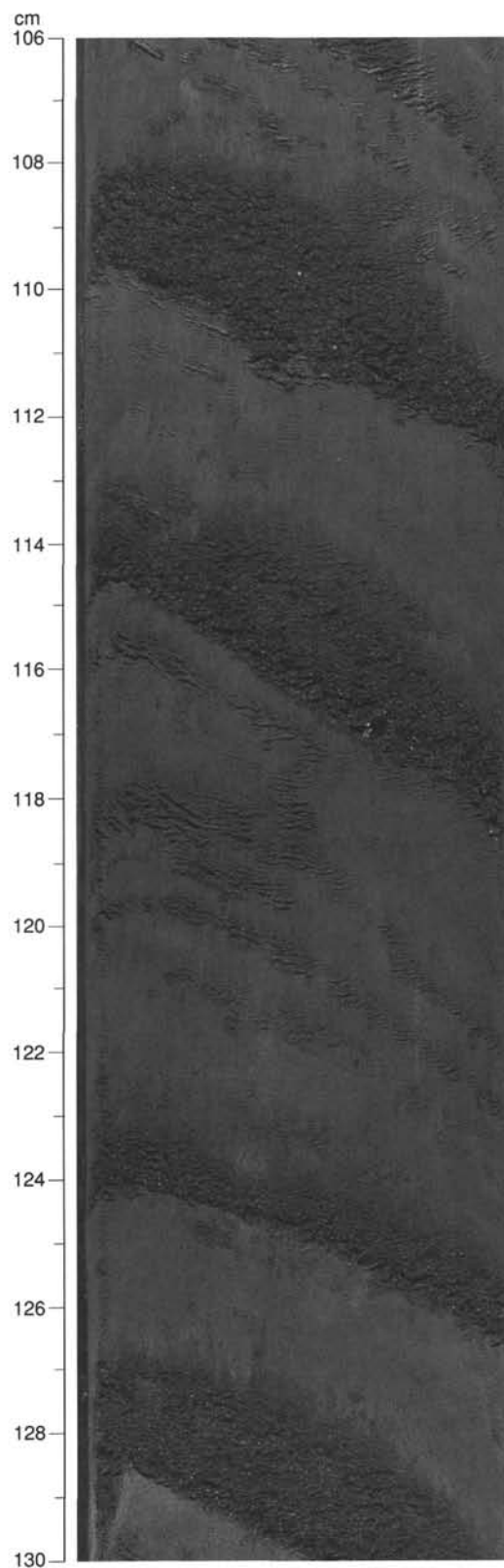


Figure 10. Photograph of interval 134-830A-3H-4, 106–130 cm, showing repeated sequences of volcanic sand fining upward to volcanic clayey silt of Subunit IB. Effects of bioturbation are evident in smeared, upper surfaces of sand layers and near-oblivation of thin sand horizons at 117–120 cm.

Unit II

Depth: 174.9–281.7 mbsf
 Interval: Sections 134-830B-14R-1, 0 cm, to 134-830B-24R-CC, 15 cm
 Thickness: 106.8 m
 Age: Indeterminate (barren)

In Hole 830B, the contact between Units I and II is marked by the occurrence of several pieces of basalt, ig-lithic breccia, and volcanic sandstone without retained matrix. Unit II consists of 106.8 m of partially lithified, very poorly sorted, very coarse, silty volcanic sed-lithic sandstone. Sand grains throughout the unit are composed of black, well-lithified volcanic siltstone; many of the grains range up to granule size (Fig. 11). The sands reside in a matrix of sandy chloritic silt. Both clasts and matrix are altered, and the unit has been deformed by tectonic brecciation (see “Structural Studies” section, this chapter). Pebbles up to 5 cm in diameter of volcanic rock, fine-grained, well-lithified volcanic sandstones, and sed-lithic breccias occur sporadically in the unit. These clasts sometimes occur in layers up to 50 cm thick of sed-lithic conglomerate and breccia.

The unit has a colorful appearance, with 1-m sequences consisting of intervals (0.2–7 cm thick) of silty sandstone in varying shades of grayish green to greenish gray, reddish black clayey silts, white zeolite veins, gray clay laminae, and black volcanic sand lenses (Fig. 11). These sections alternate with thick (up to 60 cm) layers of dark gray, volcanic sed-lithic sandstone similar in composition and texture to the green sandstones.

Hole 830C

Hole 830C was washed to a depth of 235 mbsf and cored 115.6 m to a depth of 350.6 mbsf, recovering 19.4 m of volcanic sed-lithic sandstone. We grouped this sandstone into Unit II with similar rocks from Hole 830B.

Unit II

Depth: 235.0–350.6 mbsf
 Interval: Sections 134-830C-1R-1, 0 cm, to 134-830C-12R-CC, 14 cm
 Thickness: 115.6 m
 Age: Indeterminate (barren)

In Hole 830C, Unit II consists of 115.6 m of partially lithified, very poorly sorted, very coarse, volcanic sed-lithic sandstone. The sand grains throughout the unit are composed of black, well-lithified volcanic siltstone; many of the grains range up to granule size. The color, degree of lithification, grain size, and distribution of sand grains in this unit at this hole are the same as described in Unit II at Hole 830B. Pebbles of volcanic rocks and fine-grained, well-lithified volcanic sandstones up to 5 cm in diameter occur sporadically throughout the unit, sometimes isolated and sometimes in horizons of sed-lithic conglomerate or breccia up to 40 cm thick. Mineralogy, colors, texture, and structure are essentially the same as Unit II in Hole 830B.

BIOSTRATIGRAPHY**Calcareous Nannofossils**

Samples 134-830A-1H-CC and 134-830A-2H-4, 150–151 cm, contain the youngest assemblage found at Site 830. The presence of *Emiliana huxleyi* in association with *Gephyrocapsa oceanica*, *G. caribbeanica*, *Calcidiscus leptoporus*, *Ceratolithus telesmus*, *Rhabdosphaera claviger*, and *Helicosphaera kamptneri* places these samples in Zone CN15 (Fig. 12). A moderate degree of reworking of Miocene material is

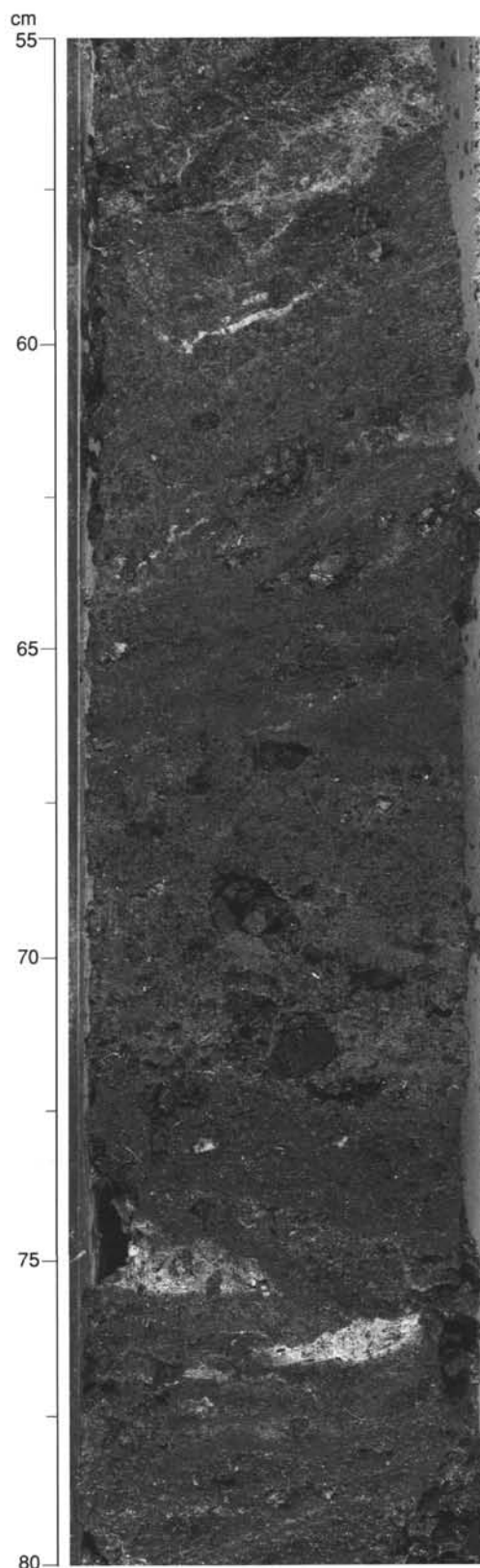


Figure 11. Photograph of interval 134-830B-18R-1, 55–80 cm, showing the sedimentary fabric that characterizes Unit II. White veins are zeolites. The coarse sandstones and silts in this interval include a thick layer of greenish gray silty sandstone (67–71.5 cm), and lenses of red, gray, white, and grayish green sandy siltstone.

Depth (mbsf)	Core	Recovery	Nannofossil zone	Planktonic foraminifer N-zone	Benthic foraminifers		Age
					Assemblage	Paleodepth	
0	1H		CN15	N22	I	Middle bathyal	Pleistocene
10	2H						
20	3H		Barren		Indeterminate		
30	4H						
40	5H		II		Lower bathyal		
50	6H		CN14		Barren	Indeterminate	
60	7X						
70	8X						
80	9X		Barren				
90	10X						
100	11X						

Figure 12. Biostratigraphic summary of Hole 830A.

indicated by the presence of *Discoaster pentaradiatus*, *Cyclogolithus floridanus*, *C. abisectus*, and *Discoaster brouweri*.

Samples 134-830A-2H-CC through 134-830A-8X-CC contain an assemblage typified by *G. oceanica*, *G. caribbeanica*, *H. kamptneri*, and *R. claviger* and have thus been placed within Zone CN14. This assemblage is also contained in Sections 134-830B-1R-CC through 134-830B-13R-CC of Hole 830B (Fig. 13). The reworking of Miocene and Pliocene nannofossils is variable in these samples.

Most samples taken at Site 830 were barren. All samples from below Section 134-830B-13R-CC were devoid of nannofossils, as were all samples from Hole 830C.

Planktonic Foraminifers

A rich assemblage of planktonic foraminifers from Hole 830A (Samples 134-830A-1H-CC to -11X-CC) and the upper 174.9 mbsf of Hole 830B (Samples 134-830B-1R-CC to -13R-CC) was recovered from core-catcher samples. Assignment of these sequences to the Pleistocene (Zone N22) is based on the

presence of *Globorotalia truncatulinoides*. The planktonic foraminiferal assemblage includes *Globorotalia menardii*, *G. tosaensis*, *G. unguolata*, *G. inflata*, *G. tumida*, *G. tumida flexuosa*, *G. crassaformis*, *Globigerina rubescens*, *G. bulloides*, *Globigerinita glutinata*, *Globigerinella aequilateralis*, *Globigerinoides sacculifer*, *G. ruber*, *G. conglobatus*, *G. immaturus*, *Candeina nitida*, *Neogloboquarina dutertrei*, *Pulleniatina obliquiloculata*, and *Sphaeroidinella dehiscens*.

Reworking of late Pliocene fauna is recognized throughout the Pleistocene succession. This is evidenced by the occurrence of *Sphaeroidinellopsis seminulina*, *S. kochi*, *Pulleniatina primalis* (dextral), and *Globigerinoides extremus*. Samples from Section 134-830B-14R-CC to -24R-CC and from Section 134-830C-1R-CC to -12R-CC are composed predominantly of volcanic clasts with no microfossils.

Benthic Foraminifers

Benthic foraminifers were studied from core-catcher samples taken from Holes 830A, 830B, and 830C. Hole 830A

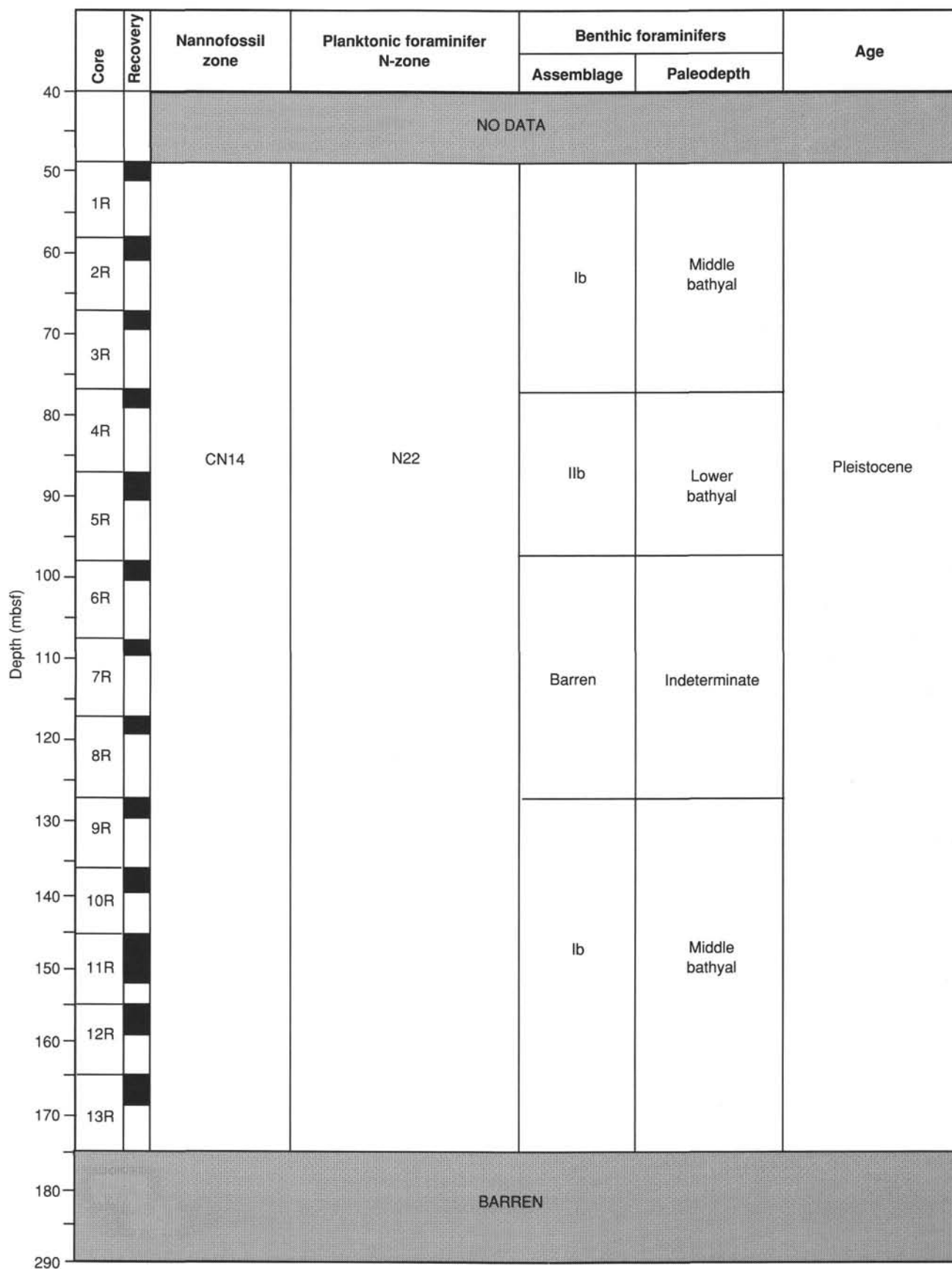


Figure 13. Biostratigraphic summary of Hole 830B.

contained well-preserved benthic foraminifers that varied in abundance from common to rare. Hole 830B contained rare, moderately preserved specimens. All of the samples in Hole 830C were barren as were the following samples in Holes 830A and 830B: Samples 134-830A-3H-CC, 134-830A-4H-CC, 134-830A-6X-CC through 134-830A-11X-CC, 134-830B-6R-CC through 134-830B-8R-CC, and 134-830B-14R-CC through 134-830B-24R-CC.

Hole 830A

The assemblages in Samples 134-830A-1H-CC and 134-830A-2H-CC are typified by *Cibicides aknerianus*, *Bulimina striata*, *Cibicides wuellerstorfi*, *Pullenia bulloides*, and *Uvigerina proboscidea*. The presence of *Cibicides wuellerstorfi* suggests that the sediments in this interval were deposited in the lower part of the middle bathyal zone.

Sample 134-830A-5H-CC contains an assemblage typified by *Bulimina striata*, *Cibicides aknerianus*, *Melonis sphaeroides*, *Melonis barleeanus*, and *Uvigerina hispidocostata*. The presence of *M. barleeanus* and *M. sphaeroides* suggests that the sediments from this interval were deposited in the lower bathyal zone.

The presence of *Bulimina striata* in Samples 134-830A-1H-CC, 134-830A-2H-CC, and 134-830A-5H-CC may indicate the presence of methane in the sediments at the time of deposition as suggested by Akimoto et al. (1990). Additional analyses must be undertaken in order to assess the quantity of *Bulimina striata* in the samples and to investigate the possible existence of additional methanophiles such as *Rutherfordoides* sp. A.

Hole 830B

Samples 134-830B-1R-CC to 134-830B-3R-CC and 134-830B-9R-CC to 134-830B-13R-CC contain an assemblage typified by the presence of *Bulimina aculeata*, *Cassidulina carinata*, *Cibicides aknerianus*, *C. wuellerstorfi*, *Uvigerina hispidocostata*, and *Uvigerina proboscidea*. This assemblage indicates that the sediments from these intervals were deposited in the lower part of the middle bathyal zone.

Samples 134-830B-4R-CC and 134-830B-5R-CC contain assemblages including *Cibicides wuellerstorfi*, *Melonis barleeanus*, *Melonis pacificus*, *Pyrgo murrhina*, and *Uvigerina hispidocostata*. The presence of the paleobathymetric indicators *Melonis barleeanus* and *Melonis pacificus* suggests that the sediments within this interval were deposited in lower bathyal depths.

As in Hole 830A, the presence of *Bulimina striata* in Samples 134-830B-3R-CC, 134-830B-5R-CC, 134-830B-9R-CC, and 134-830B-10R-CC suggests that the sediments in these samples were possibly methane-bearing at the time of deposition. Post-cruise investigations into the abundances of these methane-associated foraminifers will be necessary in order to reach conclusions regarding their paleoecologic significance at this site.

Radiolarians

The only radiolarians in the 40 samples examined from this site are very rare fragments found in Core 134-830A-1H.

IGNEOUS PETROLOGY

Only a few igneous rocks were encountered at Site 830, occurring as clasts in a very poorly sorted, very coarse-grained volcanoclastic sandstone with a sandy silt matrix. They are found at the top of lithostratigraphic Unit II, between 174.9 and 184.6 mbsf, Hole 830B (Core 134-830B-14R). Additional isolated pebbles were also recovered from deeper in Hole 830B, between 252.4 and 262.2 mbsf (Core

134-830B-22R) and in Hole 830C between 235.0 and 263.7 mbsf (Cores 134-830C-1R, -2R, and -3R; see "Lithostratigraphy" section, this chapter).

Although they share similar mineralogy and appear to be closely related, the clasts can be divided into two types:

Group A: Lavas (Sample 134-830B-14R-1, 12–17 cm, piece 3; Sample 134-830B-22R-1, 39–40 cm; Sample 134-830C-3R-1, 1–2 cm; and Sample 134-830C-3R-CC, 16–18 cm);

Group B: Volcanic breccia (Sample 134-830B-14R-1, 47–56 cm, piece 8; Sample 134-830B-14R-1, 57–61 cm, piece 9; Sample 134-830C-1R-1, 49–52 cm; and Sample 134-830C-3R-1, 61–65 cm).

Lavas

These rocks vary in modal composition from moderately olivine-clinopyroxene-phyric basalt to highly plagioclase-phyric basalt or basaltic andesite, the latter type being the more common. Fresh olivine is never found and pseudomorphs of serpentine and calcite indicating the presence of previous olivine phenocrysts are relatively rare. Clinopyroxene of augitic composition is found either as phenocrysts (3%–8% by volume) or in the groundmass, showing a variable shape from euhedral to subhedral. In Sample 134-830C-3R-1, 16–18 cm, clinopyroxenes show glomeroporphyritic texture, with several crystals clustered together. Clinopyroxene phenocrysts range in diameter from 0.2–2 mm and groundmass grains are <0.2 mm. The crystals show variable degrees of alteration, being replaced by chlorite and calcite. Plagioclase, which is normally euhedral, is the most common mineral phase in the rocks, being widely represented either as phenocrysts (0.1–3 mm in size) or in the groundmass (0.1–0.5 mm in size). It is clouded by inclusions, which can comprise up to 10%–15% of the crystal volume: they are preferentially oriented along the cleavage direction and appear to be completely altered to chlorite. The plagioclase itself is often altered, being replaced to a variable extent by calcite, sericite, and clay minerals. When plagioclase is well preserved, its composition can be estimated using albite twinning. The usual phenocryst composition is between An₅₅ and An₆₅ and groundmass grains are between An₃₀ and An₄₀. Some crystals show reverse zoning. Opaque minerals, ranging in size from 0.01 to 1 mm, are present in the lavas, mainly in the groundmass. Tiny, elongate crystals of ilmenite are fairly abundant in Sample 134-830B-22R-1, 39–40 cm.

The groundmass is either glassy or may contain variable amounts of plagioclase, clinopyroxene, and opaque minerals (in decreasing order of abundance). Glass is almost always altered to chlorite and clay minerals. Intersertal and fluidal textures are common. Vesicles, which are filled with chlorite, calcite, and zeolites, can amount to as much as 20% of the total volume of the rock. Some cavities contain calcite lined with chlorite. Calcite and zeolites are common in veins (0.1–0.2 mm).

Volcanic Breccias

This rock type is composed of fragments, mainly of volcanic origin and crystals. In some clasts, rock fragments predominate, whereas in others, crystals are more abundant. The rock fragments consist of variably altered basalts, ranging from aphyric to highly plagioclase-phyric basalts. Plagioclase crystals range in size from 2 to 5 mm, and comprise up to 30% of the volume of some fragments. Although the compositional variation of the volcanic clasts is wider than that described for the lavas of the first group, the relative mineral abundances and textural relationships are very similar. Thus, the petrographic description of the volcanic fragments is not repeated

here. Fragments are rounded to subrounded and sometimes do not show a clear, sharp boundary, but seem to pass gradually into the more homogeneous volcanic groundmass, in such a way that it is difficult to distinguish the clast from its matrix. Some fragments are lobate or irregular in shape and partially engulf isolated crystals. One fragment of a partially recrystallized calcareous mudstone and two of fine-grained gabbro were also found in Section 134-830C-3R-1.

Isolated crystals in these volcanic breccias are mainly clinopyroxene and plagioclase, and rarely olivine and amphibole. Single mineral fragments, subangular to angular in shape, are often highly fractured, and, more rarely, deformed. The grain size of the crystals is <2 mm and they are apparently similar in composition to phases in the associated lava fragments and in the clasts of group A.

The matrix of these breccias consists of fine-grained volcanic material with small laths of plagioclase, opaque minerals, and clay minerals that are interpreted as the alteration products of glass. Patches of a highly oxidized reddish volcanic matrix are also observed.

Although chemical analyses have not been carried out on this material, the modal assemblages and textural features indicate a similar origin for the clasts of lavas (group A) and volcanic breccias (group B). The great variety of lavas in the breccias, the shapes of the fragments, and their relationships with the groundmass and the isolated crystals suggest that the clastic material is the product of an explosive event, perhaps one that occurred during the formation of nearby Espiritu Santo Island or Malakula Island, in early to middle Miocene time. Lavas and breccias are probably derived from reworking of a volcanoclastic formation of the same islands.

IGNEOUS GEOCHEMISTRY

Major and several trace elements (Nb, Zr, Y, Sr, Rb, Zn, Cu, Ni, Cr, and V) for three basalt samples and one volcanic sand sample recovered from Holes 830B and 830C were analyzed aboard ship by X-ray fluorescence (see "Explanatory Notes" chapter, this volume). The coarse volcanic sand analyzed occurs in lithostratigraphic Unit IB (silt interbedded with sand), whereas the basalt samples occur as clasts in a poorly lithified volcanic and lithic sandstone of lithostratigraphic Unit II (see "Lithostratigraphy" section, this chapter), and were described as "lavas" (see "Igneous Petrology" section, this chapter). The three samples of basalt analyzed (Samples 134-830B-22R-1, 32–33 cm, 134-830C-2R-1, 6–8 cm, and 134-830C-3R-1, 3–4 cm) were larger than pebble size and homogenous in hand specimen. These samples are also moderately to highly altered and are unlikely to retain their original compositions.

Sample 134-830A-3H-7, 36–38 cm, a volcanic sand, was sieved to separate grains from 38 to 63 μm in diameter. The separated coarse fraction was then put into a 1-N HCl solution to remove carbonates. The residue contained 25% plagioclase, 15% clinopyroxene, 5% magnetite, and 55% rock fragments or grains containing microcrystalline minerals. The last component shows variable colors of white, pale green, green, orange red, and gray, probably reflecting different degrees of oxidation and alteration. The material may represent reworked volcanic ash, volcanoclastic sediment, or a mixture of the two, hence the use of the term volcanic sand.

Lavas

Analytical results are listed in Table 3. The analyzed lavas are all basalts with a narrow silica range between 49.3 and 50.8 weight percent (wt%). MgO contents are relatively low (4.58 to 6.67 wt%) despite the low silica contents, indicating that they are moderately fractionated. Ni and Cr contents are in

Table 3. Major and trace element analyses of volcanic rocks from Site 830.

Hole	830A	830B	830C	830C		
Core, section	3H-7	22R-1	2R-1	3R-1	Espiritu	Malakula
Interval (cm)	36–38	32–33	6–8	3–4	Santo	Island
Depth (mbsf)	25.86	252.72	244.46	254.13	SR75	ML656
Major elements (wt%)						
SiO ₂	60.42	49.29	50.35	50.78	49.93	49.98
TiO ₂	0.83	1.32	1.46	1.18	0.93	1.19
Al ₂ O ₃	15.51	18.22	18.34	16.07	16.90	19.95
Fe ₂ O ₃ (t)	6.08	10.62	10.24	10.93	10.80	10.90
MnO	0.14	0.21	0.24	0.31	0.14	0.33
MgO	3.28	4.58	5.15	6.67	4.19	4.36
CaO	8.85	11.47	9.36	10.84	8.08	9.91
Na ₂ O	3.22	2.99	3.29	2.23	4.15	3.00
K ₂ O	0.86	0.60	0.41	0.45	0.85	0.51
P ₂ O ₅	0.02	0.26	0.27	0.22	0.21	0.10
Total	99.20	99.54	99.10	99.65	96.18	100.23
LOI	2.29	4.41	3.51	7.07	4.26	3.32
Trace elements (ppm)						
Nb	3	6	4	3		
Zr	108	141	169	112		
Y	13	27	38	24		
Sr	340	361	244	347		
Rb	12	7	5	7		
Zn	14	71	101	73		
Cu	20	130	53	93		
Ni	14	30	25	50		
Cr	114	25	8	113		
V	163	281	238	310		
Ce	10	25	17	17		
Ba	254	184	274	153		

Note: Sample 134-830A-3H-7, 36–38 cm, is the "volcanic sand." Examples from Espiritu Santo Island and Malakula Island are also listed for comparison. The analysis of the Espiritu Santo Island lava is from Mallick and Greenbaum (1977); that of the Malakula Island lava is from Gorton (1974). Fe₂O₃(t) = total iron as Fe₂O₃; LOI = loss on ignition. For SR75, LOI refers to the sum of H₂O⁺ and H₂O⁻.

the ranges of 25–50 parts per million (ppm) and 8–113 ppm, respectively, also indicating moderate fractionation. However, since these samples are fairly altered, their MgO contents probably do not represent the original values. The petrological observation that some of the olivines are replaced by calcite indicates a loss of MgO. The altered nature of the basalt samples is also shown by high loss on ignition (LOI) values of 3.51–7.07 wt%. Another characteristic of these lavas is their high aluminum content (16.07–18.34 wt%), which was not the case for igneous rocks from Sites 828 and 829. The high aluminum contents are associated with high modal plagioclase, although contents of Sr (244–361 ppm) and Ba (153–274 ppm) are not unusually high. The alkali contents of these lavas fall in the subalkalic field of the total alkali vs. silica diagram, but close to the boundary with the alkalic fields (Fig. 14). This is consistent with their relatively low potassium content (0.41–0.60 wt%). However, again, these contents are unlikely to represent the original values due to alteration.

For altered rocks like these, high field strength (HFS) elements such as Zr are better indices of fractionation. If we plot oxides or elements, such as TiO₂, Rb, Ba, and Y, against Zr for these three samples, they lie on trends indicative of some fractionation processes (Fig. 15). However, this is not the case with several major elements whose concentrations have probably been modified by alteration. It seems likely that the three basalts are differentiation products of a similar parental magma.

Trace element patterns normalized for mid-ocean ridge basalt (MORB) (Pearce, 1982) are similar for the three basalts (Fig. 16). All three have slightly negative Nb anomalies that are characteristic of island-arc patterns. They all have dis-

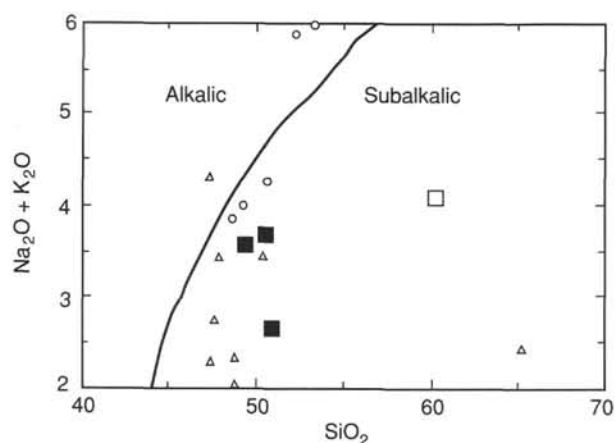


Figure 14. SiO_2 vs. $\text{Na}_2\text{O} + \text{K}_2\text{O}$ diagram for samples from Site 830 (basalts = solid squares, volcanic sand = open square), Site 829 (triangles), and Site 828 (circles). The boundary between alkalic and sub-alkalic magma series is from Miyashiro (1978). (Note that some of the samples from Sites 828 and 830 are highly altered.)

tinctly high peaks at Ba and a gently falling slope from Ce to Ti. Such trends are not observed among basaltic samples from Sites 828 and 829. In Figure 16C, representative patterns for basalts from Sites 828 and 829 (Samples 134-828A-15N-1, 23–25 cm; 134-828A-15N-2, 62–63 cm; and 134-829A-43R-3, 94–96 cm) are also shown for comparison. The samples from Sites 828 and 829 have been interpreted as transitional between MORB and island-arc tholeiite (IAT) (see “Igneous Geochemistry” chapters for Sites 828 and 829, this volume). The patterns for basalts from Site 830 are unlike MORB, but resemble those of arc basalts. They differ from IAT mainly in their higher concentrations of most of the incompatible elements. In fact, most elements, especially large ion lithophile (LIL) elements and Zr, plot above those of IAT and island-arc calc-alkaline basalts (IACA) in this diagram. However, their characteristics are generally intermediate between IAT and IACA. The only feature of basalts from Site 830 that is characteristic of IAT is the relatively low peak at Ce. These basalts are also moderately differentiated and plagioclase accumulation might have played a role in producing the present compositional characteristics.

The patterns for basalts from Site 830 resemble those from Aoba, Ambrym, and Epi volcanoes of the Central Chain of the New Hebrides Island Arc in that they exhibit a Ba peak. For Aoba, Ambrym, and Epi islands, the analyses with similar major element chemistry to those of Site 830 were selected. The difference is that the latter have more distinct peaks at Ce and P, which are characteristic of calc-alkaline basalts. At present, we do not have trace element data from the Central Chain volcanic islands that show similar MORB-normalized patterns to those from Site 830. The geographic location of Site 830 indicates that the southern part of Espiritu Santo Island and the northern part of Malakula Island are the most likely sources for these basalts. Both Robinson (1969) and Mallick and Greenbaum (1977) reported the occurrence of highly plagioclase-phyric basalts from Espiritu Santo Island. Similar highly plagioclase-phyric basalts also occur in Malakula Island, although intrusive rocks are more abundant (Mitchell, 1966, 1971; Gorton, 1974; Macfarlane and Carney, 1987). Their phenocryst assemblage includes plagioclase (15%–30%), clinopyroxene (0%–5%), and olivine (0%–2%), and thus these island rocks are comparable to volcanic clasts recovered from Site 830. Their major element chemistry, listed in Table 3, is also similar to samples from Site 830. They

show high aluminum contents and relatively low MgO contents for the low SiO_2 concentrations. Even with the limited geochemical data available at present, we conclude that these basaltic clasts were derived from the southern part of Espiritu Santo Island or from the northern part of Malakula Island.

Volcanic Sand

Apart from a very low P content, the MORB-normalized pattern for the volcanic sand is strikingly similar to that of the basalts analyzed from this site. Low P may result from an underrepresentation of groundmass in the separated fraction. Other differences are lower total Fe_2O_3 , TiO_2 , Zn, Cu, and V contents in the volcanic sand compared with the basalts, which may be ascribed to selective deposition of heavy Fe-Ti oxides during transportation of the rock fragments. It is thus reasonable to think that this volcanic sand originated from rocks (or volcanic ash) related to the basalts described above.

SEDIMENT AND FLUID GEOCHEMISTRY

The geochemical objectives of Site 830 were the same as at Sites 827 and 829: to identify the diagenetic and hydrologic origins of fluids in accretionary wedge sediments. This site is located ~7 km east of the collision zone between the Bougainville Guyot, composed mostly of carbonate sediments, volcanoclastic, and volcanic rocks, and the New Hebrides Island Arc (Collot et al., 1985) and therefore represents a slightly different tectonic setting from Sites 827 or 829. The composition of accreted sediments and the style of deformation was therefore expected to differ from Sites 827 and 829. All sedimented convergent margins that have been drilled, for example, the Middle America trench (Aubouin, von Huene, et al., 1982), the Barbados accretionary complex (Biju-Duval, Moore, et al., 1984; Mascle, Moore, et al., 1988), the Peru Margin (Suess, von Huene, et al., 1988), and the Nankai Trough (Taira, Hill, Firth, et al., 1991) are dominated by siliciclastic sediments.

Results

A total of 12 fluid samples were collected from whole-round sections of cores at the three holes drilled at Site 830 (Table 4). Three samples were obtained with the APC and the remaining nine were obtained with the RCB. All parts of the solid samples that appeared to be contaminated by drilling fluids were removed prior to squeezing, but sulfate concentrations in the deeper samples suggest that some drilling fluids may have been inadvertently included in the fluid samples. A variety of solutes were measured in the fluids (see “Explanatory Notes” chapter, this volume); these values are plotted against depth in Figure 17.

The water yield from the sediment dropped rapidly from the sediment-water interface to a depth ~50 mbsf, but from 50 to 200 mbsf approximately constant volumes of fluid were squeezed from the samples (Fig. 18). These results are consistent with measurements of water content in the sediments (see “Physical Properties” section, this chapter). One 13-cm-long sample (Sample 134-830B-23R-1, 42–55 cm), located at 262.6 mbsf in the highly altered volcanic rocks of lithostratigraphic Unit II (see “Lithostratigraphy” section, this chapter), yielded no fluid although it was squeezed at 35,000 psi for more than 3 hr. The lack of fluid is not surprising because volcanic rocks usually contain little or no water although other samples collected from this unit did yield water; Sample 134-830C-12R-1, 28–53 cm, provided ~0.4 cm^3/cm of fluid and its solute composition (Table 4) indicates that it is true formation fluid and was not contaminated by drilling fluid.

The carbon contents of the sediment are reported in Table 5. The CaCO_3 contents are plotted against depth in the

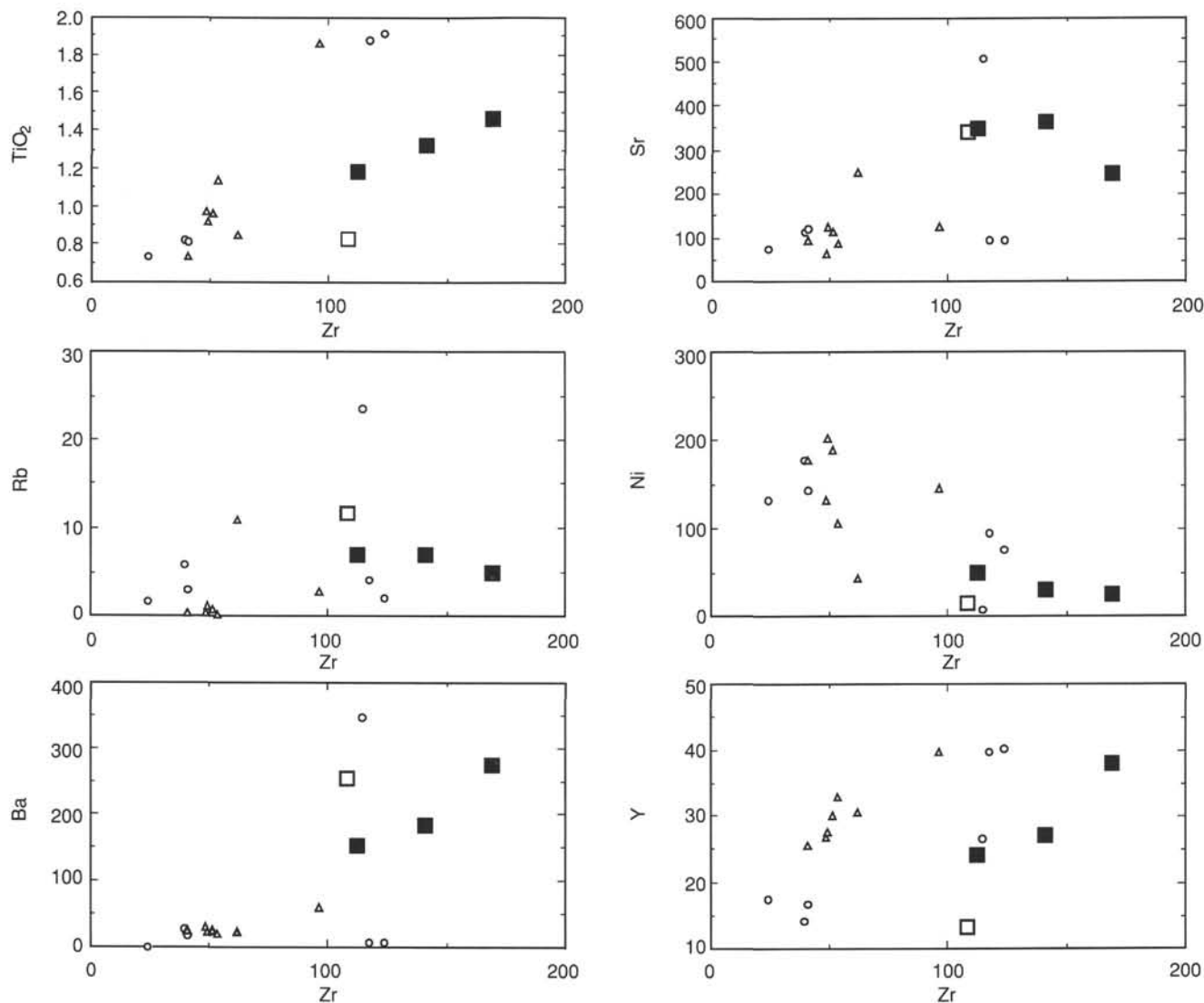


Figure 15. Zr variation diagrams for samples from Site 830 (basalts = solid squares, volcanic sand = open squares), Site 829 (triangles), and Site 828 (circles).

“Lithostratigraphy” section (this chapter) and the organic carbon contents are plotted vs. depth in Figure 19.

Chloride and Salinity

The chloride concentration increases to 620 mM at a depth of 214 mbsf (Fig. 17). Below this depth within Unit II, the chloride concentration decreases to 603 mM. Salinity decreases rapidly between the upper two samples and then increases with depth in the volcanic rocks of Unit II. Both the chloride concentration gradient and the salinity gradient, however, exhibit minor perturbations in their overall trends; the chloride concentration increases from the sediment-water interface to 59.5 mbsf and then is approximately constant to a depth of 117.8 mbsf. The salinity exhibits opposite characteristics; it is constant to 59.5 mbsf and then increases sharply to a depth of 117.8 mbsf.

Sodium, Potassium, Calcium, and Magnesium

Within Unit I, shallower than 180 mbsf, the sodium concentration gradient differs from the potassium gradient (Fig. 17). The sodium concentration decreases continuously to 403

mM at 157 mbsf, but the potassium exhibits a minimum of 6.4 mM at 60 mbsf. Within Unit II, deeper than 180 mbsf, both the sodium and potassium concentrations are less than seawater values; the sodium concentration is only 172 mM at 341 mbsf and there is no detectable potassium.

Calcium and magnesium concentrations also exhibit wide ranges in their values (Fig. 17). The calcium concentration increases to 28.9 mM at 141 mbsf, but then increases to 208.2 mM by only 214 mbsf and 229.2 mM at 341 mbsf. The magnesium concentration clearly exhibits a minimum of 33.8 mM, corresponding to the potassium minimum at 60 mbsf, and a maximum of 41.7 mM, corresponding to the potassium maximum at 141 mbsf (Table 4). The pore fluid in Unit II contains low magnesium concentration at 215 mbsf, the sample contains only 3.5 mM magnesium, and there is no measurable magnesium in the sample located at 341.2 mbsf.

Ammonia, Phosphate, Alkalinity, Silica, and Sulfate

The concentration profiles of alkalinity, silica, and ammonia are similar to the concentration profiles of potassium, magnesium, and sodium. Each of these solutes exhibits a

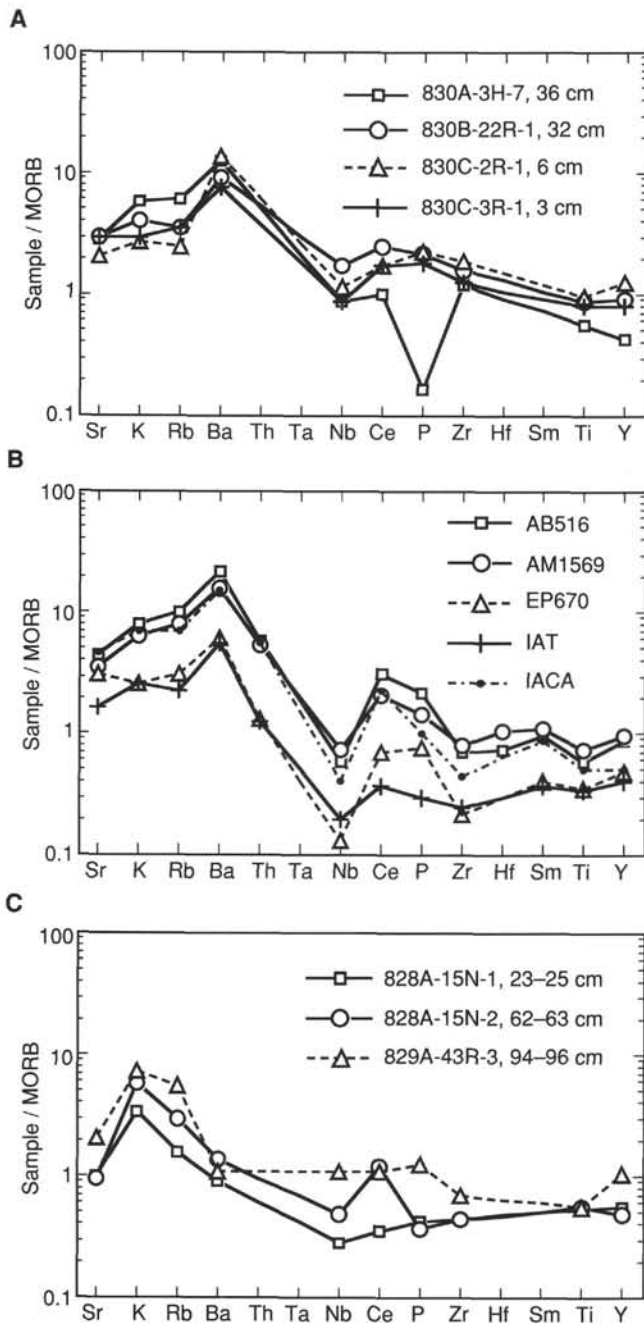


Figure 16. A. MORB-normalized trace element plots (Pearce, 1982) for the volcanic samples from Site 830. B. Samples from island-arc tholeiite (IAT), island-arc calc-alkaline basalt (IACA), Aoba (AB516), Ambrym (AM1569), and Epi (EP670). C. Basalts from Site 828 and 829. IAT and IACA data from Wilson (1989, p. 176) and those of Aoba, Ambrym, and Epi from Gorton (1977).

minimum at depths around 75 mbsf and low concentrations in the samples collected from the volcanic rocks in Unit II (Fig. 17). The minimum in ammonia concentration is less pronounced than other components and little ammonia exists in the deepest samples. Within Unit I however, the ammonia concentration reaches a fairly high value of 1849 μM at depths of 141 mbsf; surprisingly, the phosphate and alkalinity values are low throughout the sediments (Table 4).

Associated with the high ammonia concentrations, sulfate reduction is nearly complete by a depth of 79 mbsf (Fig. 17).

Sulfate is present below this depth, however, with concentrations ranging between 0.5 and 2.5 mM in Unit I (79–157 mbsf) and between 14.7 and 9.5 mM in Unit II. The sulfate contained in Unit II is unlikely to be a result of drilling contamination because of the lack of potassium and the low magnesium and high calcium concentrations. It is thus possible that the sulfate observed between 79 and 157 mbsf represents diffusion away from a source of sulfate contained within Unit II or sulfate reduction may be incomplete because of the low organic carbon contents within this unit.

Methane

The methane concentration is greater than previously observed during Leg 134 (Fig. 20) and heavier hydrocarbons (ethane and propane) were first observed at Site 830. The methane concentration varies sporadically between 30 and 90 mbsf, is lower between 90 and 110 mbsf, and exhibits a maximum of $\sim 800,000$ ppm around 145 mbsf. Essentially no methane was observed in the rocks of Unit II.

Discussion

The steepest concentration gradients at Site 830, particularly magnesium, calcium, sodium, and potassium, occur across the interface between lithostratigraphic Unit I and Unit II. Results from previous Deep Sea Drilling Project (DSDP) legs indicate that these solute concentrations are often controlled by alteration of volcanic ash and basement rock (Gieskes, 1981; Lawrence and Gieskes, 1981) and the concentration gradients observed often can be explained by diffusion away from reaction zones at the sediment-basement interface (McDuff and Gieskes, 1976; McDuff, 1981). Diagenesis is also reflected by the occurrence of numerous authigenic minerals throughout the volcanic rocks of Unit II. The composition of these minerals has not yet been determined through X-ray diffractometry, but petrographic identification indicates that zeolite, feldspar, and carbonate minerals are common. These minerals are distributed mostly in veins, implying that they may have formed from fluids flowing through fractures.

Mixing between the highly altered Unit II fluids and less altered Unit I fluids should be clearly exhibited because of the large differences in the compositions of these fluids; for example, fluid flow from Unit II may cause the observed magnesium and potassium minima and the slight calcium maximum between a depth of 60 and 79 mbsf (Fig. 21). The maximum and minima, however, could also result from local diagenesis of volcanic ash at this horizon, although there is no corresponding major change in lithology (see "Lithostratigraphy" section, this chapter). The silica concentration and alkalinity values also exhibit minima at this horizon, similar to the fluid in Unit II.

Because of the lack of a major lithologic change between 60 and 79 mbsf, however, the path of fluid flow is not obvious. The sporadic variations in the methane concentration (Fig. 20) suggest that flow could be concentrated along thin sandy zones observed in this unit. The major element chemistry may exhibit smoother profiles because of diffusion away from these zones. The sediments in this interval also exhibit numerous small normal faults and fractures (see "Structural Studies" section, this chapter), which could provide a conduit for fluid flow by increasing permeability. Deep fluids may have migrated upward from the point of their origin within the Unit II rocks along a diffuse fault zone located ~ 3 km east of the site (see "Seismic Stratigraphy" section, this chapter).

Summary

Intense alteration of pore fluid occurs in volcanic rocks of Unit II at Site 830. The decrease in the fluid content of the

Table 4. Pore-fluid chemistry, Site 830.

Core, section, interval (cm)	Depth (mbsf)	pH	Salinity (%)	Chloride (mM)	Sodium (mM)	Potassium (mM)	Magnesium (mM)	Calcium (mM)	Sulfate (mM)	Alkalinity (mM)	Phosphate (μM)	Ammonia (μM)	Silica (μM)
134-830A-													
1H-3, 145-150	4.5	7.9	35.0	552	469	12.0	46.4	8.4	22.8	3.7	4.8	216	456
3H-4, 145-150	22.5	7.8	32.0	564	467	10.6	38.1	8.2	4.9	2.7	1.8	605	319
5H-1, 145-150	36.4	8.1	32.0	568	456	9.1	35.8	10.3	4.1	2.5	1.8	952	319
134-830B-													
2R-1, 140-150	59.5		32.0	575	448	6.4	33.8	21.7	1.3		0.9	1518	300
4R-1, 100-110	78.5	8.2	32.5	577	451	7.6	34.7	25.0	0.5	1.2	1.0	1570	314
6R-1, 134-150	98.4	8.1	33.5	578	439	7.3	38.3	24.8	1.4	1.4	0.8	1547	338
8R-1, 134-150	117.8	8.0	34.0	584	436	9.1	41.6	23.4	1.9	1.7	0.9	1786	456
10R-2, 0-19	141	8.1	34.0	587	429	10.0	41.7	28.9	1.7	1.5	0.9	1849	453
12R-2, 0-18	156.8	7.9	34.0	597	403	9.9	36.8	57.9	2.5	1.3	0.6	1629	488
18R-1, 135-155	214.8		43.5	620	216	0.0	3.5	208.2	14.7		0.5	0	153
134-830C-													
10R-2, 0-10	323		42.5	603									
12R-2, 28-53	341.2	8.1	42.0	613	172	0.0	0.0	229.2	9.5	0.4	0.5	5	137

sediments implies that they were rapidly dewatered, but the conduits for fluid flow are not as evident as at Site 829, perhaps because no major fault planes were intersected at Site 830. Possible evidence for flow is exhibited by maxima and minima in the concentration profiles, although local diagenetic reactions could also account for the profiles.

STRUCTURAL STUDIES

Description of Tectonic Features

Cores recovered from Hole 830A display only a few structures related to tectonic activity (Fig. 22A). The uppermost core of Hole 830A (Core 134-830A-1H) and Cores 134-830A-7X through -10X contain horizontal bedding planes. Bedding attitudes (corrected using multishot data) in Cores 134-830A-2H through -6H increase in dip from 5° to more than 40° downhole and dip toward the southeast. Those structural features observed in the Pleistocene volcanic silts (Sections 134-830A-3H-4 and 134-830A-6H-1) display normal faults with centimeter-scale displacements. Figure 23 shows an excellent example of a set of conjugate normal faults and a vertical tensional gash filled by silt.

Rocks of Hole 830B are more deformed than those recovered from Hole 830A. All structures observed in Hole 830B (Fig. 22B) result from brittle deformation. In the upper part of the hole (Cores 134-830B-1R through -13R), the steeply dipping faults cut the Pleistocene silt and siltstones. In some cases, a normal sense of movement along the faults could be observed; displacements range from a few millimeters to centimeters. In interval 134-830B-1R-1, 22-36 cm, a normal fault with 1-cm displacement is overlain by a layer of silt and the toe of the fault scarp is filled with coarse-grained sediment (Fig. 24), which indicates syndimentary faulting. From Core 134-830B-15R to the bottom of Hole 830B a sequence of very coarse-grained volcanic sandstone and fine-grained breccia have been subjected to strong, brittle deformation. These brecciated rocks are considered cataclases (Fig. 25). Numerous white veins or concretions of zeolite crosscut the rocks.

The deformation features in Hole 830C are similar to those of the lower part of Hole 830B (Fig. 22C). The main rock type in Hole 830C is a coarse-grained volcanic sandstone with some intercalations of volcanoclastic breccia. The rocks have undergone intense brittle deformation and are interpreted as cataclases. In Cores 134-830C-8R and -9R a weakly developed planar fabric is visible, which may be interpreted as a zone of higher strain; the sense of motion could not be determined. A fault within this zone (interval 134-830C-8R-2,

10-23 cm), which cuts the planar fabric, shows a normal sense of movement (Fig. 26).

Discussion

Based on structural observations, cores recovered at Site 830 can be divided into two units (tectonic Units A and B) that correlate with the lithostratigraphic units (see "Lithostratigraphy" section, this chapter). Tectonic Unit A is composed of 170 m of Pleistocene volcanic silt and siltstone and was affected only by normal faulting and fracturing. Tectonic Unit B consists of coarse volcanic sandstone and fine breccia and was subjected to cataclastic deformation. The strong contrast in the tectonic style of the upper and lower units of Site 830 suggests that the cataclastic deformation occurred before the deposition of the Pleistocene silt and siltstone. The age of this severe brittle deformation is unknown because the ages of the rocks have not been determined. Therefore, this deformation is not necessarily related to the indentation of the Bougainville Guyot but could be an older event.

PALEOMAGNETISM

Archive halves from Holes 830A, 830B, and 830C were measured with the cryogenic magnetometer. Most sections were alternating-field (AF)-demagnetized at 5-cm intervals using a peak field intensity of 10 mT. When time permitted, sections were progressively demagnetized using peak fields of 2, 5, 10, and 15 mT. Cores 134-830A-2H through -6H were oriented *in situ* using the multishot orientation technique (see "Paleomagnetism" section, "Explanatory Notes" chapter, this volume). Sixty-three discrete samples taken from the working halves of cores recovered from all holes at Site 830 were progressively AF-demagnetized so that the directional stability and coercivity spectra of each section could be determined.

Magnetostratigraphy

The natural remanent magnetization (NRM) intensities of the un lithified volcanic silt in Cores 134-830A-1H and -2H (0-16.5 mbsf) and the first three sections of Core 134-830A-3H (16.5-20.7 mbsf) (lithostratigraphic Subunit IA, see "Lithostratigraphy" section, this chapter) are on the order of 10^{-1} A/m (Fig. 27). Twenty-two samples from these cores were progressively AF-demagnetized in 10-mT intervals up to 50 mT (Fig. 28). After removal of a drilling-induced component characterized by median destructive fields of 10-25 mT (Figs. 28 and 29), a stable component of magnetization was isolated whose inclination is negative, implying normal polarity. Di-

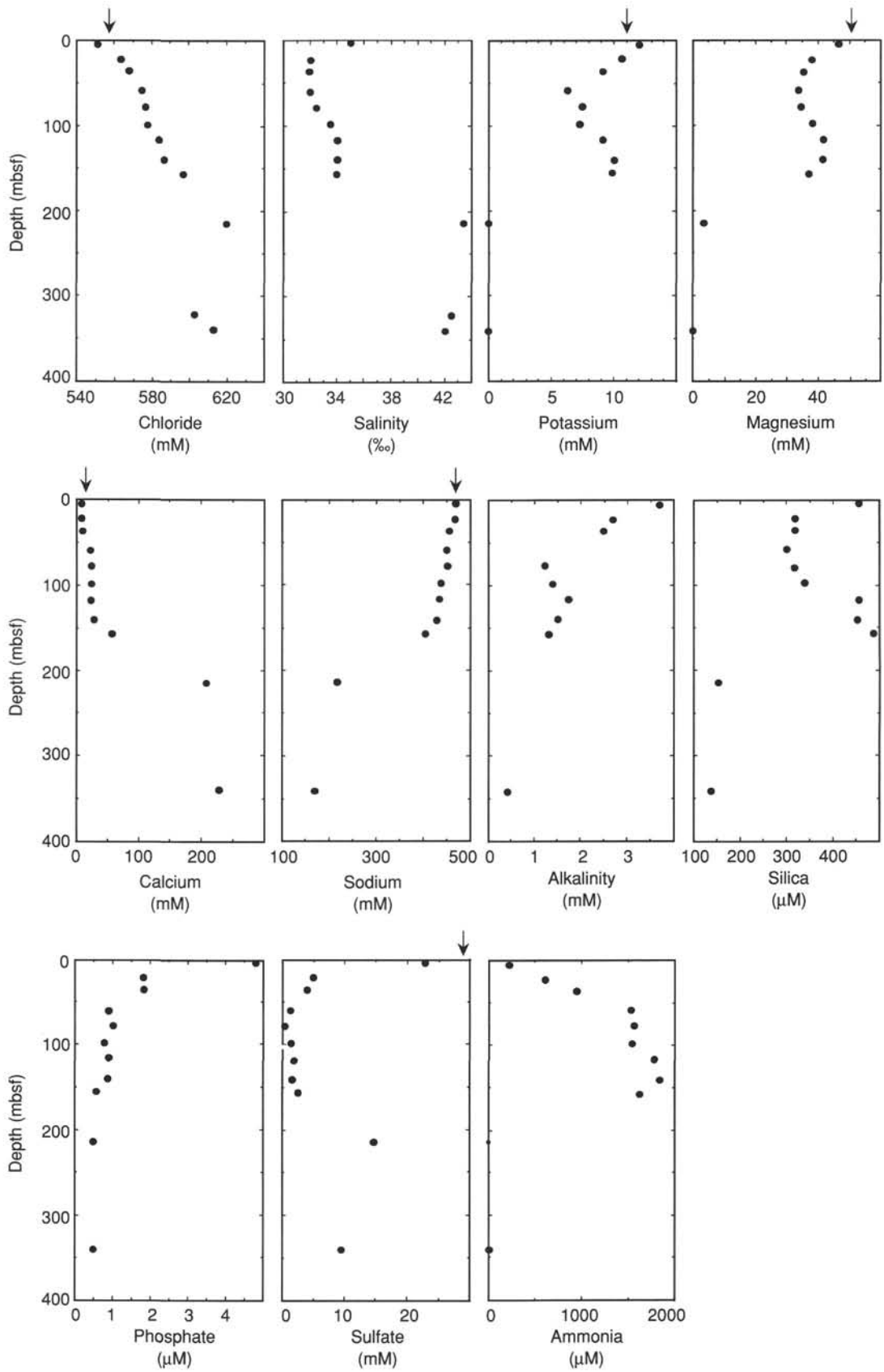


Figure 17. Pore-fluid gradients, Site 830. The arrows indicate seawater concentrations.

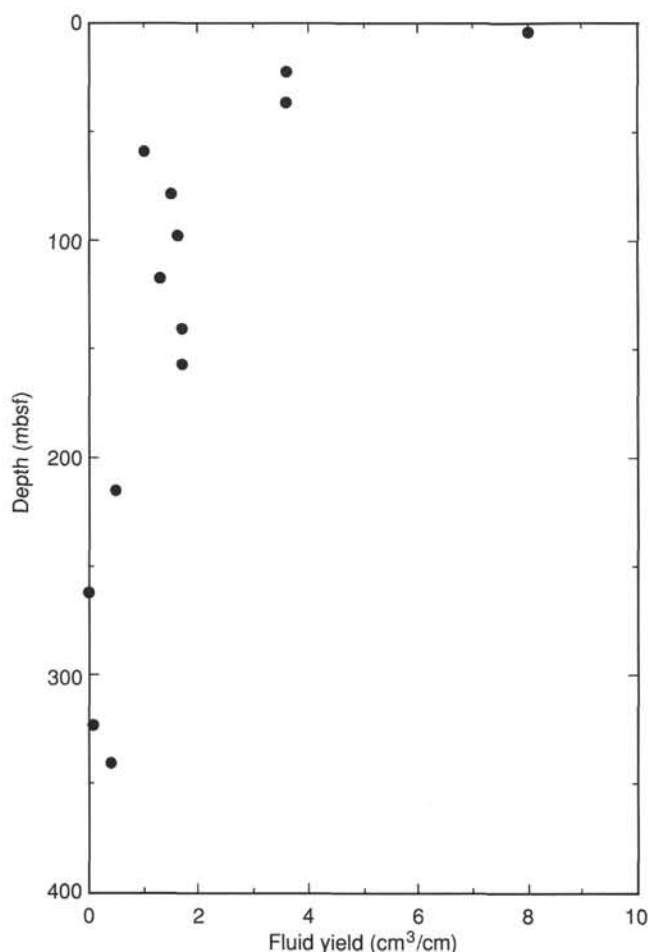


Figure 18. The yield of water per centimeter of core that was squeezed, Site 830. This value is only a qualitative measure of the water contained in the sample because some variable amount of the sample was removed from each sample prior to squeezing.

rections of 15 AF-demagnetized samples from Cores 134-830A-2H and -3H have been corrected using data from both multishot orientation and bedding attitudes (Fig. 30). Their mean has a declination of 347.7° and an inclination of -32.8° , similar to the present-day field direction at Site 830 (declination of 0° , inclination of -29°). Lithostratigraphic Subunit IB (21.0–47.0 mbsf) contains clayey sandy silt with graded interbeds of volcanic sand; smear-slide analysis reveals as much as 30% magnetite in these sands (see “Lithostratigraphy” section and core descriptions, this chapter). From about 21–42 mbsf (Section 134-830A-3H-4 to -6H-2), the NRM intensity of the discrete samples increases from <1 to 2 A/m (Fig. 29). After correction using multishot data and bedding attitudes and removal of a soft component of remanence by AF demagnetization to 10 mT, directions are characterized by northwesterly declinations and steep upward inclinations (Fig. 29). The difference in directions between Subunits IA and IB may result from a combination of (1) incomplete removal of drilling-induced overprints, (2) incorrect multishot orientation, (3) the presence of low-coercivity magnetite in the beds of volcanic sand in Subunit IB, and (4) possible tectonic rotation of Site 830. The stable magnetizations recorded by Cores 134-830A-1H to -6H are all of normal polarity, which suggests that the volcanic silt was deposited during the Brunhes Chron.

Table 5. Sediment carbon contents, Site 830.

Core, section, interval (cm)	Depth (mbsf)	Total carbon (wt%)	Inorganic carbon (wt%)	TOC (wt%)	CaCO ₃ (wt%)
134-830A-					
H-1, 3–5	0		1.69		14.1
1H-3, 3–5	3.0	3.38	3.03	0.35	25.2
1H-5, 3–5	6.0		2.53		21.1
2H-2, 27–30	8.8		3.38		28.2
2H-4, 50–53	12.0	2.12	1.89	0.23	15.7
2H-6, 85–88	15.4		2.11		17.6
3H-1, 122–125	17.7		1.98		16.5
3H-3, 122–125	20.7	2.52	2.26	0.26	18.8
3H-5, 35–38	22.9		2.65		22.1
3H-7, 45–48	26.0		1.62		13.5
4H-1, 70–73	26.7		0.85		7.1
4H-3, 60–63	29.6	1.60	0.99	0.61	8.2
4H-3, 70–73	29.7		0.76		6.3
5H-1, 100–102	31.4		0.81		6.7
5H-3, 85–87	34.3	1.25	0.96	0.29	8.0
5H-5, 85–87	37.3		0.70		5.8
6H-1, 55–59	40.5	1.33	1.17	0.16	9.7
6H-3, 57–59	43.5		0.01		0.1
7X-1, 57–58	49.1	1.30	1.17	0.13	9.7
7X-CC, 22–23	49.7		1.14		9.4
8X-CC, 16–18	58.4	1.59	1.26	0.33	10.5
9X-CC, 28–30	68.2	1.78	1.60	0.18	13.3
10X-1, 24–26	77.8	0.95	0.81	0.14	6.7
134-830B-					
1R-1, 142–145	48.5		1.14		9.5
2R-2, 100–102	60.6	1.28	1.12	0.16	9.3
3R-1, 126–128	69.0	1.38	1.18	0.20	9.8
4R-2, 10–13	78.7	1.28	1.11	0.17	9.2
5R-2, 137–140	90.3	1.34	1.13	0.21	9.4
6R-1, 100–103	98.1	1.58	1.55	0.03	12.9
7R-1, 105–108	107.9	1.23	1.05	0.18	8.7
8R-1, 84–87	117.3	1.81	1.45	0.36	12.1
9R-2, 37–40	128.1	2.23	1.89	0.34	15.7
10R-1, 47–49	136.4	2.21	1.94	0.27	16.2
11R-1, 44–46	146.0		1.72		14.3
11R-3, 36–38	149.0		1.32		11.0
12R-1, 57–59	155.9	1.76	1.53	0.23	12.7
13R-1, 54–56	165.7	2.29	1.92	0.37	16.0
15R-1, 63–65	185.2	0.13	0.08	0.05	0.7
17R-1, 22–25	204.0	0.31	0.18	0.13	1.5
18R-1, 47–50	213.9	0.26	0.14	0.12	1.2
19R-1, 60–63	223.7	0.19	0.09	0.10	0.7
20R-1, 50–53	233.4	0.29	0.15	0.14	1.2
21R-1, 50–53	243.1	0.25	0.24	0.01	2.0
22R-1, 50–53	252.9	0.19	0.15	0.04	1.2
23R-1, 33–34	262.5	0.46	0.40	0.06	3.3
23R-2, 63–64	263.4		0.07		0.6
24R-1, 48–50	272.5	0.52	0.40	0.12	3.3
134-830C-					
1R-1, 60–63	235.6	1.29	1.23	0.06	10.2
2R-1, 30–33	244.7	1.75	1.59	0.16	13.2
4R-2, 66–68	265.9	1.09	1.27	0.00	10.6
5R-1, 20–22	273.5		2.77		23.1
7R-1, 37–40	293.0		0.51		4.2

Note: TOC = total organic carbon.

Lithostratigraphic Subunit IC (47.0–96.9 mbsf in Hole 830A and 48.5–174.9 mbsf in Hole 830B) consists of interbedded sandy volcanic silts and silty sands. Recovery of this subunit was poor; thus, magnetostratigraphic interpretation is difficult. Two samples from this subunit (Samples 134-830B-13R-1, 139–141 cm, and 134-830B-13R-2, 115–117 cm) exhibit positive inclinations (Fig. 30), which indicate a reversed polarity. Additional paleomagnetic data are required to confirm that the polarity of the interval is indeed reversed, and additional biostratigraphic data are required to interpret the reversed interval in terms of the geomagnetic polarity time scale.

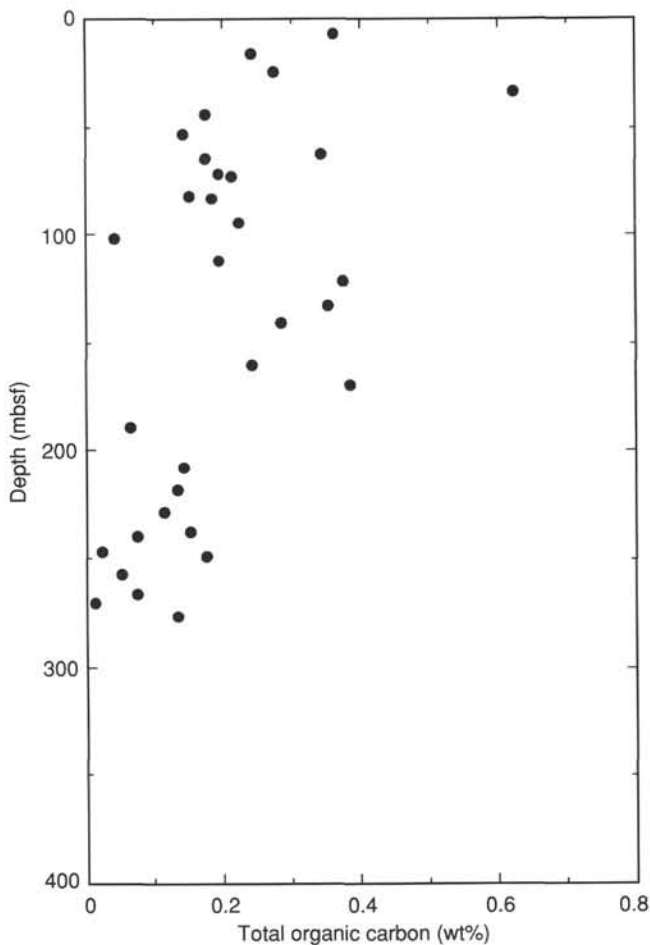


Figure 19. Total organic carbon content of sediments at Site 830 plotted vs. depth.

Lithostratigraphic Unit II (174.9–281.7 mbsf in Hole 830A and 235.0–350.6 mbsf in Hole 830B) comprises partially lithified silty volcanic sed-lithic sandstone, whose biostratigraphic ages cannot be determined because of the absence of microfossils. One sample from this subunit (Sample 134-830B-18R-1, 112–114 cm) exhibits positive inclination and a reversed polarity (Fig. 30). Poor recovery and extensive overprinting of samples from Hole 830C make interpretation of magnetic polarity impossible.

Magnetic Susceptibility

The magnetic susceptibility of all cores was routinely measured at 2.5-cm intervals. The downhole profile of susceptibility at Site 830 is shown in Figures 29D and 31. Magnetic susceptibility increases from $<1 \times 10^{-2}$ SI in lithostratigraphic Subunit IA to $>10 \times 10^{-2}$ SI in Subunit IB, a trend that reflects the abundance of volcanogenic minerals and the high concentration of magnetite in Subunit IB. Susceptibility decreases to an average of around 2.2×10^{-2} SI in Subunit IC. Poor core recovery in both Subunit IC and Unit II resulted in an incomplete record of susceptibility downhole that is difficult to interpret.

SEDIMENT ACCUMULATION RATES

Sediment accumulation rates could not be estimated for Holes 830A and 830B because only one datum level is represented in these sections. Samples recovered from Hole

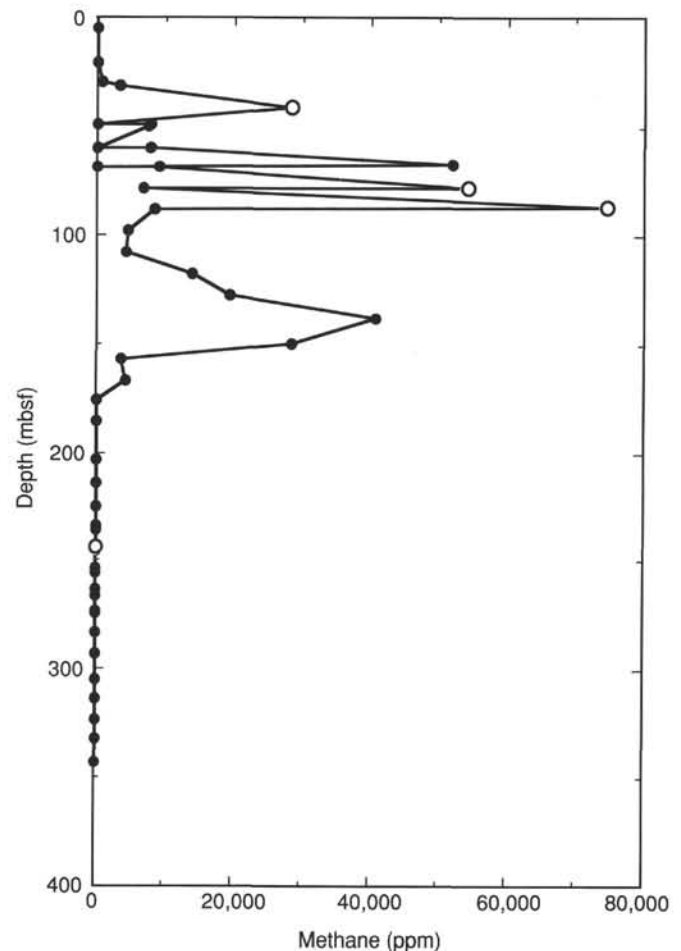


Figure 20. The concentration of methane in the headspace analyses plotted vs. depth. The open symbols represent samples that contain ethane and propane.

830A and from the upper 184.6 m of Hole 830B are Pleistocene (planktonic foraminifer Zone N22 and nannofossil Zone CN14/15). Samples from the lower part of Hole 830B (184.6–281.7 mbsf) and samples from Hole 830C are composed predominantly of volcanoclastic rocks that contain no microfossils.

PHYSICAL PROPERTIES

Measurements of index properties and Hamilton Frame sonic velocity were completed on sediments and rocks at Site 830. Full APC/XCB cores from Hole 830A were measured with the gamma-ray attenuation porosity evaluator (GRAPE) and the *P*-wave logger (PWL) on the multisensor track. Undrained shear-strength measurements were completed on Hole 830A cores that were recovered using APC and XCB. Because of better core recovery and less disturbance, measurements of physical properties of samples from Hole 830A (55% recovery) were of higher quality than those from Hole 830B (20% recovery) and from Hole 830C (16% recovery). All measurements at Site 830 were made according to the procedures described in the “Explanatory Notes” chapter in this volume.

Index Properties

Values of porosity (wet and dry), bulk density (wet-, dry-, and grain), and water content (dry and wet) for Site 830 are

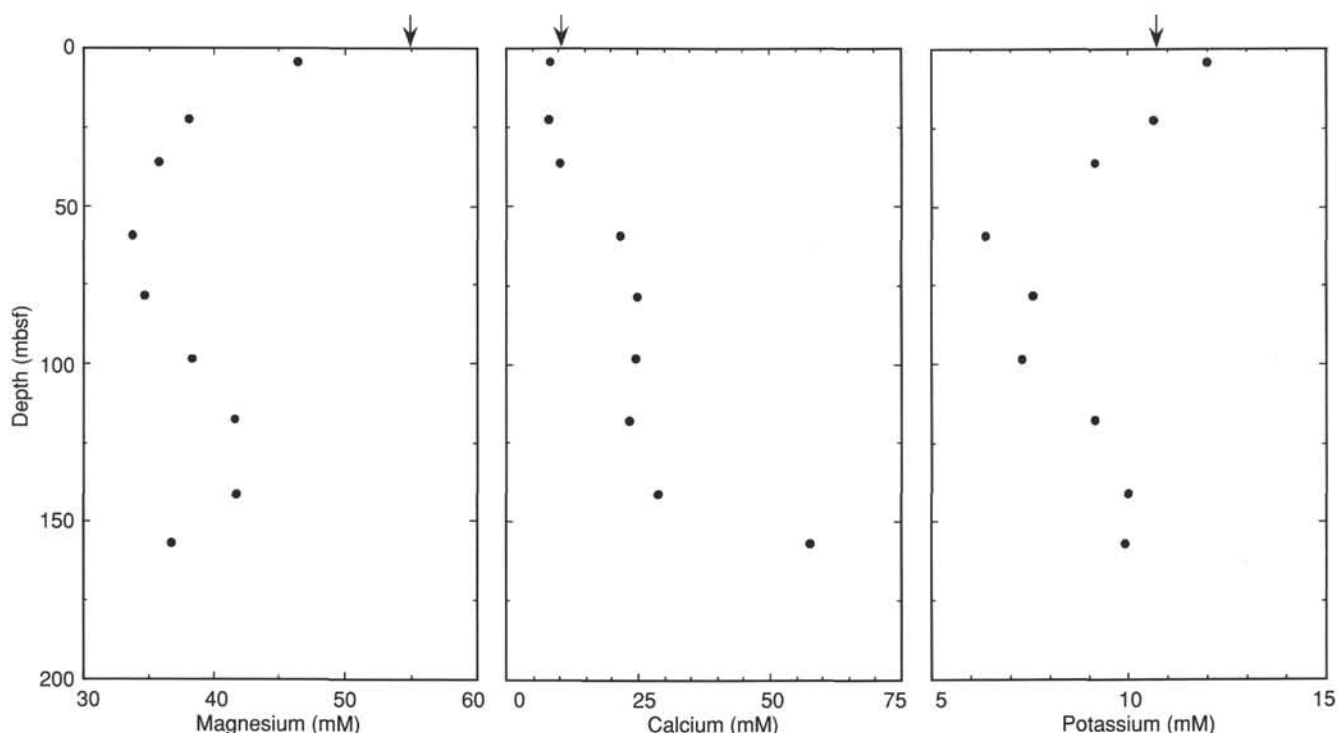


Figure 21. The magnesium, calcium, and potassium concentrations of pore fluids in the sediments of Unit I, from 0 to 200 mbsf, plotted against depth, Site 830. The arrows indicate seawater concentrations.

listed in Table 6. Figure 32 illustrates the variation of porosity, water content, and bulk density as a function of depth below seafloor. Bulk density trends often mirror those of porosity and water content; therefore, bulk density and porosity are plotted vs. depth along with the lithostratigraphic units in Figure 33.

At Site 830, porosity ranges from 23.5% to 71.8%, water content ranges from 11.0% to 84.7%, and bulk density ranges from 1.56 to 2.52 Mg/m³. Two lithostratigraphic units were described at Site 830 (see “Lithostratigraphy” section, this chapter): lithostratigraphic Unit I (0–174.9 mbsf) contains volcanic sediments and lithostratigraphic Unit II (174.9–350.6 mbsf) comprises volcanoclastic sand with a matrix of chloritic sandy silt.

The index properties data can also be separated into two zones. The index zones are associated with the lithostratigraphic units as follows:

Index Zone 1 = Lithostratigraphic Subunits IA and IB (0–47 mbsf); and

Index Zone 2 = Lithostratigraphic Subunit IC and Unit II (47.0–350.6 mbsf).

Sampling frequency in index Zone 1 (0.36 samples/m) was more than three times the sampling frequency in index Zone 2 (0.11 samples/m); consequently, the trends are clearer in index Zone 1. Index Zone 1 is composed of unlithified volcanic silt (fine-grained and clayey to sandy), and interbeds of volcanic sand occur from 21 mbsf (see “Lithostratigraphy” section, this chapter). Porosity and water content decrease rapidly, whereas bulk density increases rapidly in index Zone 1. From the surface to the base of index Zone 1 (0.03–43.5 mbsf), porosity decreases from 71.8% to 43.3%, water content decreases from 84.7% to 24.7%, and bulk density increases from 1.60 to 2.24 Mg/m³. In index Zone 2, porosity and water content decrease much less quickly, and between 49.9 and 322.9 mbsf, a slow decrease from 52.7% to 23.7% and 35.9%

to 11.2% occurs. The gradient of porosity and water content is nearly vertical below 200 mbsf. From 49.1 mbsf to near the base of Hole 830C (at 322.9 mbsf), bulk density increases from 2.05 to 2.41 Mg/m³. The rapid decrease of porosity and water content and concomitant increase in bulk density suggest that the collision with the Bougainville Guyot is inducing tectonic dewatering of the sediments at Site 830.

Sonic Velocity

Sonic velocities were measured using both the PWL and the Hamilton Frame in Hole 830A. In Holes 830B and 830C, velocities were measured exclusively with the Hamilton Frame. Hamilton Frame sonic velocity measurements are listed in Table 7, and the variation in velocity vs. depth is shown in Figure 32. PWL and Hamilton Frame measurements agree well with each other, and because of this and the consistent use of the Hamilton Frame in all holes, only the measurements made in the Hamilton Frame are discussed below.

At Site 830, vertical velocity ranges from 1538 to 4440 m/s and horizontal velocity ranges from 1536 to 4233 m/s. The vertical and horizontal velocities are essentially isotropic in lithostratigraphic Unit I, but become somewhat anisotropic in lithostratigraphic Unit II.

The velocity data at Site 830 correspond well with the lithostratigraphic units. In lithostratigraphic Unit I (0–174.5 mbsf), vertical velocity increases slightly from 1538 m/s at the surface to 1962 m/s at the base of the unit (0.03–165.7 mbsf). The velocities become scattered and fewer measurements could be made due to decreased recovery in Unit II (174.5–350.6 mbsf). Vertical velocity varies from 1576 to 4440 m/s and horizontal velocity varies from 2007 to 4233 m/s. Most horizontal velocity values (15 of 17) range between 2007 and 3419 m/s. Maximum anisotropy occurs at 244.7 mbsf, where the horizontal velocity is 1217 m/s greater than the vertical

A

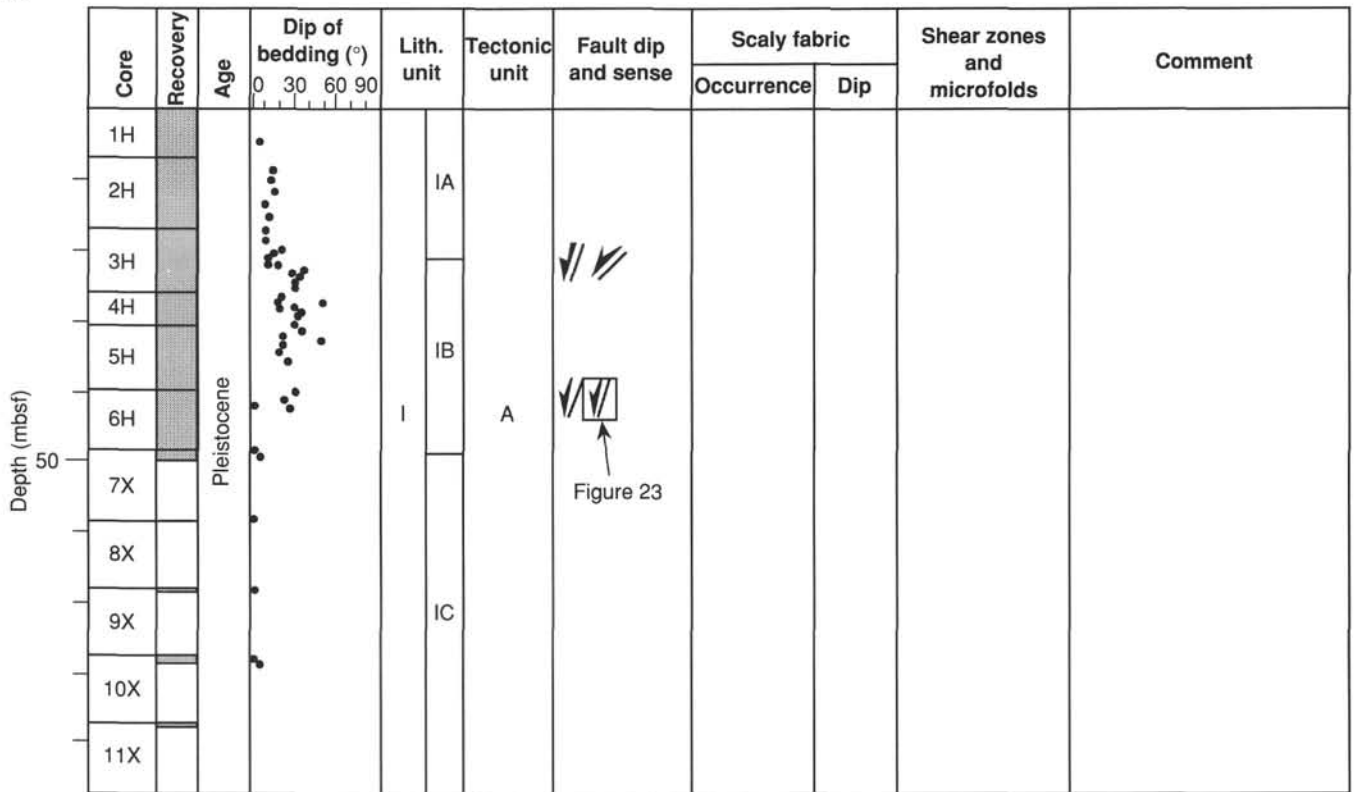


Figure 22. Structural logs of Hole 830A (A), Hole 830B (B), and Hole 830C (C).

velocity. Anisotropy (increased horizontal velocities) may be an indication of the lateral tectonic effects at this site.

Shear Strength

Shear-strength data for Site 830 are listed in Table 8, and are plotted as a function of depth below seafloor in Figure 34.

The shear-strength data increase strongly from 5.1 kPa at the mudline to about 100 kPa at the base of lithostratigraphic Subunit IA (0–21 mbsf). Below this, the data are more scattered, from 60.9 kPa at 22.8 mbsf to 134.9 kPa at 40.5 mbsf. At the contact between Subunits IB and IC (47.5 mbsf), two low values, 27.9 kPa (47.7 mbsf) and 40.3 kPa (49.1 mbsf), were measured, which can be correlated to a local increase in porosity and water content. Below 49.1 mbsf, recovery was poor and the cores were lithified, so shear strength was not measured.

Thermal Conductivity

At Site 830 thermal conductivity could be performed only to a depth of 50 mbsf in Hole 830A. Values increase quickly from about 1.0 to 1.4 W/(m · K) between the seafloor and 30 mbsf (Fig. 35), and range from 0.84 W/(m · K) (20.25 mbsf) to 1.39 W/(m · K) (26.75 mbsf) (Table 9). This increase in thermal conductivity correlates well with index properties, mirroring the rapid decrease in water content (from 85%–25%) and increase in bulk density (1.60 to 2.20 Mg/m³) from 0 to 30 mbsf (Fig. 32). From 30 to 50 mbsf thermal conductivity values remain constant at around 1.25 W/(m · K). No measurements could be completed below 50 mbsf because the cores were too lithified and deformed by tectonics and drilling disturbance.

Summary

The most notable change of physical properties at Site 830 is the very rapid decrease of porosity and water content in lithostratigraphic Subunits IA and IB (Fig. 32). Hole 828A on the North d’Entrecasteaux Ridge drilled through a similar sequence of silty volcanic sediments in the first 100 mbsf. At that site, porosity remained constant at about 60% from 0–100 mbsf, whereas at Site 830 porosity decreased from 71.8% at the surface to less than 40% at 100 mbsf, and to 23.5% at 283.1 mbsf (Fig. 32). Water content decreased from 84.7% at the surface to about 23% at 100 mbsf, and to 11.0% at 283.1 mbsf. These data are similar to results presented by Bray and Karig (1985), who reported after examining the Nankai Trough and other subduction zones that low porosities in accretionary prisms are evidence that tectonic processes associated with accretion increase the efficiency of dewatering. Because of the permeable nature of silty volcanic sediments, fluids have little trouble diffusing through the grain matrix or flowing up through faults and shear zones. Rapid dewatering provides evidence that the collision zone of the Bougainville Guyot with the New Hebrides Island Arc is a regime of tectonic compression.

DOWNHOLE MEASUREMENTS

Operations

Well-logging operations at Hole 830C consisted of two logging runs. Logging operations began with the rigging up of the logging cables at 0600 local time (L), 12 November 1990, and ended with the rigging down of the logging cables at 1430 L, 12 November 1990. The first logging run used the “seismic

B

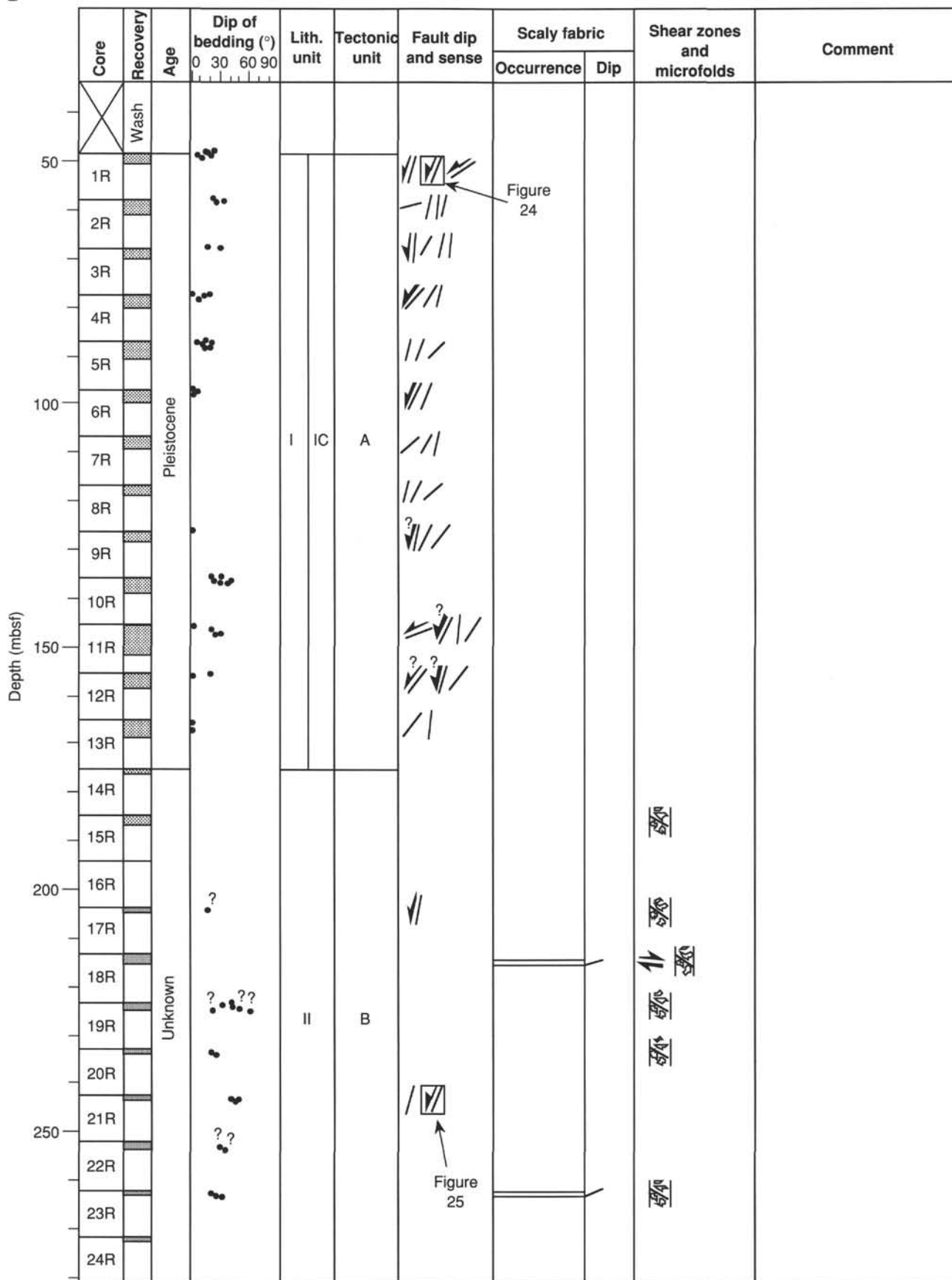


Figure 22 (continued).

C

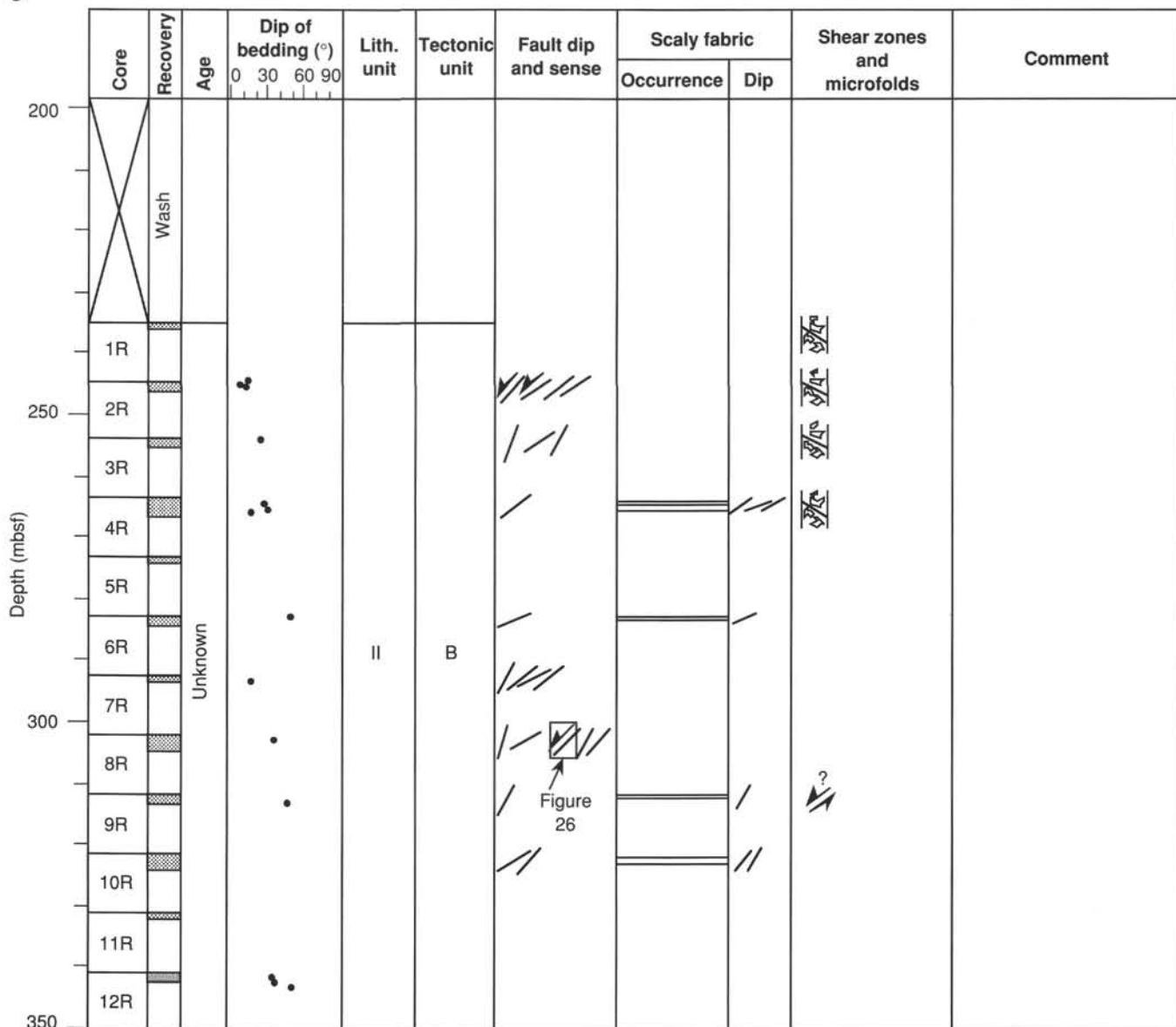


Figure 22 (continued).

stratigraphic combination” logging string. This logging string measures resistivity, sonic velocity, bulk density, minimum and maximum hole size, natural gamma radioactivity, and temperature. The end of the drill pipe was held at 51.6 mbsf (1071.6 m below rig floor). The first pass of the logging run was from the bottom of the open hole at 272.3 to 11.0 mbsf. The second pass (repeat section) was from 157.7 to 11.0 mbsf. The second logging run employed the “geochemical combination” logging string. This logging string measures natural gamma radioactivity, porosity, aluminum content, and elemental concentrations of calcium, silicon, iron, sulfur, chlorine, and hydrogen, along with temperature. The first pass of this logging run was from 247.0 to 34.6 mbsf. The second pass was from 77.2 mbsf to 4 m above sea floor. The second pass logged the upper part of the hole through the drill pipe.

The formation microscanner string and the digital borehole televiwer strings were not run in this hole because of the large drill-hole diameter. Hole conditions were deteriorating, as shown by increasing amount of fill during the operations.

The total drilled depth of the hole was 350.6 mbsf, while the first logging run could not get deeper than 272.3 mbsf, and the second logging run touched bottom at 247.0 mbsf.

Results and Interpretation

The results of the logging in Hole 830C are presented in the Log Summary at the end of this chapter. Lithostratigraphic Unit I (0–174.9 mbsf) consists of clayey volcanic silt to siltstone interbedded with silty volcanic sand to sandstone. Unit I is divided into three subunits: Subunit IA (0–21 mbsf), Subunit IB (21–47 mbsf), and Subunit IC (47–174.9 mbsf). Lithostratigraphic Unit II (174.9–350.6 mbsf) consists of a very poorly sorted, very coarse, silty volcanic sed-lithic sandstone (see “Lithostratigraphy” section, this chapter).

The natural gamma-ray logs (computed and total gamma ray) show a small-scale variability but no systematic change in the upper unit down to about 165 mbsf. The gamma-ray logs drop in value over the interval from 165 to 180 mbsf. The drop is most pronounced in the total gamma-ray log. The core

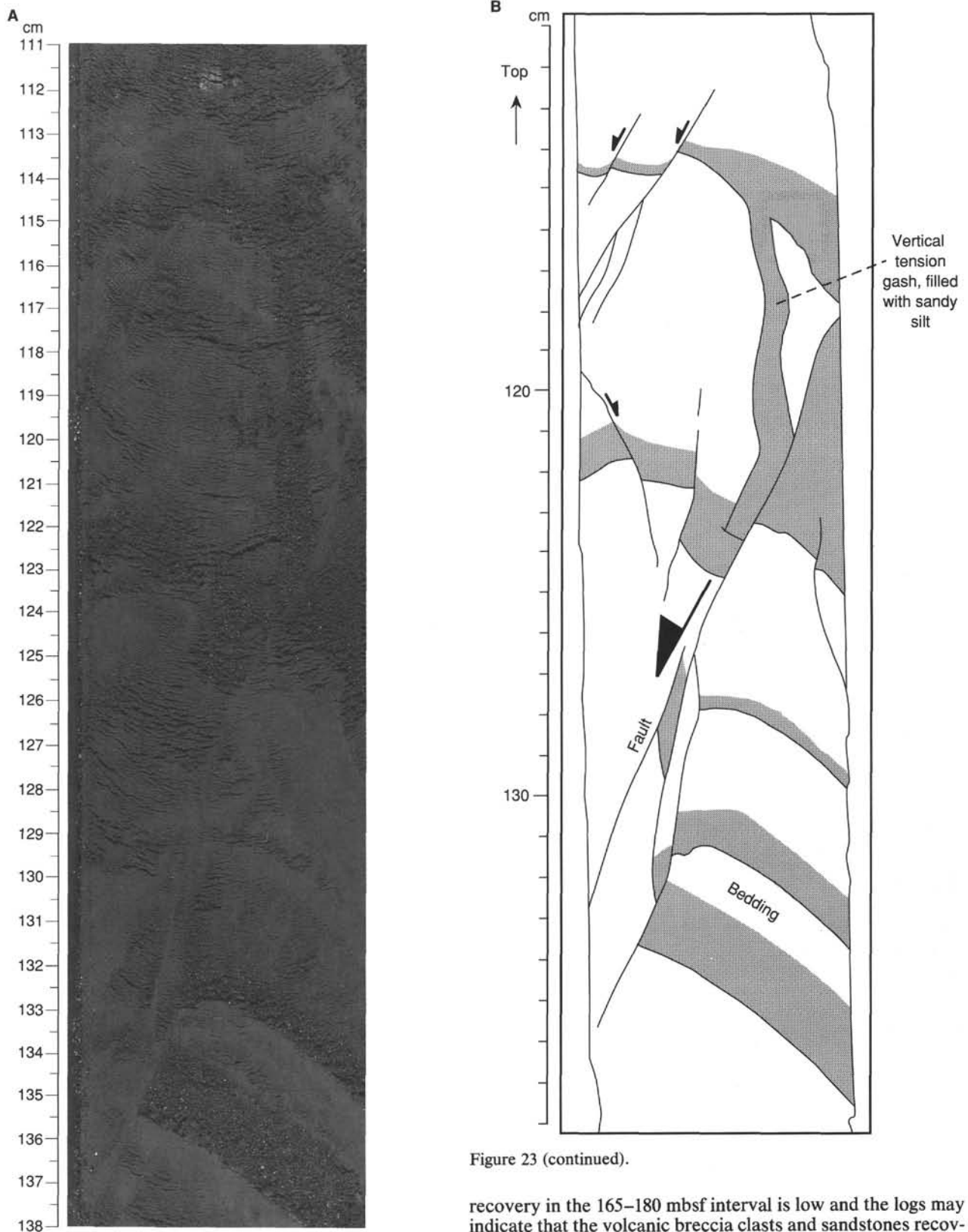


Figure 23 (continued).

Figure 23. Photograph (A) and sketch (B) of the conjugate set of normal faults observed in interval 134-830A-6H-1, 111-138 cm. The location is indicated in Figure 22A.

recovery in the 165-180 mbsf interval is low and the logs may indicate that the volcanic breccia clasts and sandstones recovered in Core 134-830B-14R are common in this interval. The gamma-ray values increase again over the interval 195-208 mbsf but there is nothing distinctive in the recovered lithology of this section other than the fact that it is the top of the poorly sorted, coarse, sed-lithic sandstone of Unit II. The gamma-ray values drop below 208 mbsf to values comparable to the

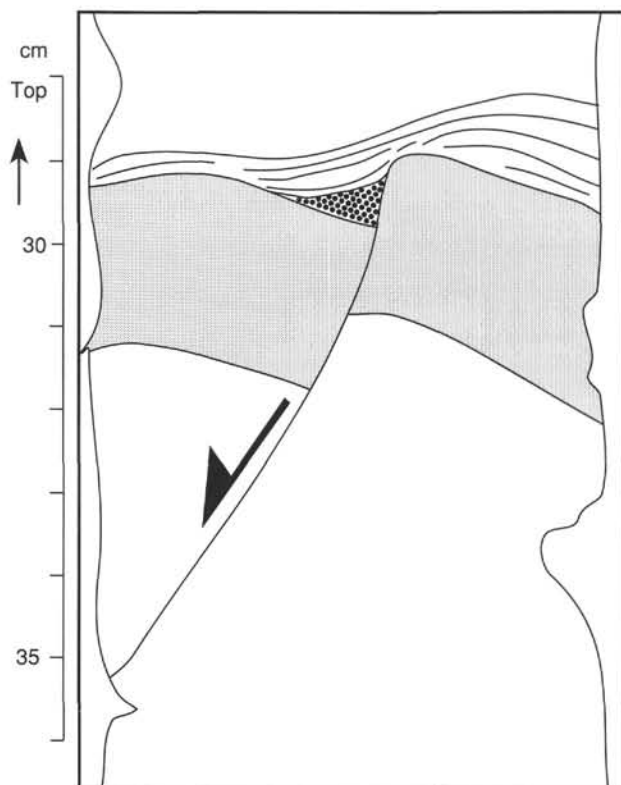


Figure 24. Sketch of the synsedimentary fault observed in interval 134-830B-1R-1, 28–36 cm. The location is indicated in Figure 22B.

165–180 mbsf interval without a corresponding change in lithology.

The thorium, uranium, and potassium logs are derived from the natural gamma-ray logs using the known gamma-ray spectrum of these elements and the calibrated spectral responses of the logging tools. The uranium log is low and somewhat variable. The only significant feature is the local doubling of concentration between 195 and 198 mbsf. The thorium values are also low but show somewhat more character. The values from 42 to 75 mbsf are distinctly higher than those from 78 to 170 mbsf. The values in the 175 to 195 mbsf depth interval are very low. Potassium values show little variation downhole, though they are generally lower below 175 mbsf. The values locally increase between 195 and 208 mbsf.

The resistivity logs (focused, medium, and deep) and the sonic traveltime log show great similarity in character. These logs are primarily controlled by density, porosity, and fracturing within the formation. They all show a slight increase in resistivity and decrease in traveltime with depth down to 165 mbsf with very little small-scale variability. Below 165 mbsf there is a large increase in resistivity and decrease in traveltime and a higher amplitude variability. These results together with the results discussed above suggest that a more logical boundary between lithostratigraphic Units I and II would be within Core 134-830B-13R (168 mbsf) rather than at the start of Core 134-830B-14R (175 mbsf). The resistivity and sonic logs have relatively constant mean values from 165 to 200 mbsf (with much small-scale variability) and then gradually increase from 205 to 215 mbsf. Below that depth they again have relatively constant mean values, although the resistivity logs show a sharp drop in value in the 248–253 mbsf interval. All of these variations are within lithostratigraphic Unit II.

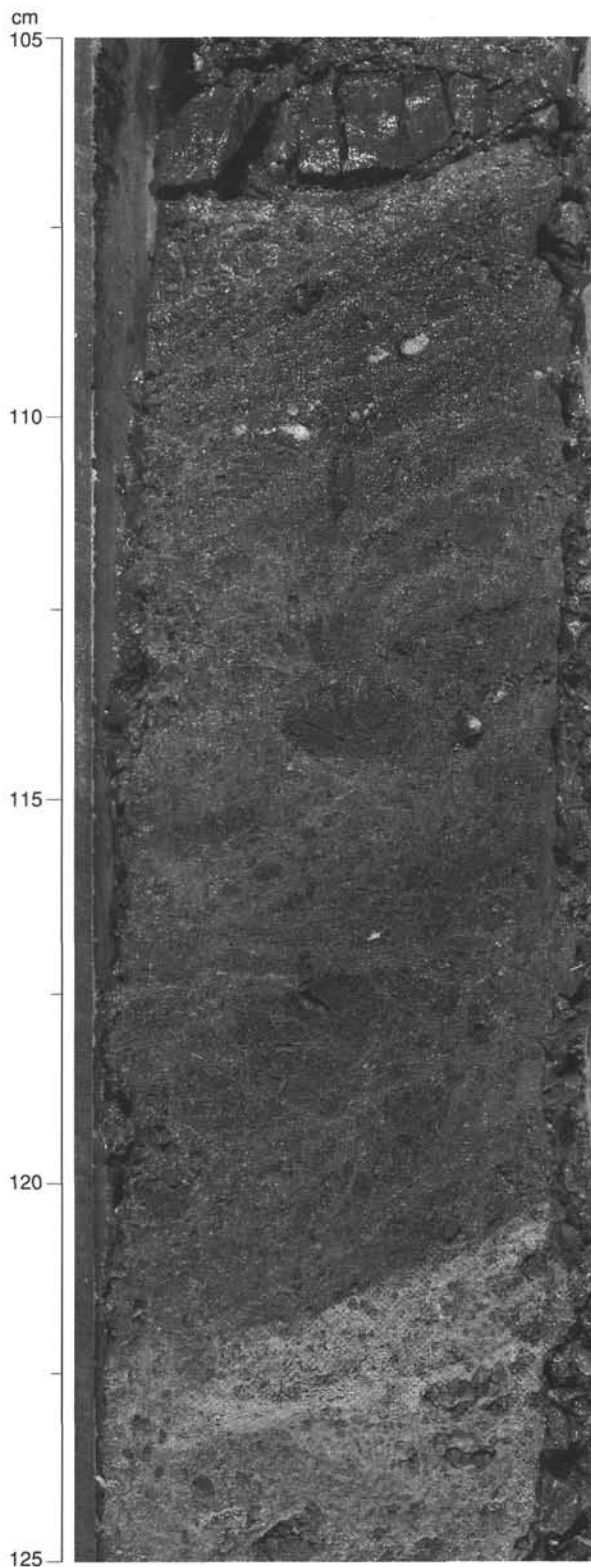


Figure 25. Photograph of the cataclasite in interval 134-830B-20R-1R, 105–125 cm. The location is indicated in Figure 22B.

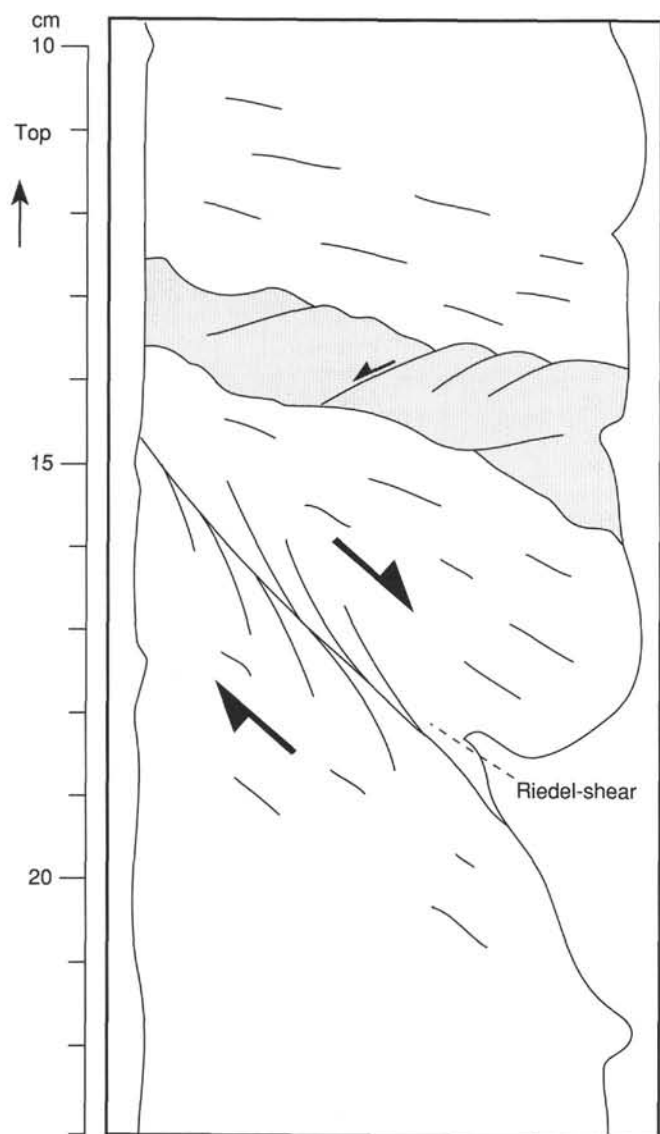


Figure 26. Sketch of the tectonic fabric observed in interval 134-830C-8R-2, 10-23 cm. The sketch represents the working half of the core. The location is indicated in Figure 22C.

The bulk-density log requires special discussion. This log obtains measurements using neutron scattering from a radioactive source on the caliper arm. The values of bulk density are only valid when the caliper arm is in contact with the wall of the borehole. An examination of the caliper log shows that over much of Hole 830C the long axis of the elliptical hole cross section was beyond the reach of the caliper arm. As a result, most of the variability shown in the density log must be regarded as spurious.

The photoelectric effect log (PEF) is a measure of the mean atomic number of the formation by measuring the Compton scattering of gamma rays. The PEF measured in lithostratigraphic Unit I is high, indicating a dense formation with an abundance of high atomic number elements, such as iron. The PEF log is scattered in Unit II in the lower part of Hole 830B, but the PEF values are lower, consistent with the higher porosity measured by the neutron porosity log.

The geochemical logs are all *normalized* logs. The geochemical logging tool normalizes the sum of the calcium, silicon, iron, sulfur, chlorine, and hydrogen outputs to one.

Post-cruise log analysis is done to convert these logs, together with selected other logs, to elemental abundances. This processing is calibrated by the shipboard and shore-based laboratory measurements of the composition of core samples. These results will be presented in the *Scientific Results* volume for Leg 134.

The chlorine and hydrogen yields are higher in Unit II (below 170 mbsf), perhaps because of a large hole diameter which complicates the interpretation of the yields from the rock matrix. The geochemical logs show that most of the matrix log signal in Hole 830C comes from silicon and iron, with calcium as lesser contributor and sulfur present only in trace amounts. The large hole diameter means that a large fraction of the tool response is from the borehole fluid. Calcium is slightly more abundant in lithostratigraphic Unit I than in Unit II, but further distinctions are hard to make at this time. Silicon shows a distinct change in character at 165 mbsf with more variability in Unit II than in Unit I. Iron has lower values in the upper part of Unit II (170-210 mbsf) than either in Unit I or the lower part of Unit II. Sulfur is only present in trace amounts in Units I and II.

The aluminum log shows a clear distinction between lithostratigraphic Units I and II. There is a gradual increase from 3 to 6 wt% from 30 to 60 mbsf, corresponding to the transition from Subunits IA to IB to IC. Within Subunit IC there is considerable variability but the concentration is generally 5-6 wt%. The transition to Unit II at 168 mbsf is marked by an abrupt decrease to 1-2 wt%. These values are also rather variable, with the interval near 213 mbsf having values of 4 wt%.

The overall results from the logs confirm the division of the hole into two units, but suggest that the boundary is at 168 mbsf rather than at 175 mbsf (see "Lithostratigraphy" section, this chapter). Distinctions are noted between Subunits IA, IB, and IC, but they are not as dramatic as the interunit boundary. Several of the logs suggest that there are coherent subunits within the lithostratigraphically undifferentiated Unit II. These subunits might have intervals from 168 to 195 mbsf, 195 to 210 mbsf, and below 210 mbsf. Discovery of the precise nature of these subunits awaits the results of further processing of the logs, especially the geochemical log results.

Heat Flow

Three successful runs of the water sampler temperature probe (WSTP) temperature tool were performed at Site 830. The data reduction procedures used were the same as those used at Sites 827 and 829. The thermal conductivity values used in the data reduction are given in Table 9 and Figure 35 (see "Physical Properties" section, this chapter).

The individual temperature measurements are discussed below: Run 5H in Hole 830A (Fig. 36) was done at a depth of 30.4 mbsf. The shallow water depth of this site meant that the mudline temperatures were still in the area where there is a significant vertical temperature gradient in the water. This considerably complicates the interpretation of mudline temperatures, as the mudline reference depths before and after penetration are only approximate. In deep water this makes little difference since bottom waters are usually almost isothermal. The run had no disturbances during the measurement. The reduction to equilibrium temperature is plotted in Figure 37.

Run 9X in Hole 830A (Fig. 38) was done at a depth of 67.9 mbsf. This run had a good mudline reference temperature before and after the penetration, as more care was taken on this run (but the difference in temperatures caused by the slightly differing depths is still readily apparent). No distur-

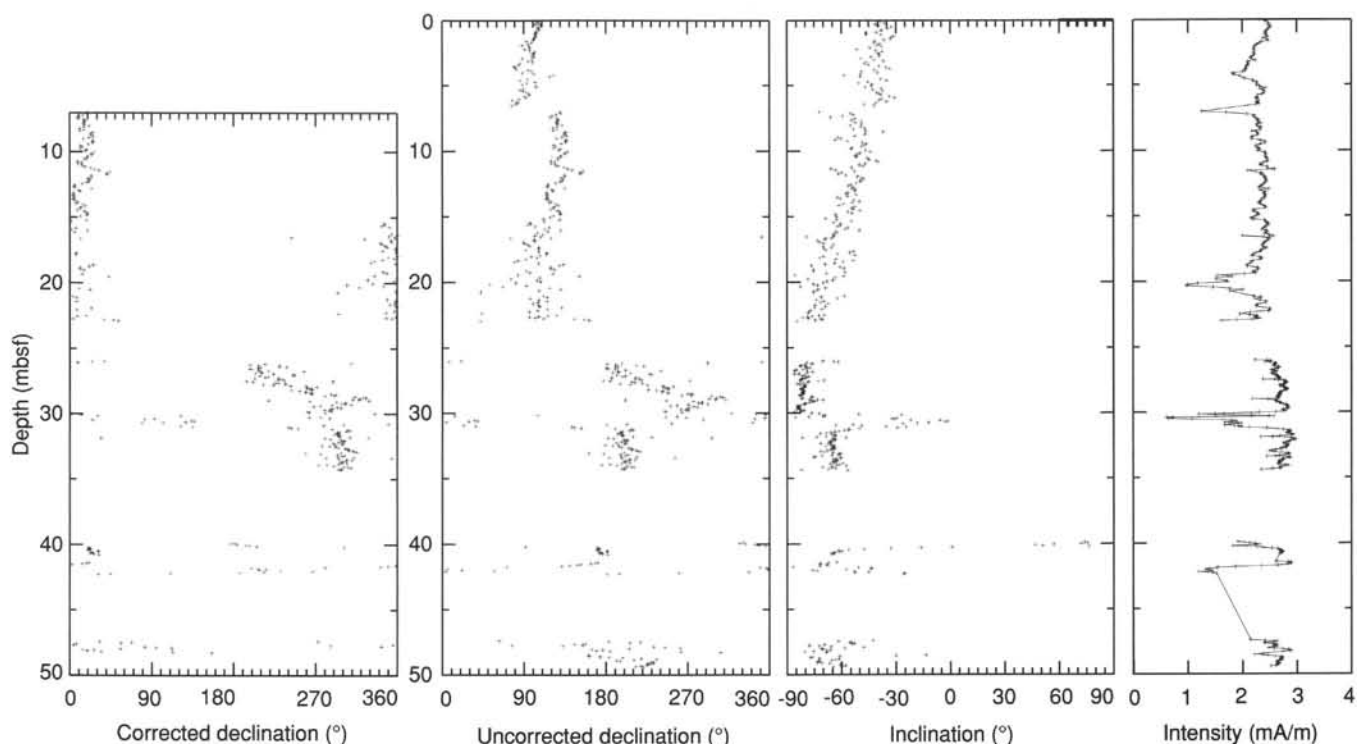


Figure 27. Remanent magnetization (after AF demagnetization at 10 mT) as a function of sub-bottom depth of archive halves from Hole 830A.

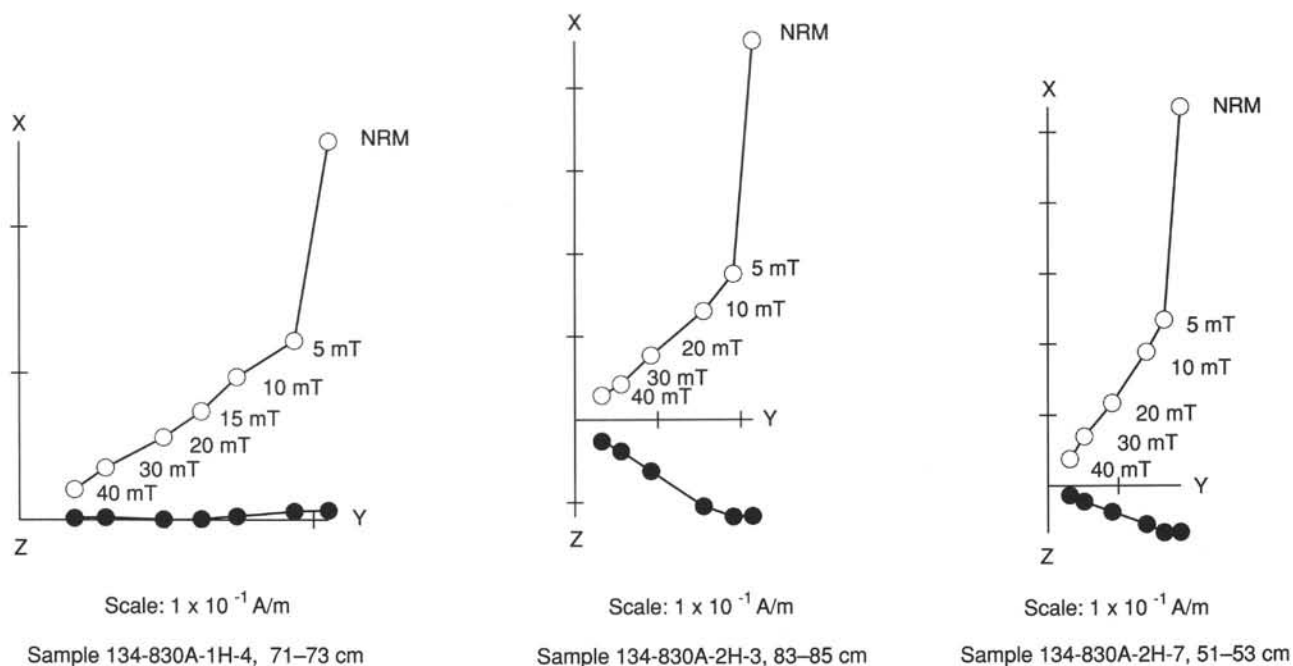


Figure 28. Representative vector endpoint diagrams showing the results of AF demagnetization plots of discrete samples from Cores 134-830A-1H and -2H before orientation and structural corrections. Open circles represent vector endpoints projected onto the vertical plane; solid circles represent endpoints projected onto the horizontal plane.

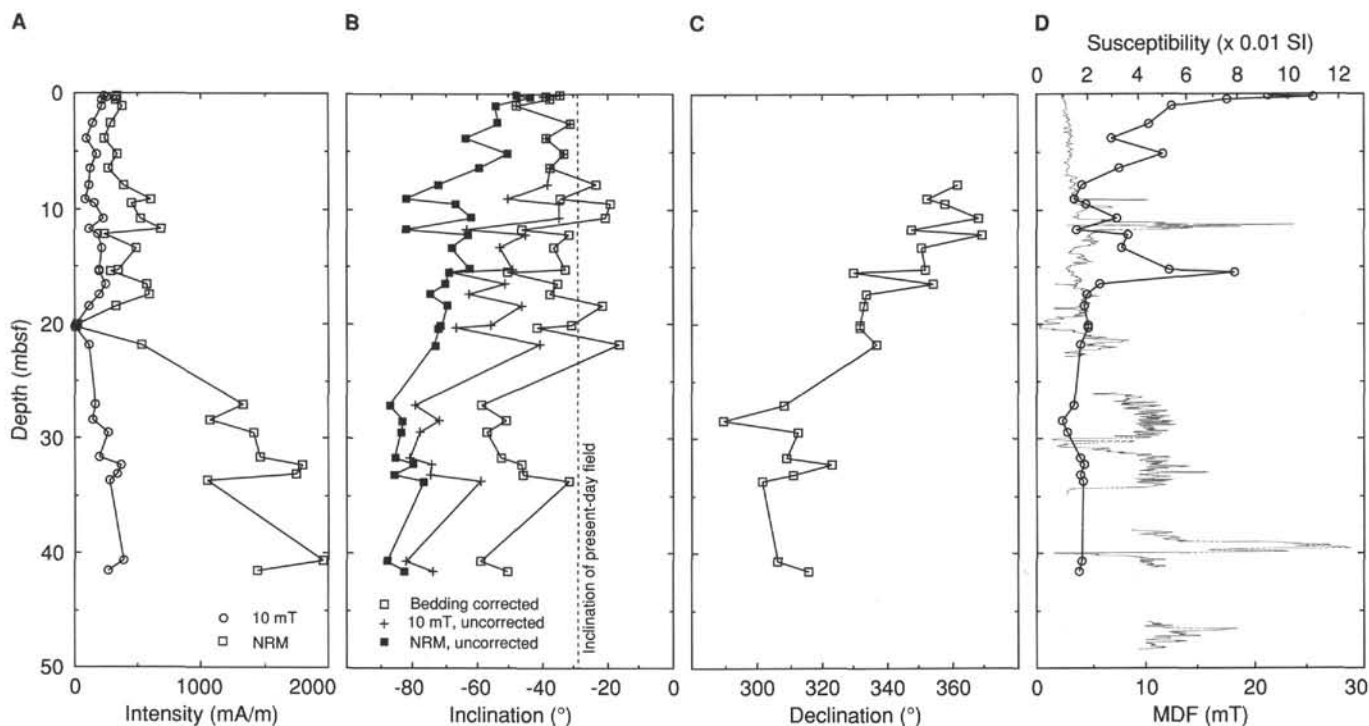


Figure 29. The variation as a function of sub-bottom depth of (A) intensity of NRM and stable magnetization after AF demagnetization at 10 mT, (B) inclination (before and after orientation correction), (C) declination (after bedding orientation and corrections), and (D) magnetic susceptibility and median destructive field (MDF) of cores from Hole 830A.

bances occurred during the measurement. The reduction to equilibrium temperature is plotted in Figure 39.

Run 12X in Hole 830A (Fig. 40) was done at a depth of 96.9 mbsf. This run also had good mudline reference temperatures before the penetration (but again note the different temperature after the penetration) and only a slight disturbance after 42 min during the measurement. The reduction to equilibrium temperature is plotted in Figure 41.

The three equilibrium temperatures are plotted against integrated thermal resistivity in Figure 42. The temperatures are plotted as absolute values because of the difficulties with the mudline temperatures discussed above. The slope of the plotted linear regression indicates that the heat flow is 17.0 mW/m². This is the lowest value measured so far on Leg 134. The two deepest measurements and the bottom-water temperature have a better straight-line fit with an indicated heat flow of 16.0 mW/m², but the discrepancy of the 30.4 mbsf value is only 0.2°K, similar to the discrepancies found at Site 827.

SUMMARY AND CONCLUSIONS

Site 830 is located at 15°57'S, 166°46.79'E to 15°57'S, 166°46.71'E in water depths ranging from 1018.4 to 1008.9 mbsl. This site is located on the forearc slope of the central New Hebrides Island Arc immediately east of where Bougainville Guyot is impinging upon the forearc slope, 30 km south of the southern tip of Espiritu Santo Island and 7 km east of the Australia-India convergence boundary. Here the DEZ is colliding with the arc. East of the point of impingement, the upper forearc slope is folded and faulted, with the most intense area of deformation being immediately eastward of the impact zone in an area that exhibits an anticlinal dome (Fig. 1). To the east of the anticlinal dome a series of imbricate thrust sheets, gently dipping to the east, can be interpreted

from the seismic reflection profile (Fig. 43). Site 830 is located just eastward of the anticlinal dome and at the westward toe of the most westerly thrust sheet.

Three holes were drilled at Site 830. Hole 830A was drilled and cored with the APC and XCB to 96.9 mbsf, recovering 53.77 m for a recovery rate of 55.5%. Hole 830B was washed to 48.5 mbsf and drilled with the RCB to a total depth (TD) of 281.7 mbsf but was cored only 233.2 m, recovering 48.77 m for a recovery rate of 20.9%. Hole 830C was washed to 235.0 mbsf and drilled with RCB to a TD of 350.6 mbsf and was cored 115.6 m, recovering 19.4 m for a 16.8% core recovery rate.

Two major lithostratigraphic units were defined and described for this site (Fig. 44). Lithostratigraphic Unit I (0–174.9 mbsf) is a very dark gray, volcanic silt and siltstone of Pleistocene age that is subdivided into three subunits. Subunit IA (0–21.0 mbsf, Hole 830A) consists of a 21-m-thick fine-grained, unlithified silt with numerous ash layers. Subunit IB (21.0–47.0 mbsf, Hole 830A) is a 26.0-m-thick clayey sandy silt with numerous normally graded interbeds of black sand. Subunit IC (47.0–174.9 mbsf, Holes 830A and 830B) is a 127.9-m-thick interbedded sandy silt and sand.

Lithostratigraphic Unit II (174.9–350.6 mbsf) is a colorful sequence of partially lithified, very poorly sorted, very coarse, volcanoclastic silty sed-lithic sandstone. The sequence is highly altered and contains intervals of grayish green to greenish gray and reddish black clayey silts, isolated pebbles of volcanic rocks, and fine-grained, well-lithified volcanic sandstone and breccias. The upper (174.9–184.9 mbsf) part of this unit is a sed-lithic breccia with 3- to 5-cm clasts of breccia and sandstone. Two types of igneous rocks are found in Unit II: lavas and volcanic breccia. The lavas are commonly andesite, but moderately olivine-clinopyroxene-phyric basalt

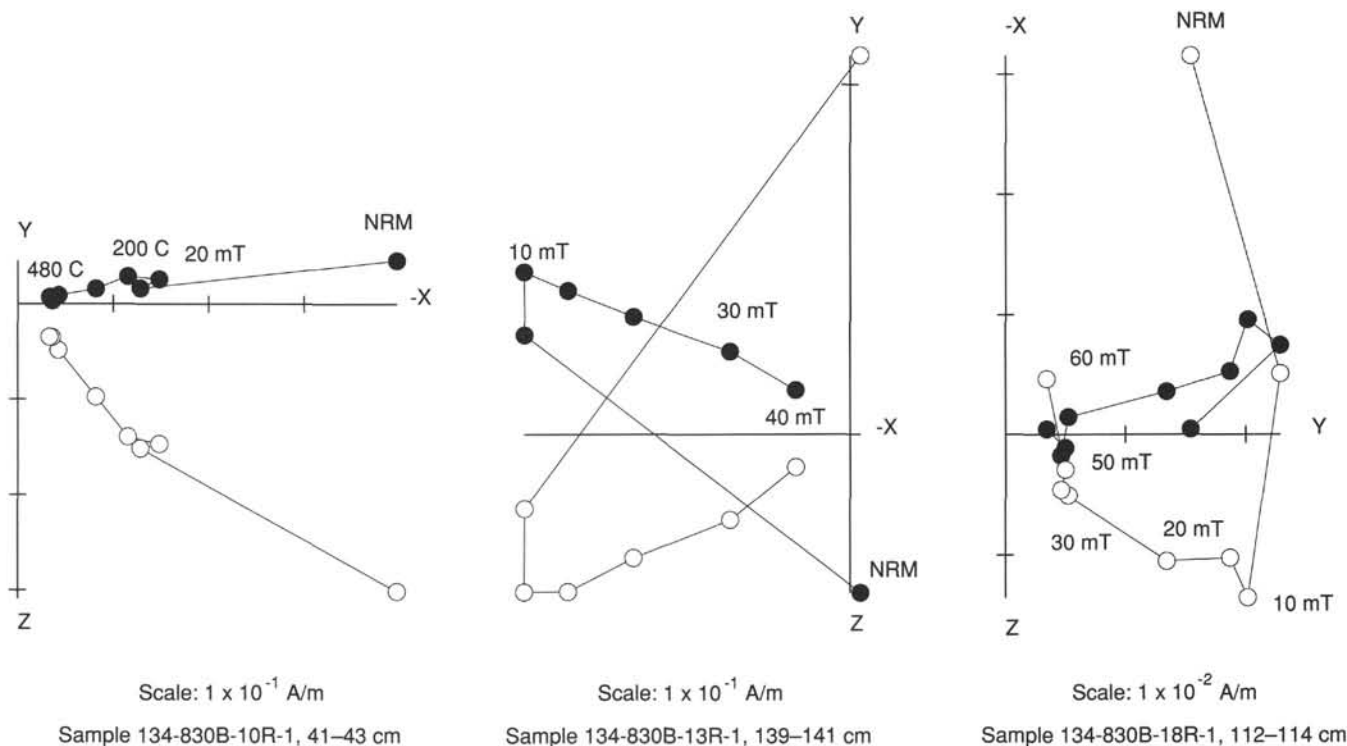


Figure 30. Representative vector endpoint diagrams showing the results of AF demagnetization of samples from Subunit IC and Unit II that exhibit positive inclinations. Open circles represent vector endpoints projected onto the vertical plane; solid circles represent endpoints projected onto the horizontal plane.

also occur. The volcanic breccia is composed of volcanic rock fragments; two fragments of fine-grained gabbro were found within this breccia. Overall, the rocks of Unit II appear to be the product of explosive events, based on the brecciated and quenched nature of the rock. Perhaps they were formed in association with the volcanic activity that built Espiritu Santo and Malakula islands. Petrology of Unit II is similar to the monolithic, volcanoclastic coarse breccias of the early Miocene Buvo Division of the Lower Santo Volcanics Subgroup exposed along the southwest end of Espiritu Santo Island, which were derived by fragmentation of basaltic and andesitic lavas and regarded as submarine accumulations near volcanic source vents (Mallick and Greenbaum, 1977). Similar types of rocks were formed in the central region of Malakula Island and consist of volcanic breccias and unsorted, unstratified submarine and subaerial autobreccias of the lower Miocene Matanui Volcanic Series, which are the product of submarine volcanoes (Mitchell, 1971). In addition, patches of highly oxidized volcanic matrix observed throughout Unit II suggests that subaerial erosion may have taken place.

Structural analyses of cores obtained at Site 830 indicate that the stratigraphy can be divided into two tectonic units, which correlate well with the lithostratigraphic units. For example, tectonic Unit A corresponds with lithostratigraphic Unit I, and tectonic Unit B corresponds with lithostratigraphic Unit II, the boundary of the two units being at 174.9 mbsf (Fig. 44). Tectonic Unit A is disturbed only by minor, steeply dipping faults and fractures, whereas tectonic Unit B has undergone cataclastic deformation. In the upper part of tectonic Unit A bedding attitudes vary from horizontal at 15 and 45 to 80 mbsf to 5° or more with a southeast dip at 15 to 45 mbsf. Tectonic Unit B (lithostratigraphic Unit II) is a coarse-grained, volcanoclastic, silty sed-lithic sandstone that has undergone brittle deformation and is considered a cataclastite.

The distinct differences in the tectonic style of the two units at this site suggest that either tectonic Unit B (lithostratigraphic Unit II) was structurally deformed before the deposition of tectonic Unit A (lithostratigraphic Unit I), or that differential deformation of both units may have occurred within a common stress field.

Nannofossil and foraminiferal biostratigraphic analyses indicate that lithostratigraphic Unit I is Pleistocene in age; however, the age of Unit II could not be determined because samples from this unit are barren. Both reworked Pliocene foraminifers and reworked Miocene and Pliocene nannofossils were found throughout the samples examined at Site 830. Paleomagnetic studies indicate that strata cored within lithostratigraphic Unit I (0–47 mbsf) were deposited during the Brunhes Chron (Fig. 44). On the basis of benthic foraminifers, the depositional environment of lithostratigraphic Unit I appears to have been in the middle to lower bathyal zone. Accurate sediment accumulation rates could not be determined for this unit because of the low biostratigraphic resolution.

Initial interpretation of the cores obtained at Site 830 and preliminary comparison with rock units defined on the islands of Espiritu Santo and Malakula (Mitchell, 1971; Mallick and Greenbaum, 1977) indicate that the sedimentary rocks penetrated by the drill are derived from the New Hebrides Island Arc and appear to have been deformed by the collision of the DEZ, and more recently by the Bougainville Guyot. Seismic reflection profiles show the location of this site to be near the western edge of a gentle, easterly dipping thrust sheet (Fig. 43), one of several imbricated thrusts that accommodates the foreshortening of the forearc slope by collisional processes. A series of east-dipping reflectors exist at this site and two strong reflectors, one at 1.5 s and another at 2.0 s (two-way traveltime), were the objectives of drilling (see "Seismic Stratigraphy" section, this chapter). These reflectors are

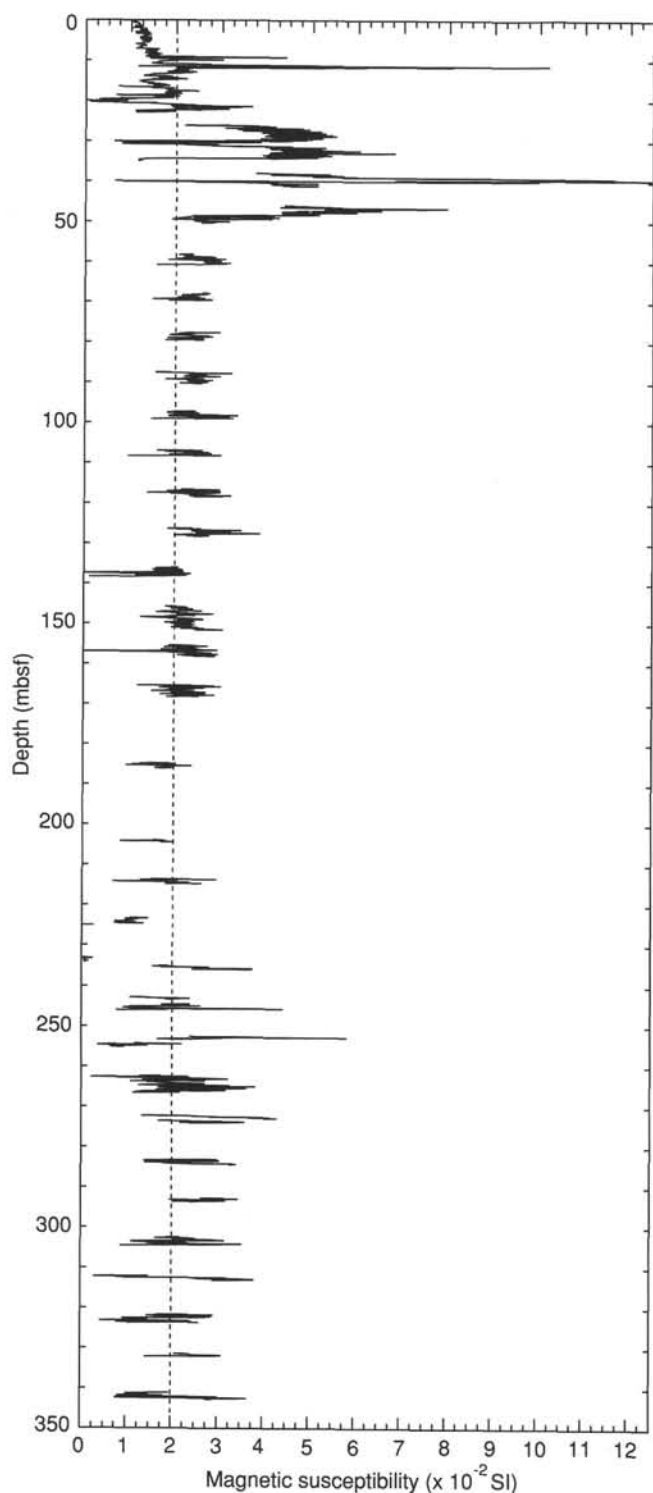


Figure 31. Magnetic susceptibility as a function of sub-bottom depth, Site 830. Dashed line indicates average magnetic susceptibility.

interpreted as stratigraphic horizons, wholly within arc rocks and disrupted by thrust faulting, that represent surfaces of carbonate blocks or the debris apron of the subducted and buried eastern part of the guyot that has been accreted to the arc. We were unable to reach these deeper reflectors and confirm the existence of guyot fragments because of hole collapse. However, we did penetrate the upper surface of the

1.5-s strong reflector. The existence of a cataclasite at this horizon suggests that severe mechanical stress has occurred here, perhaps along the plane of the stratigraphic horizon (bedding plane movement) and in association with the foreshortening of the forearc.

Study of pore fluids obtained from the cores at Site 830 was found to be significant in the understanding of diagenetic and hydrologic origins of fluids in accretionary wedges. Similar to what has been found in other accretionary wedges, such as in the Barbados (Biju-Duval, Moore, et al., 1984; Mascle, Moore, et al., 1988) and Nankai (Taira, Hill, Firth, et al., 1991) regions, dewatering of the sediments appears to have occurred as the water yield decreased sharply from the seawater interface to 50 mbsf, but chlorides increased in Hole 830B to 620 mM at 214 mbsf in lithostratigraphic Unit II, within the cataclasite of tectonic Unit B. Methane concentrations from headspace samples were higher at this site than observed in any of the previous sites of this leg. This methane was found within lithostratigraphic Unit I, but not along the cataclastic zone. Along with this methane, at 30–90 mbsf heavier hydrocarbons (ethane and propane) were found; another strong methane maximum—this time without the heavier hydrocarbons—was also found at 145 mbsf. At these depths the foraminifer *Bulimina striata*, which may indicate the existence of methane during the time of deposition (Akimoto, 1990), was found in the cores as well. The steepest concentration gradients of magnesium, calcium, sodium, and potassium found at Site 830 occur across the contact of lithostratigraphic Units I and II. This is attributed to the alteration of volcanic ash and basement rocks beneath the contact with diffusion away from the zones of intense reaction (see “Sediment and Fluid Geochemistry” section, this chapter). The deepest sample taken at this site contains the extraordinarily high calcium concentration of 229.2 mM, possibly the highest calcium concentration measured during either DSDP or ODP.

The extreme fluid compositions measured at Site 830 may result from the intense tectonic deformation that is occurring from the impact of the Bougainville Guyot with the New Hebrides Island Arc. A strong decrease in water content downsection (see “Sediment and Fluid Geochemistry” and “Physical Properties” sections, this chapter) implies compressional dewatering. Water content decreased from 84.7% at the surface to about 23.0% at 100 mbsf, and 10%–11.0% at 283.1 mbsf. Fracturing of volcanic rocks from collision facilitates increased alteration and fluid flow. Foreshortening of the forearc resulting in the formation of imbricate thrust sheets appears to have stacked small fragments of highly fractured basement rocks on fluid-rich sediments. The sandy intervals can then form conduits for mineral-rich fluid flow and the thrust zones themselves also act as conduits.

REFERENCES

- Akimoto, K., 1990. Distribution of Recent benthic foraminiferal faunas in the Pacific off Southwest Japan and around Hachijojima Island. *Sci. Rep. Tohoku Univ., Ser. 2*, 60:139–223.
- Akimoto, K., Tanaka, T., Hattori, M., and Hotta, H., 1990. Recent foraminiferal assemblages around Calyptogena colony off Hatusushima Island, Sagami Bay, central Japan. *Technical Reports of the Symposium of Deep-sea Research Using Submersible Shinkai 2000 System*. Jpn. Mar. Sci. Tech. Center, Yokosura.
- Aubouin, J., von Huene, R., et al., 1982. *Init. Repts. DSDP*, 67: Washington (U.S. Govt. Printing Office).
- Biju-Duval, B., Moore, J. C., et al., 1984. *Init. Repts. DSDP*, 78A: Washington (U.S. Govt. Printing Office).
- Bray, C. J., and Karig, D. E., 1982. Porosity of sediments in accretionary prisms and some implications for dewatering processes. *J. Geophys. Res.*, 90:768–778.

- Collot, J.-Y., Daniel, J., and Burne, R. V., 1985. Recent tectonics associated with the subduction/collision of the d'Entrecasteaux zone in the central New Hebrides. *Tectonophysics*, 112:325-356.
- Collot, J.-Y., and Fisher, M. A., 1989. Formation of forearc basins by collision between seamounts and accretionary wedges: an example from the New Hebrides subduction zone. *Geology*, 17:930-933.
- Collot, J.-Y., Pelletier, B., Boulin, J., Daniel, J., Eissen, J.-P., Fisher, M. A., Greene, H. G., Lallemand, S., and Monzier, M., 1989. Premiers résultats des plongées de la campagne SUBPSO1 dans la zone de collision des rides d'Entrecasteaux et de l'arc des Nouvelles Hébrides. *C. R. Acad. Sci. Ser. 2*, 309:1947-1954.
- Daniel, J., Collot, J. Y., Monzier, M., Pelletier, B., Butscher, J., Deplus, C., Dubois, J., Gérard, M., Maillat, P., Monjaret, M. C., Récy, J., Renard, V., Rigolot, P., and Temakon, S. J., 1986. Subduction et collision le long de l'arc des Nouvelles-Hébrides (Vanuatu): résultats préliminaires de la campagne SEAPSO (Leg 1). *C. R. Acad. Sci. Ser. 2*, 303:805-810.
- Fisher, M. A., Collot, J.-Y., and Smith, G. L., 1986. Possible causes for structural variation where the New Hebrides island arc and the d'Entrecasteaux zone collide. *Geology*, 14:951-954.
- Gieskes, J. M., 1981. Deep-sea drilling interstitial water studies: implications for chemical alteration of the oceanic crust, layers I and II. In Warne, J. E., Douglas, R. G., and Winterer, E. L. (Eds.), *The Deep Sea Drilling Project: A Decade of Progress*. Soc. Econ. Paleontol. Mineral. Spec. Publ., 32:149-167.
- Gorton, M. P., 1974. The geochemistry and geochronology of the New Hebrides [Ph.D. dissert.]. Australian National Univ., Canberra.
- , 1977. The geochemistry and origin of Quaternary volcanism in the New Hebrides. *Geochim. Cosmochim. Acta*, 41:1257-1270.
- Lawrence, J. R., and Gieskes, J. M., 1981. Constraints on water transport and alteration in the oceanic crust from the isotopic composition of pore water. *J. Geophys. Res.*, 86:7924-7934.
- Macfarlane, A., and Carney, J. N., 1987. *Geology and Mineralisation of North and Central Malakula*. Vanuatu Dept. of Geol., Mines and Rural Water Supplies.
- Mallick, D.I.J., and Greenbaum, D., 1977. *Geology of Southern Santo*. Regional Rept.—New Hebrides Geol. Surv., 1-84.
- Masclé, A., Moore, J. C., et al., 1988. *Proc. ODP, Init. Repts.*, 110: College Station, TX (Ocean Drilling Program).
- McDuff, R. E., 1981. Major cation gradients in DSDP interstitial waters: the role of diffusive exchange between seawater and upper ocean crust. *Geochim. Cosmochim. Acta*, 45:1705-1713.
- McDuff, R. E., and Gieskes, J. M., 1976. Calcium and magnesium profiles in DSDP interstitial waters: diffusion or reaction? *Earth Planet. Sci. Lett.*, 33:1-10.
- Mitchell, A.H.G., 1966. *Geology of Southern Malekula*. Regional Rept.—New Hebrides Geol. Surv., No. 3.
- , 1971. *Geology of Northern Malekula*. Regional Rept.—New Hebrides Geol. Surv.
- Miyashiro, A., 1978. Nature of alkaline volcanic rock series. *Contrib. Mineral. Petrol.*, 66:91-104.
- Pearce, J. A., 1982. Trace element characteristics of lavas from destructive plate boundaries. In Thorpe, R. S. (Ed.), *Andesites: Orogenic Andesites and Related Rocks*: New York (Wiley), 525-548.
- Robinson, G. P., 1969. *The Geology of Northern Santo*. Regional Rept.—New Hebrides Geol. Surv.
- Suess, E., von Huene, R., et al., 1988. *Proc. ODP, Init. Repts.*, 112: College Station, TX (Ocean Drilling Program).
- Taira, A., Hill, I., Firth, J., et al., 1991. *Proc. ODP, Init. Repts.*, 131: College Station, TX (Ocean Drilling Program).
- Taylor, F. W., Frohlich, C., Lecolle, J., and Strecker, M., 1987. Analysis of partially emerged corals and reef terraces in the central Vanuatu arc: comparison of contemporary coseismic and nonseismic with Quaternary vertical movements. *J. Geophys. Res.*, 92:4905-4933.
- Wilson, M., 1989. *Igneous Petrogenesis: A Global Tectonic Approach*: London (Unwin Hyman).

Ms 134A-110

NOTE: All core description forms ("barrel sheets") and core photographs have been printed on coated paper and bound as Section 4, near the back of this volume, beginning on page 581.

Table 6. Index properties data, Site 830.

Sample (cm)	Depth (mbsf)	Unit	Wet-bulk density (Mg/m ³)	Dry-bulk density (Mg/m ³)	Grain density (Mg/m ³)	Porosity		Water content	
						Wet (%)	Dry (%)	Wet (%)	Dry (%)
134-830A-									
1H-1, 3	0.03	IA	1.60	0.87	2.74	71.8	69.6	45.9	84.7
1H-3, 3	3.03	IA	1.79	1.14	2.76	62.7	60.5	36.0	56.2
1H-5, 3	6.03	IA	1.81	1.19	2.72	60.1	58.0	34.0	51.6
2H-2, 27	8.77	IA	1.83	1.22	2.72	59.3	57.1	33.2	49.7
2H-4, 50	12.00	IA	1.82	1.17	2.78	63.0	60.3	35.6	55.2
2H-6, 85	15.35	IA	1.56	1.17	2.73	37.7	47.0	24.8	33.0
3H-1, 122	17.72	IA	1.94	1.36	2.74	56.8	53.6	30.0	42.8
3H-3, 122	20.72	IB	2.02	1.51	2.73	49.1	47.2	24.9	33.2
3H-5, 35	22.85	IB	2.07	1.47	2.78	58.2	52.7	28.8	40.5
3H-7, 45	25.95	IB	2.17	1.71	2.85	44.5	42.7	21.0	26.6
4H-1, 70	26.70	IB	2.12	1.70	2.82	41.2	40.7	19.9	24.8
4H-3, 70	29.70	IB	2.20	1.76	2.75	42.4	40.0	19.8	24.6
5H-3, 85	34.25	IB	2.13	1.66	2.70	46.1	43.1	22.2	28.5
5H-5, 85	37.25	IB	2.08	1.57	2.68	50.0	46.3	24.6	32.7
6H-1, 55	40.45	IB	2.14	1.67	2.77	46.6	43.9	22.3	28.7
6H-3, 57	43.47	IB	2.24	1.80	2.81	43.3	40.6	19.8	24.7
7X-1, 57	49.07	IC	2.05	1.65	2.61	38.4	37.9	19.2	23.8
7X-CC, 22	49.72	IC	2.52	1.87	2.77	63.5	48.7	25.8	34.8
134-830B-1R-1, 142	49.92	IC	2.04	1.50	2.74	52.7	49.2	26.4	35.9
134-830A-8X-CC, 16	58.36	IC	2.36	1.93	2.75	41.8	37.6	18.2	22.2
134-830B-2R-2, 100	60.60	IC	2.15	1.67	2.71	46.2	43.0	22.0	28.3
134-830A-9X-CC, 28	68.18	IC	2.13	1.68	2.73	44.5	42.2	21.4	27.2
134-830B-									
3R-1, 127	68.97	IC	2.06	1.56	2.69	48.4	45.7	24.1	31.7
4R-2, 10	78.70	IC	2.14	1.68	2.75	44.1	42.1	21.1	26.8
5R-2, 137	90.27	IC	2.12	1.66	2.7	44.5	42.2	21.5	27.4
6R-1, 100	98.10	IC	2.20	1.78	2.73	41.1	38.8	19.1	23.6
7R-1, 105	107.85	IC	2.21	1.80	2.77	39.9	38.2	18.5	22.7
8R-1, 84	117.34	IC	2.21	1.79	2.8	41.9	39.8	19.4	24.0
9R-1, 37	126.57	IC	2.23	1.76	2.78	46.4	42.6	21.3	27.1
10R-1, 46	136.36	IC	2.32	1.87	2.7	43.6	38.8	19.2	23.8
11R-3, 37	148.97	IC	2.27	1.81	2.71	44.8	40.4	20.2	25.3
12R-1, 57	155.87	IC	2.24	1.82	2.71	41.6	38.5	19.0	23.4
13R-1, 54	165.74	IC	2.22	1.82	2.68	38.5	36.3	17.8	21.7
15R-1, 63	185.23	II	2.20	1.81	2.73	37.8	36.5	17.6	21.4
17R-1, 22	204.02	II	2.43	2.14	2.67	27.8	25.9	11.7	13.3
18R-1, 47	213.87	II	2.34	2.01	2.7	31.8	30.1	13.9	16.2
19R-1, 60	223.70	II	2.36	2.05	2.63	30.6	28.4	13.3	15.3
20R-1, 50	233.40	II	2.44	2.19	2.68	24.2	23.0	10.2	11.3
21R-1, 50	243.10	II	2.40	2.16	2.57	23.5	22.0	10.0	11.2
23R-1, 33	262.53	II	2.38	2.11	2.52	25.9	23.8	11.2	12.6
24R-1, 48	272.48	II	2.35	2.05	2.52	29.9	27.1	13.0	15.0
134-830C-									
5R-1, 20	273.50	II	2.42	2.14	2.58	27.2	24.9	11.5	13.0
6R-1, 17	283.07	II	2.44	2.19	2.51	23.5	21.3	9.9	11.0
7R-1, 37	292.97	II	2.46	2.19	2.62	26.2	24.0	10.9	12.2
8R-1, 100	303.30	II	2.33	2.04	2.58	28.2	26.4	12.4	14.1
9R-1, 57	312.47	II	2.34	2.07	2.52	26.4	24.5	11.6	13.1
10R-1, 143	322.93	II	2.41	2.16	2.59	23.7	22.3	10.1	11.2
12R-1, 56	341.99	II	2.34	1.99	2.59	34.4	31.2	15.1	17.7

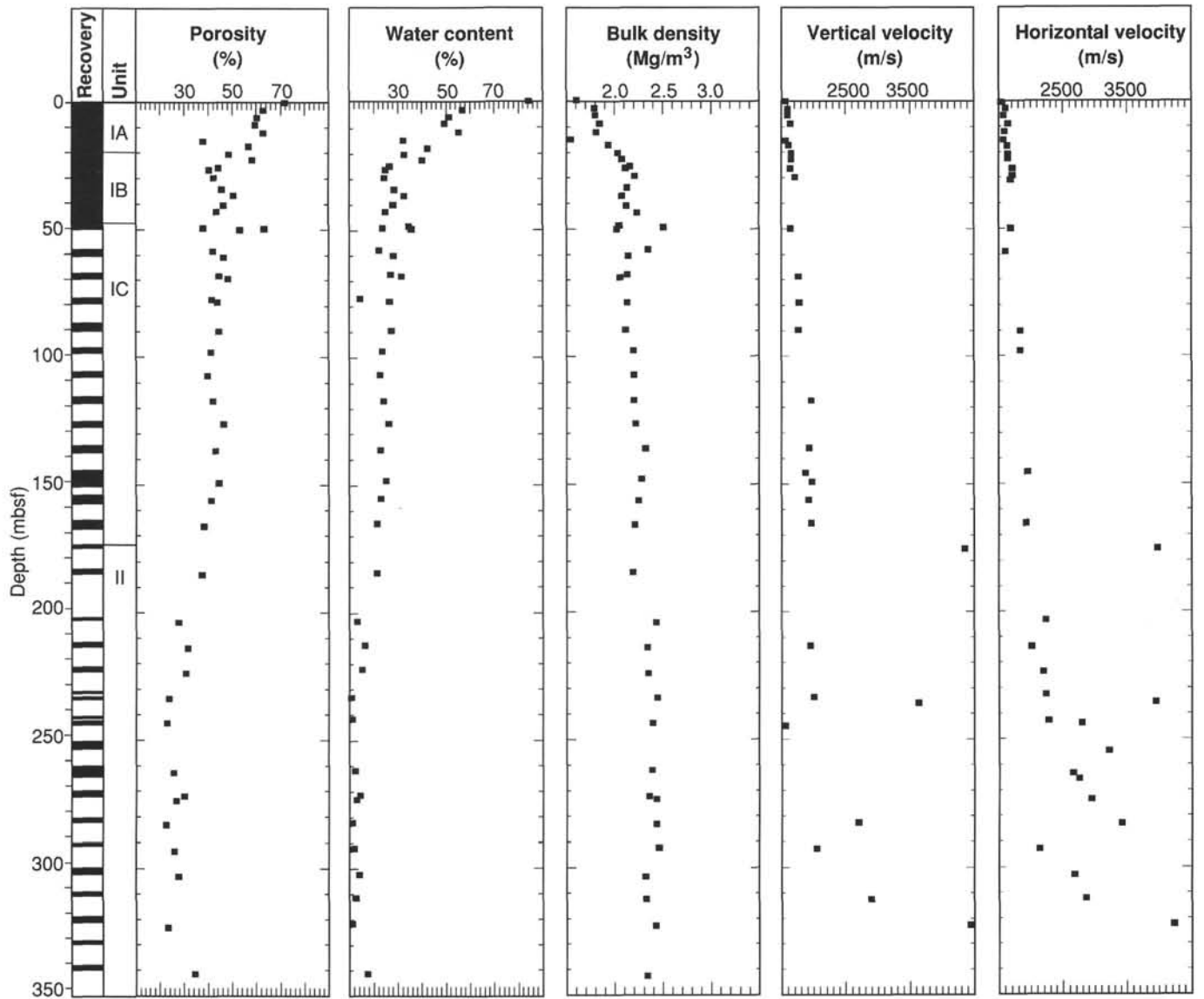


Figure 32. Porosity, water content, bulk density, and vertical and horizontal velocities vs. depth, Site 830.

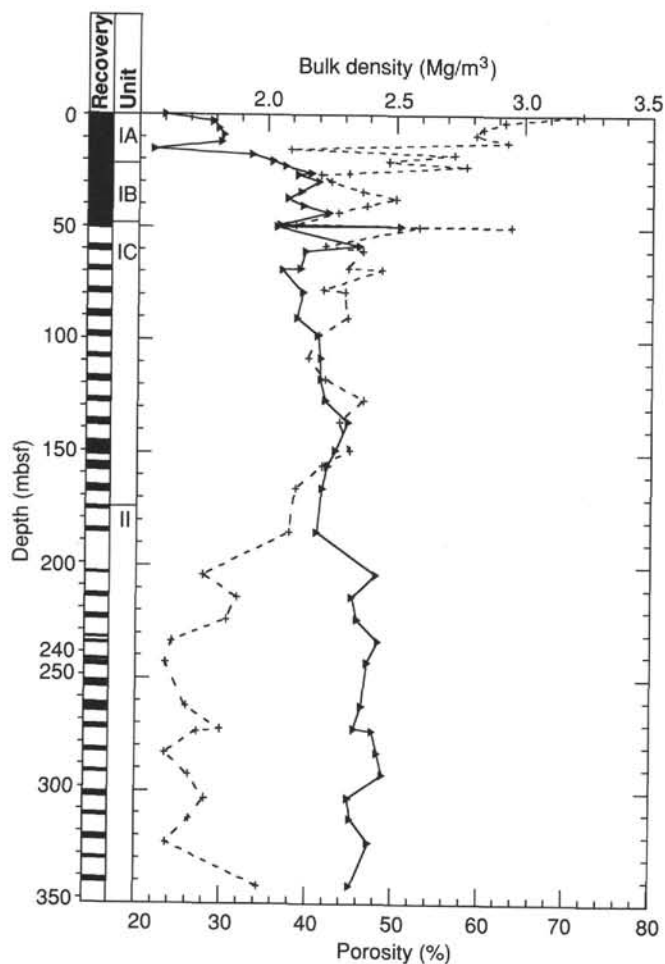


Figure 33. Bulk density (solid line) and porosity (dashed line) vs. depth, Site 830.

Table 7. Hamilton Frame sonic velocity data, Site 830.

Sample (cm)	Depth (mbsf)	Unit	Vertical velocity (m/s)	Wave type ^a	Horizontal velocity (m/s)	Wave type ^a
134-830A-						
1H-1, 3	0.03	IA	1538	C	1536	C
1H-3, 3	3.03	IA	1607	C	1599	C
1H-5, 3	6.03	IA	1592	C	1576	C
2H-2, 27	8.77	IA	1644	C	1640	C
2H-4, 50	12.00	IA			1566	S
2H-6, 85	15.35	IA	1585	C	1573	C
3H-1, 122	17.72	IA	1623	C	1625	C
3H-3, 122	20.72	IA	1639	C	1647	C
3H-5, 35	22.85	IB	1653	C	1646	C
4H-1, 70	26.70	IB	1622	C	1697	C
4H-3, 60	29.60	IB	1719	C	1717	C
5H-1, 90	31.30	IB			1706	C
134-830B-						
1R-1, 142	49.92	IC	1636	S	1688	S
2R-1, 130	59.40	IC			1612	C
3H-1, 127	68.97	IC	1778	C		
4R-2, 10	78.70	IC	1793	S		
5R-2, 137	90.27	IC	1757	C	1851	C
6R-1, 100	98.10	IC			1835	S
8R-1, 84	117.34	IC	1963	S		
10R-1, 46	136.36	IC	1942	C		
11R-1, 44	146.04	IC	1882	C	1961	C
11R-3, 37	148.97	IC	1978	C		
12R-1, 57	155.87	IC	1926	C		
13R-1, 54	165.74	IC	1962	C	1936	C
14R-1, 47	175.37	II	4358	C	3987	C
17R-1, 22	204.02	II			2234	C
18R-1, 47	213.87	II	1962	C	2007	C
19R-1, 60	223.70	II			2197	S
20R-1, 50	233.40	II	1998	S	2239	C
21R-1, 50	243.10	II			2281	S
134-830C-						
1R-1, 60	235.60	II	3632	C	3942	C
2R-1, 30	244.70	II	1576	C	2793	C
3R-1, 63	254.73	II			3220	C
4R-1, 48	264.18	II			2646	C
4R-2, 65	265.85	II			2736	C
5R-1, 20	273.50	II			2939	C
6R-1, 17	283.07	II	2703	C	3419	C
7R-1, 37	292.97	II	2042	S	2150	S
8R-1, 100	303.30	II			2681	S
9R-1, 57	312.47	II	2902	S	2865	S
10R-1, 143	322.93	II	4440	C	4233	C

^a C = compressional (P-wave) and S = shear (S-wave).

Table 8. Shear-strength data, Site 830.

Sample (cm)	Depth (mbsf)	Unit	Shear strength (kPa)
134-830A-			
1H-1, 3	0.03	IA	5.1
1H-3, 8	3.08	IA	42.5
1H-5, 8	6.08	IA	63.1
2H-2, 24	8.74	IA	55.7
2H-4, 47	11.97	IA	59.4
2H-6, 91	15.41	IA	115.1
3H-1, 127	17.77	IA	95.3
3H-3, 118	20.68	IA	92.4
3H-5, 31	22.81	IB	60.9
3H-7, 57	26.07	IB	44
4H-1, 76	26.76	IB	110.7
4H-3, 55	29.55	IB	69.6
5H-1, 92	31.32	IB	74
5H-3, 75	34.15	IB	134.9
6H-1, 62	40.52	IB	78.4
6H-6, 34	47.74	IB	27.9
7H-1, 56	49.06	IC	40.3

^a Values determined by Wykeham-Farrance spring vane-shear apparatus.

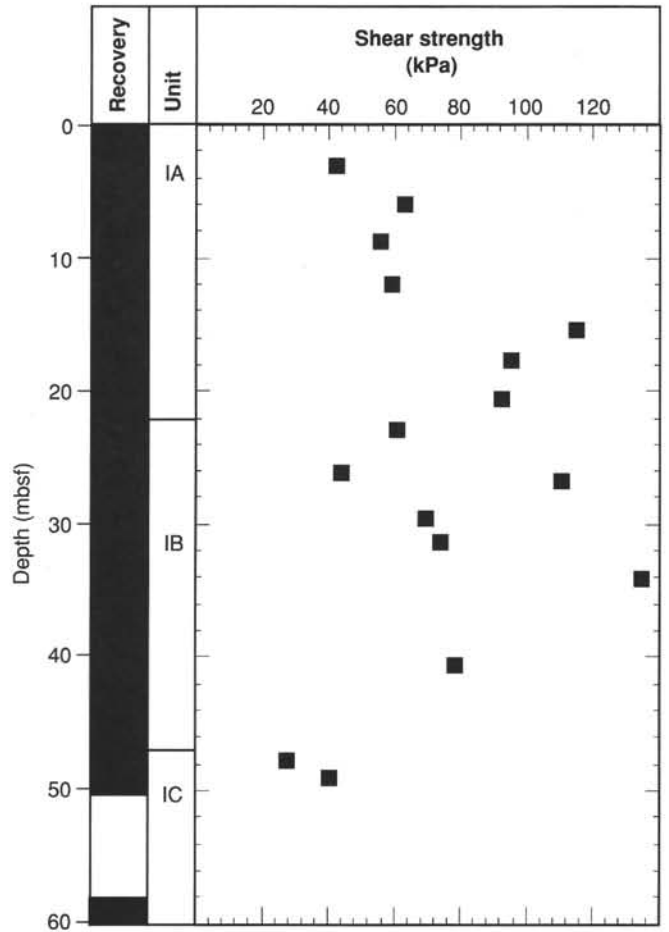


Figure 34. Shear strength vs. depth, Hole 830A.

Table 9. Thermal conductivity data, Site 830.

Sample (cm)	Depth (mbsf)	Unit	Value (W/(m · K))
134-830A-			
1H-2, 75	2.25	IA	1.0587
1H-3, 75	3.75	IA	1.0354
1H-4, 75	5.25	IA	0.9983
1H-5, 35	6.35	IA	1.0307
2H-2, 75	9.25	IA	1.1127
2H-3, 75	10.75	IA	0.9921
2H-5, 75	13.75	IA	0.9939
2H-6, 75	15.25	IA	0.9739
3H-1, 75	17.25	IA	1.2366
3H-2, 75	18.75	IA	1.0477
3H-3, 75	20.25	IA	0.8453
3H-4, 75	21.75	IB	1.1649
4H-1, 75	26.75	IB	1.3880
4H-2, 75	28.25	IB	1.2999
4H-3, 50	29.50	IB	1.1723
5H-1, 75	31.15	IB	1.1941
5H-2, 75	32.65	IB	1.2581
5H-3, 75	34.15	IB	1.1113
6H-1, 60	40.50	IB	1.2885
7X-1, 55	49.05	IC	1.2391

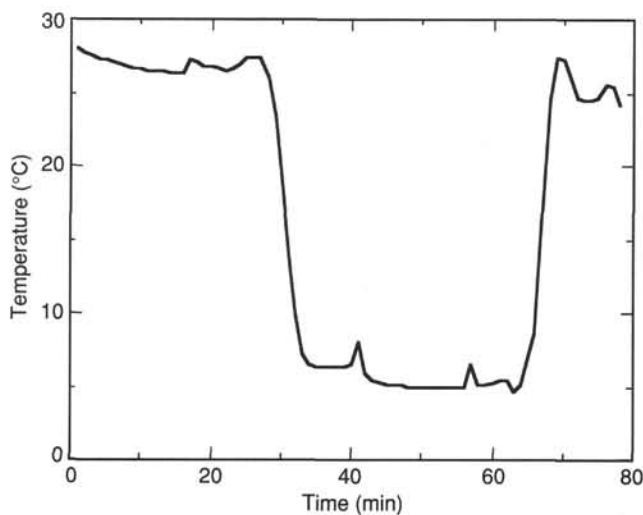


Figure 36. Temperature vs. time for water sampler temperature probe (WSTP) run 5H in Hole 830A at a depth of 30.4 mbsf.

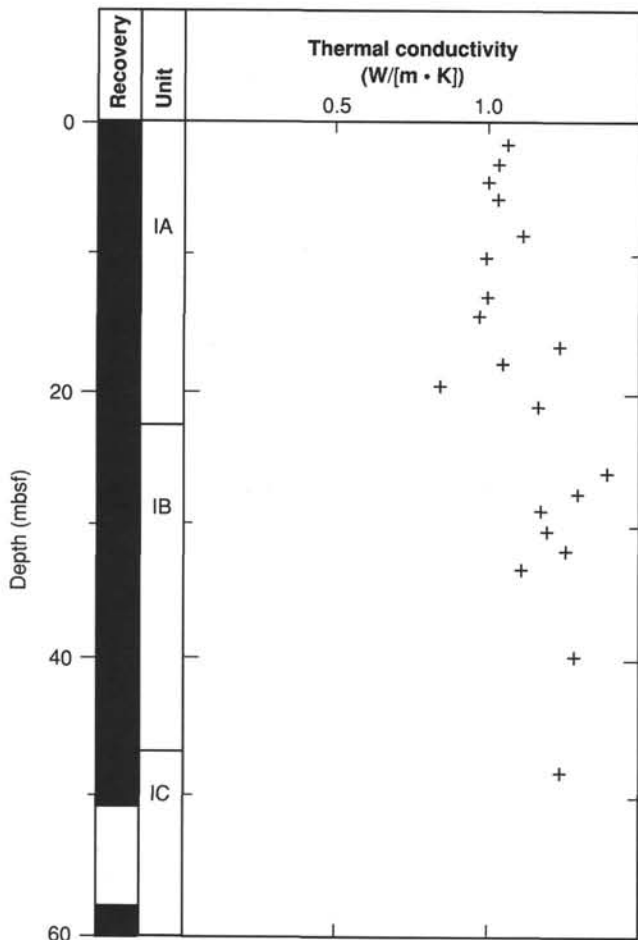


Figure 35. Thermal conductivity vs. depth, Site 830.

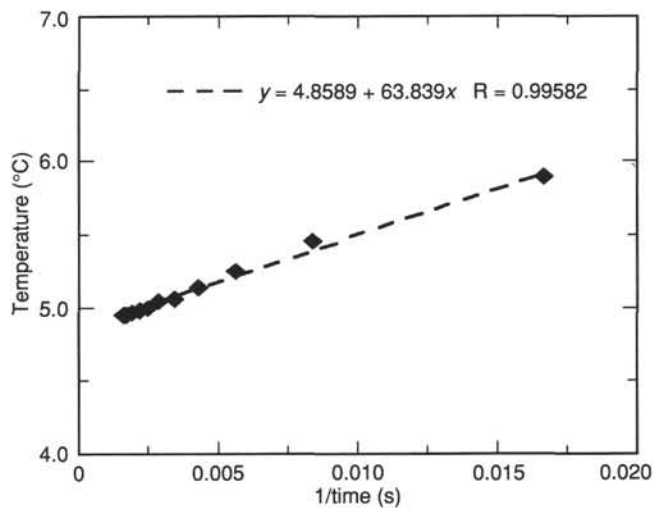


Figure 37. Reduction to equilibrium temperature for WSTP run 5H in Hole 830A. The temperature value at 1/time = 0 is the equilibrium value.

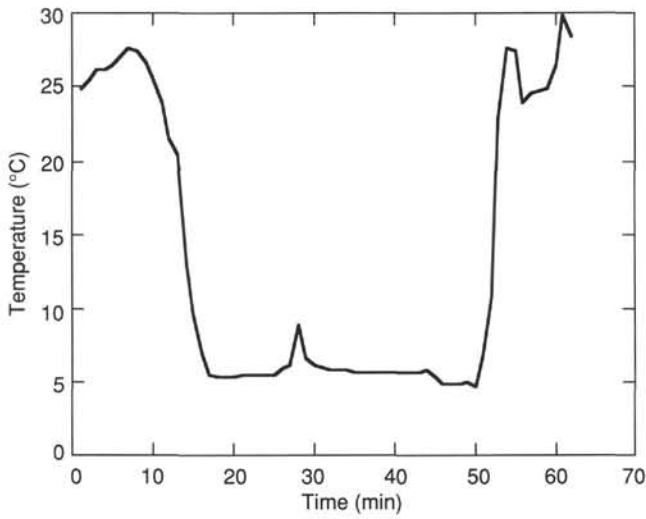


Figure 38. Temperature vs. time for WSTP run 9X in Hole 830A at a depth of 67.9 mbsf.

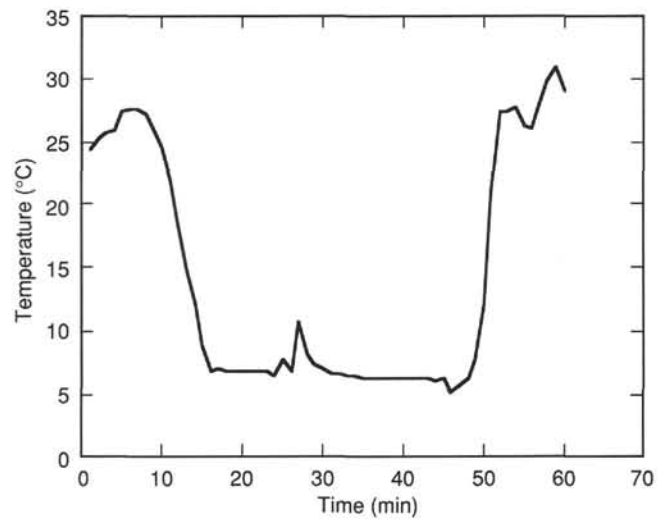


Figure 40. Temperature vs. time for WSTP run 12X in Hole 830A at a depth of 96.9 mbsf.

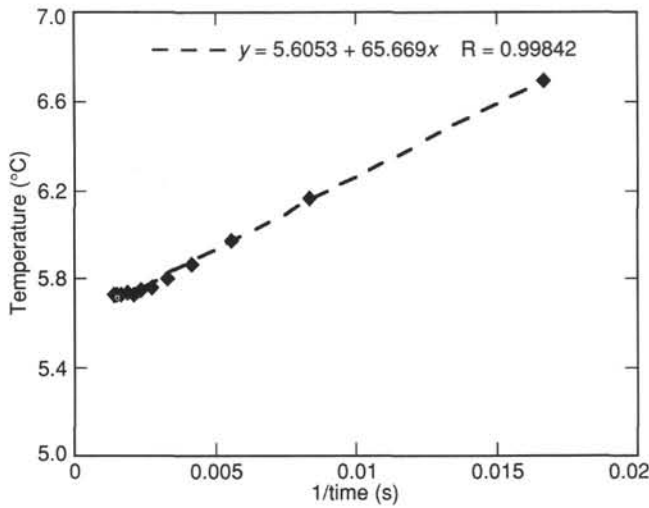


Figure 39. Reduction to equilibrium temperature (1/time = 0) for WSTP run 9X in Hole 830A.

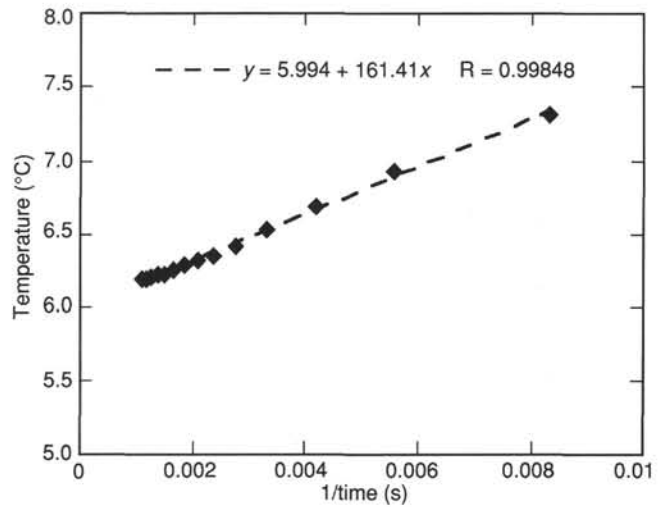


Figure 41. Reduction to equilibrium temperature (1/time = 0) for WSTP run 12X in Hole 830A.

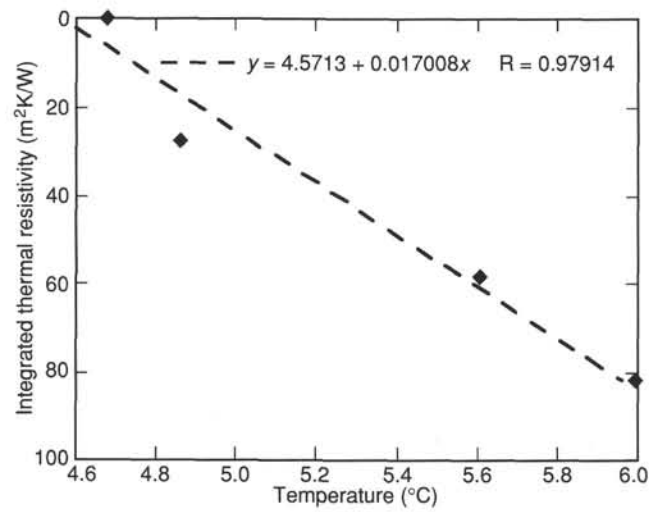


Figure 42. Temperature vs. the depth integral of thermal resistivity for Site 830. The slope of the linear regression line is the conductive heat flow.

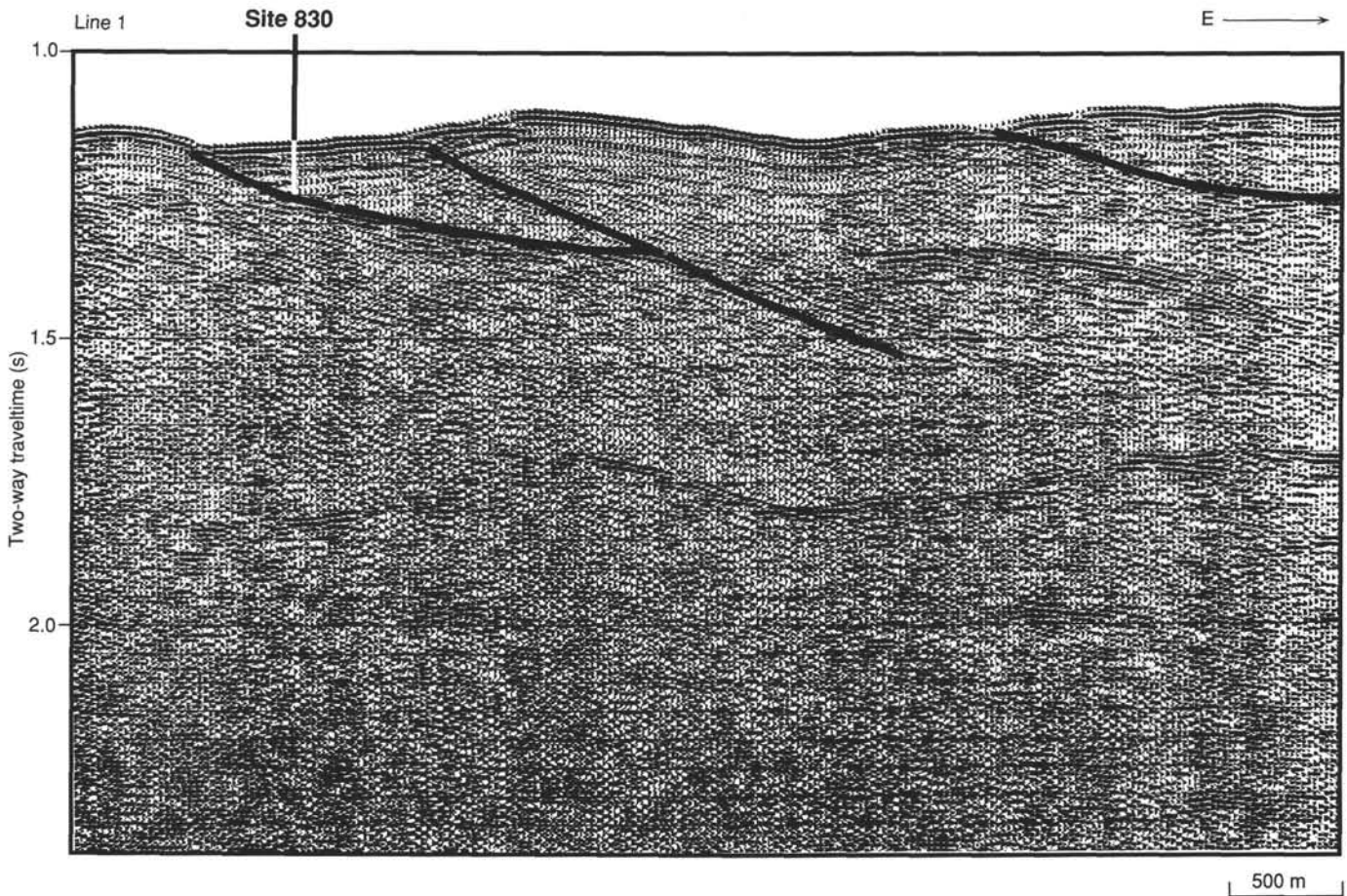


Figure 43. Single-channel seismic reflection profile collected by the *JOIDES Resolution* during the site survey for Site 830. Thrust faults shown by solid lines.

Hole 830A

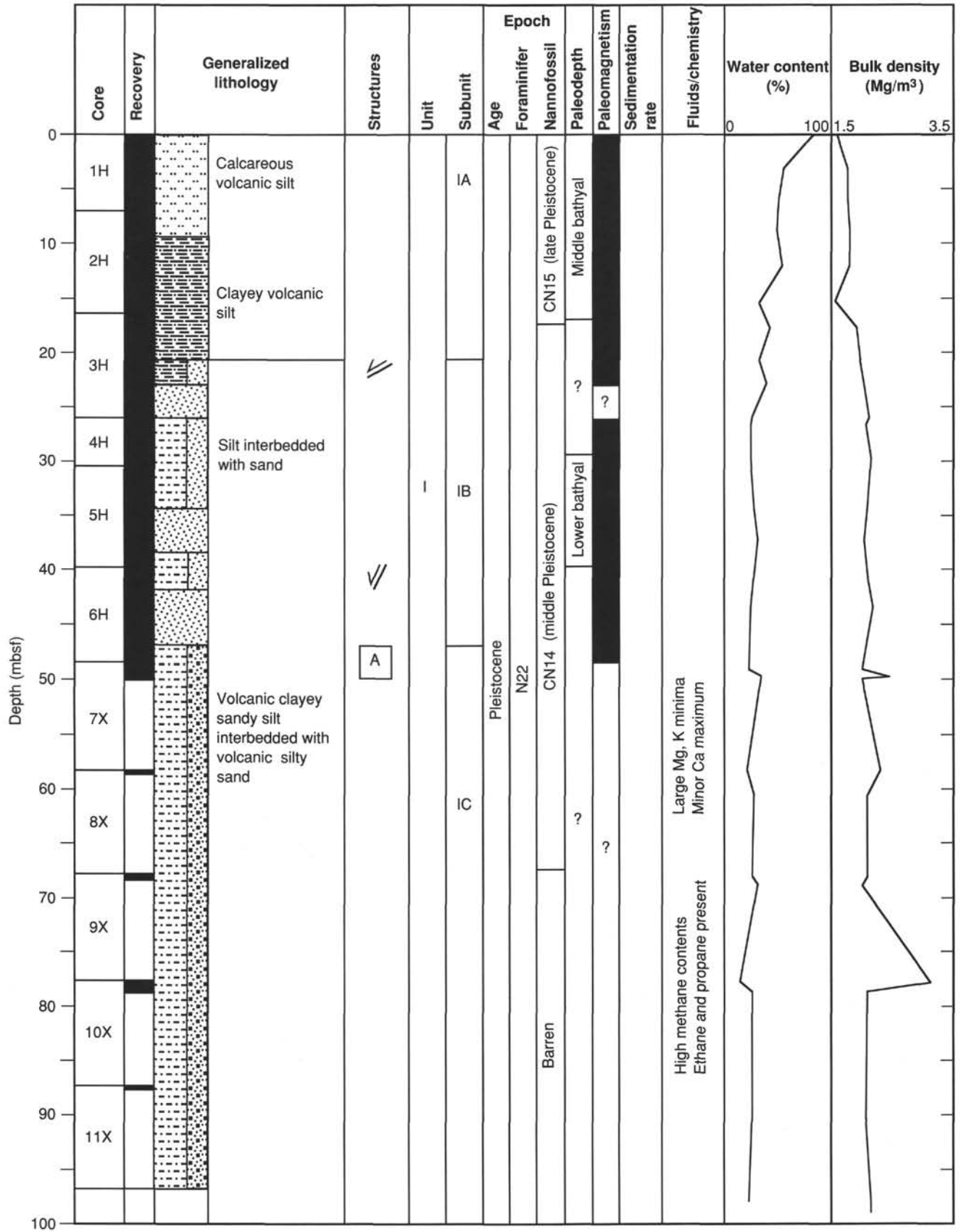


Figure 44. Master columns for Site 830 showing summary of lithostratigraphy and other information interpreted from drilling results. If no data or annotations appear in a particular column, please refer to the appropriate section of this chapter for details.

Hole 830B

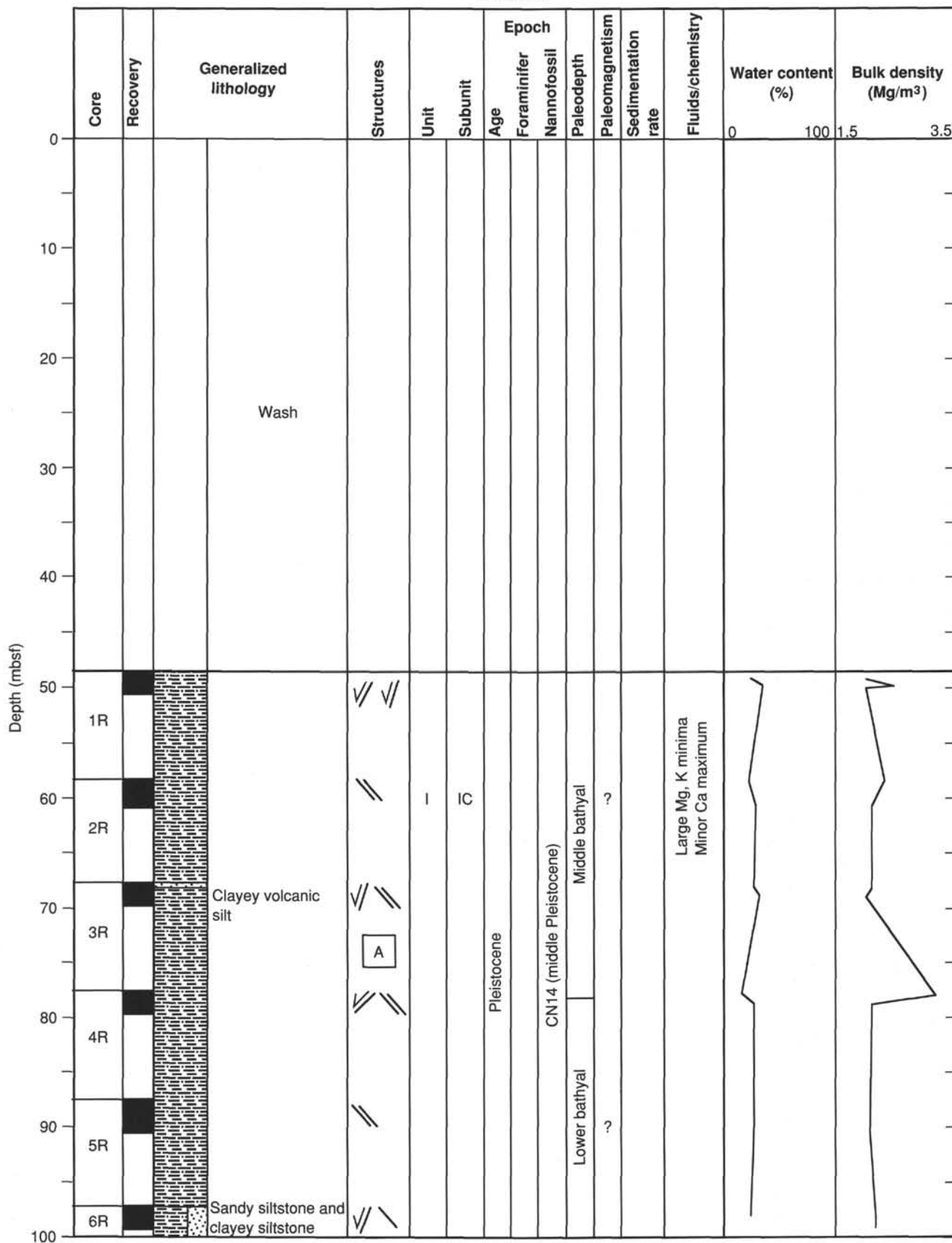


Figure 44 (continued).

Hole 830B (continued)

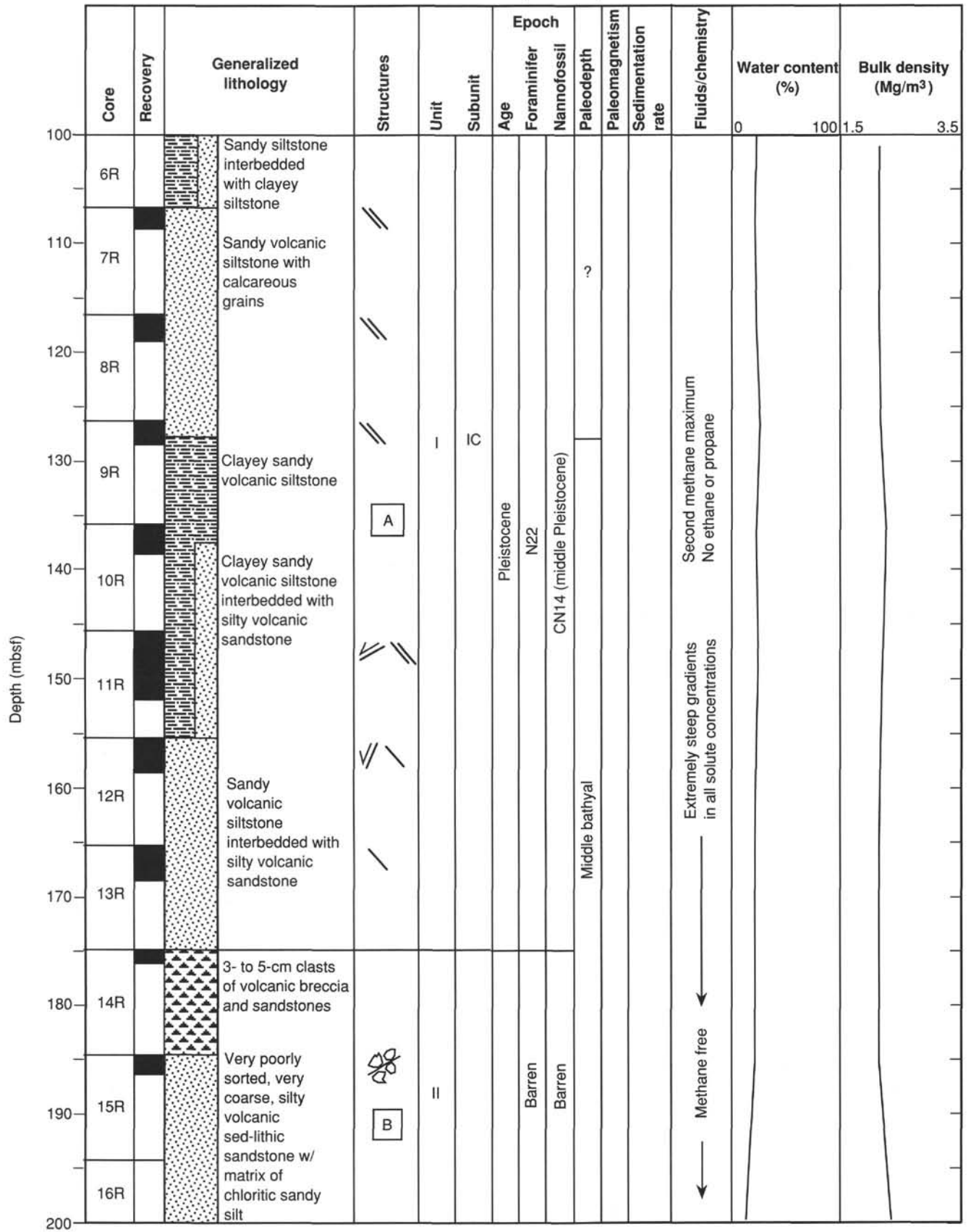


Figure 44 (continued).

Hole 830B (continued)

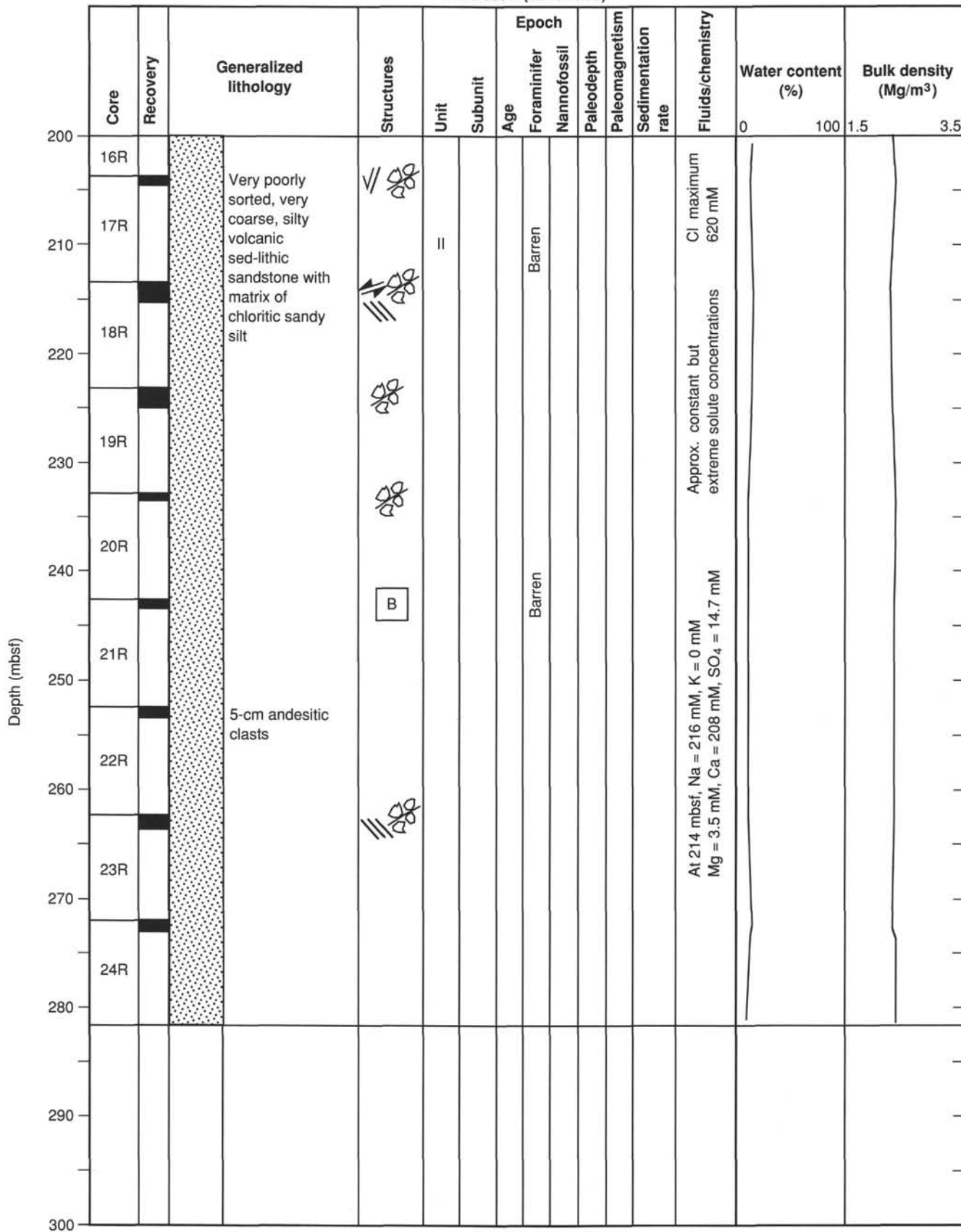


Figure 44 (continued).

Hole 830C

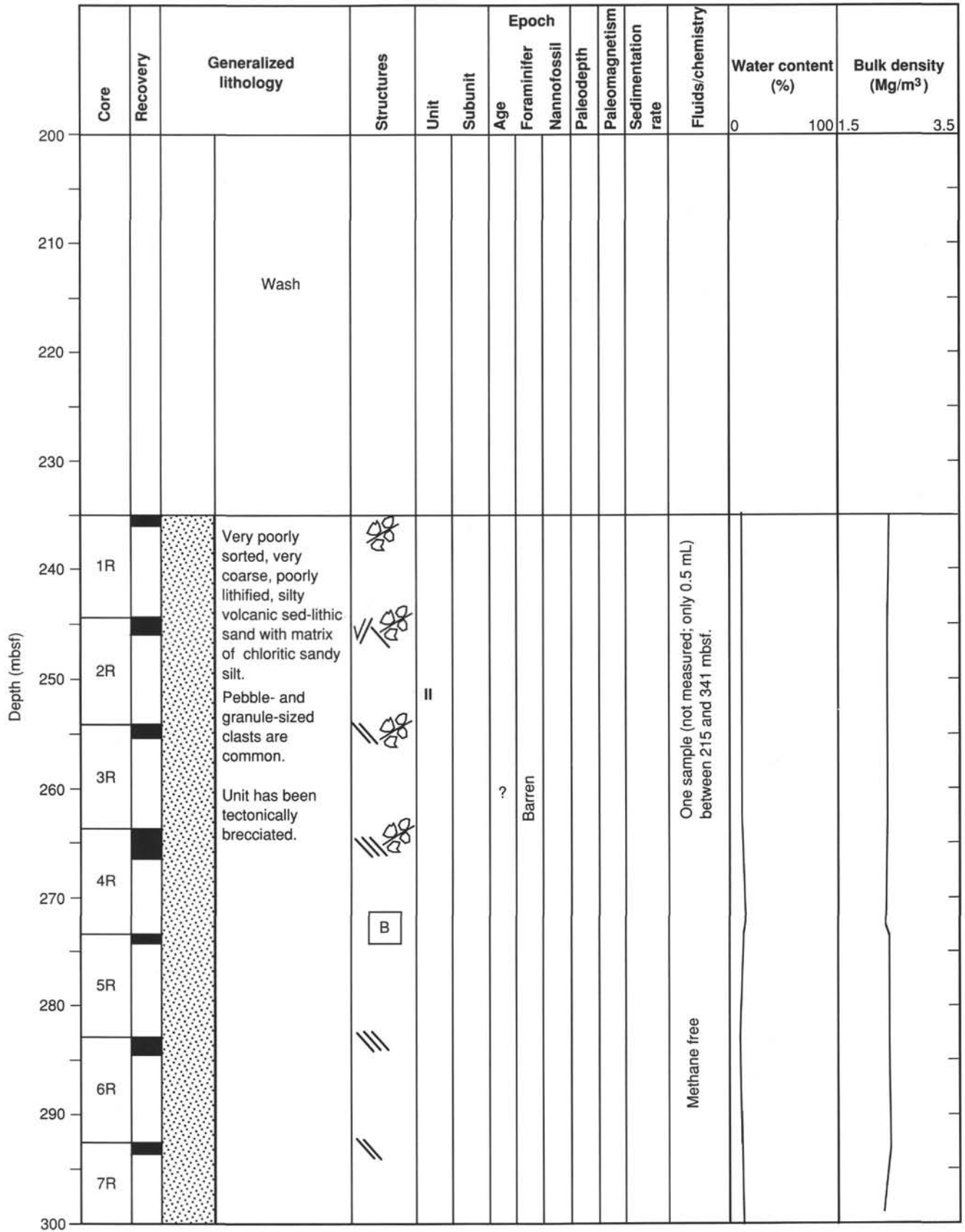


Figure 44 (continued).

Hole 830C (continued)

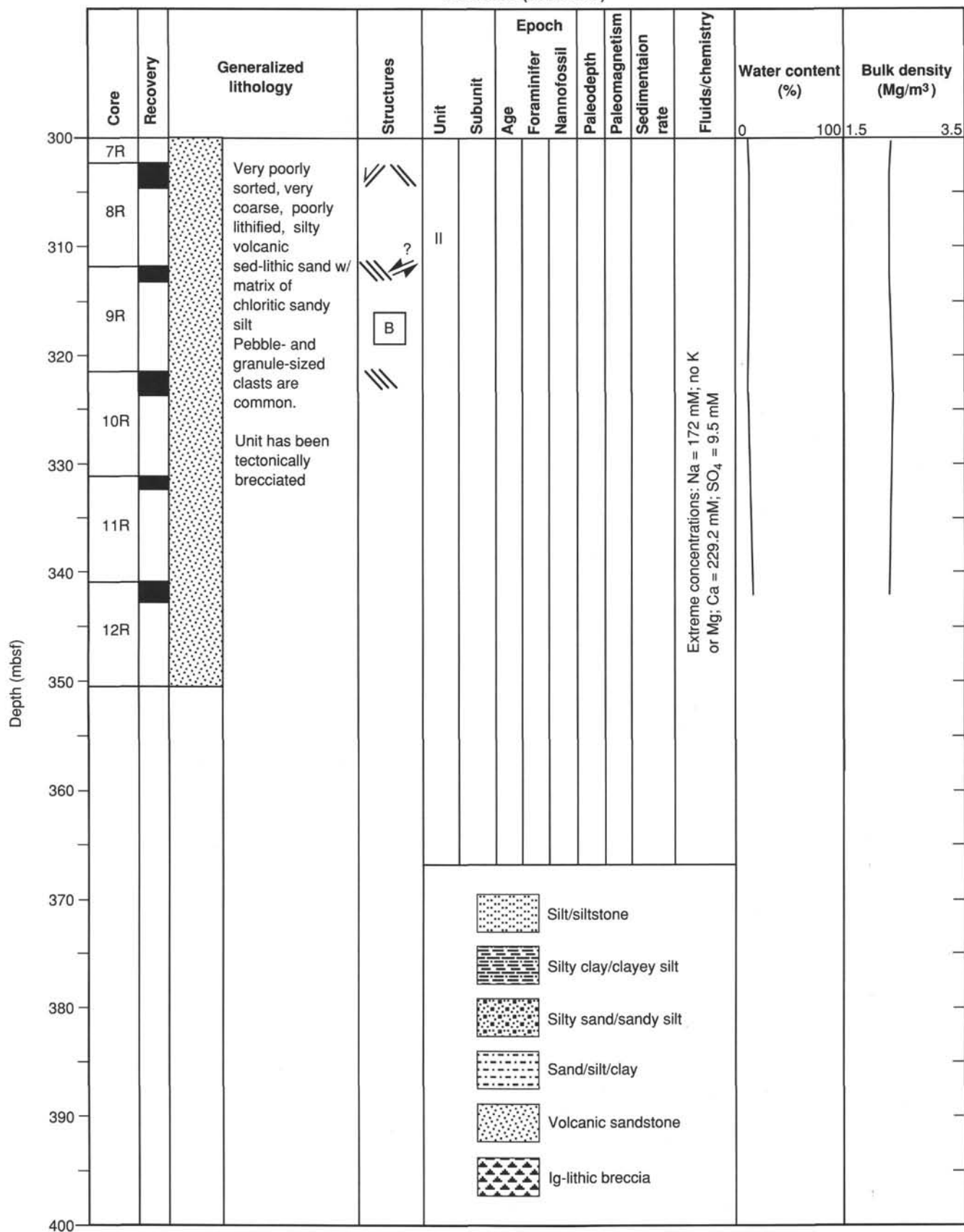
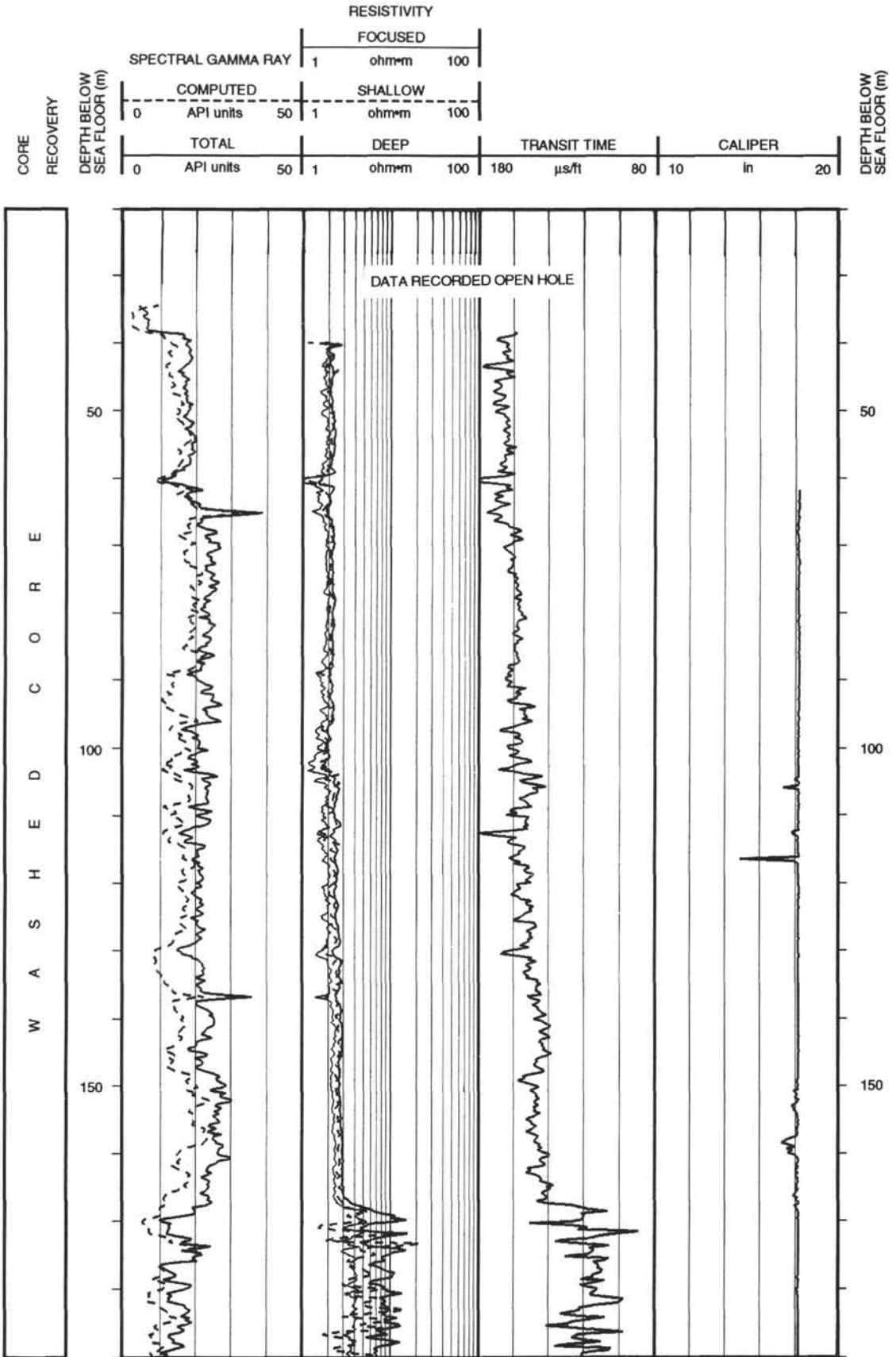
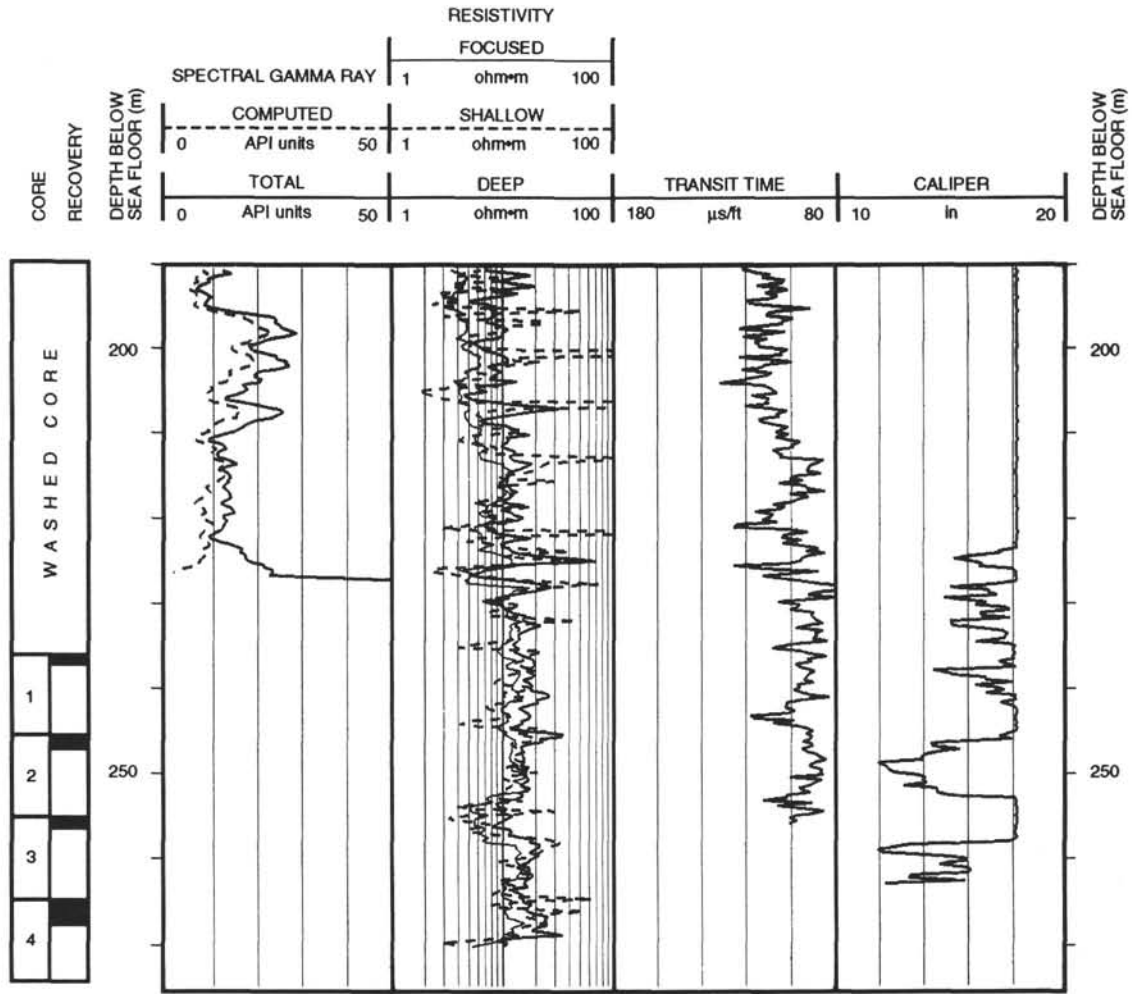


Figure 44 (continued).

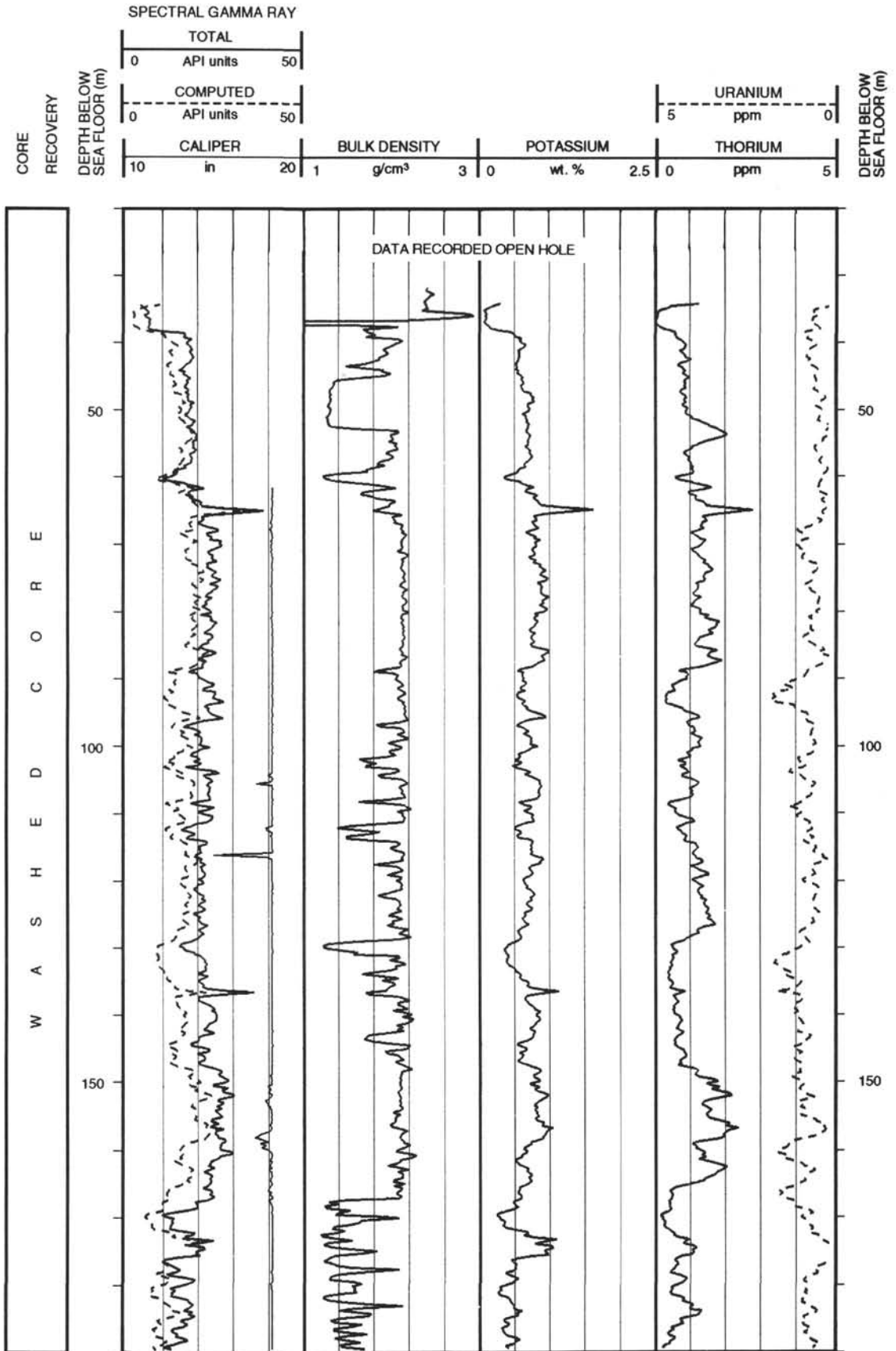
Hole 830C: Resistivity-Sonic-Natural Gamma Ray Log Summary



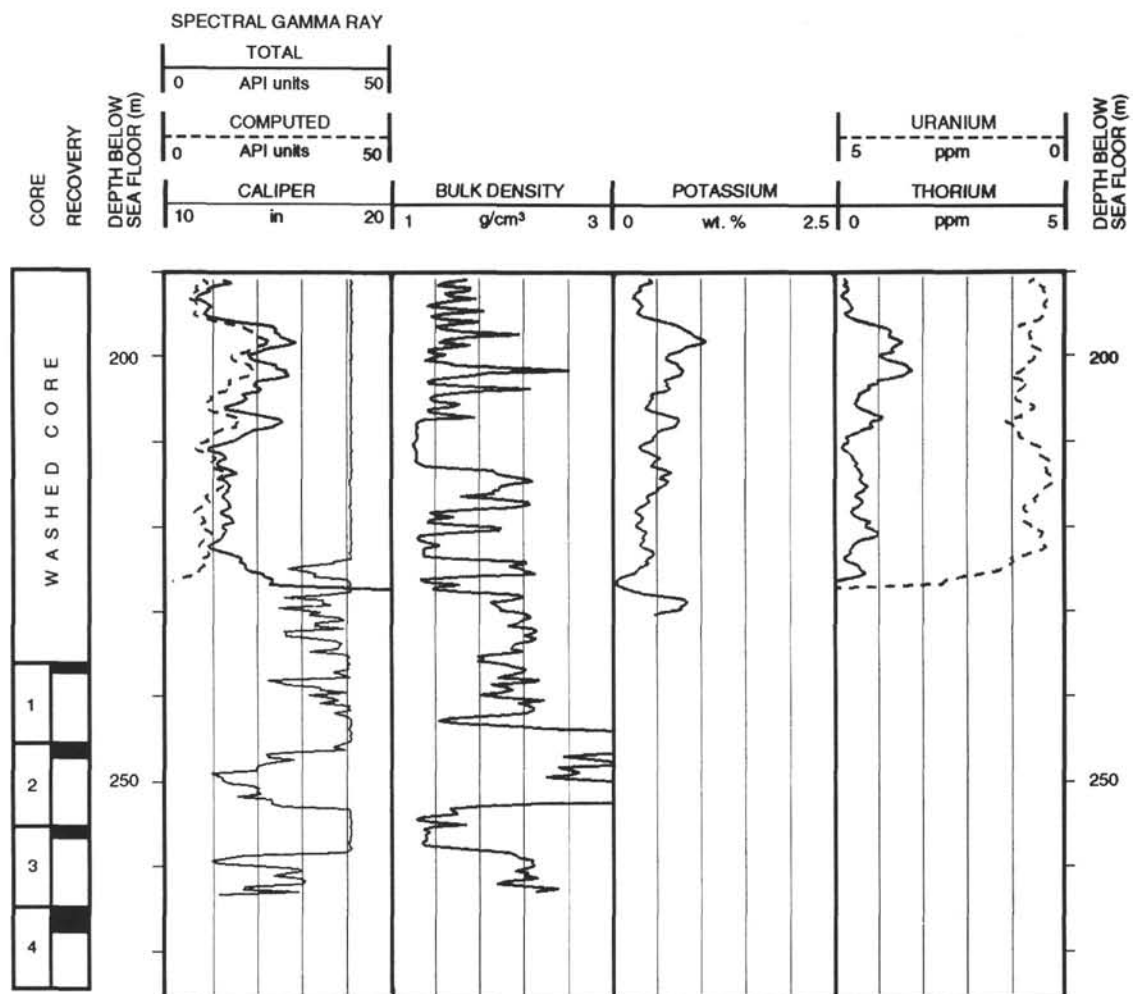
Hole 830C: Resistivity-Sonic-Natural Gamma Ray Log Summary (continued)



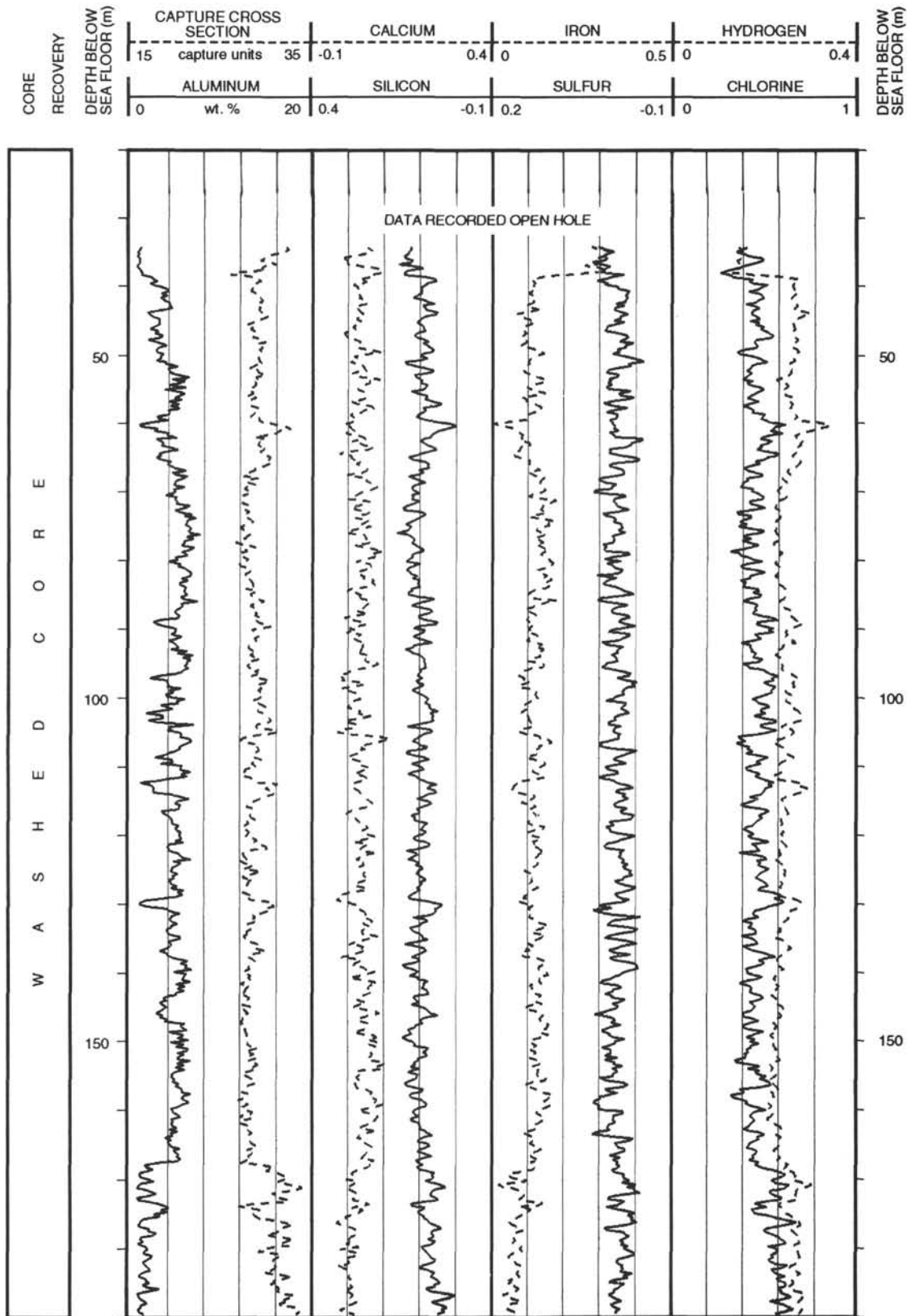
Hole 830C: Density-Natural Gamma Ray Log Summary



Hole 830C: Density-Natural Gamma Ray Log Summary (continued)



Hole 830C: Geochemical Log Summary



Hole 830C: Geochemical Log Summary (continued)

